TWO - DIMENSIONAL LATERALLY - INTEGRATED ESTUARINE NUMERICAL WATER QUALITY MODEL

VOLUME I - ANALYSIS AND RESULTS

MALCOLM L. SPAULDING

FRANK M. WHITE

DEPARTMENT OF MECHANICAL ENGINEERING AND APPLIED MECHANICS

UNIVERSITY OF RHODE ISLAND

KINGSTON, RHODE ISLAND

1974

THIS WORK WAS SUPPORTED BY THE UNIVERSITY OF RHODE ISLAND SEA GRANT PROGRAM. ADDITIONAL COPIES OF MARINE TECHNICAL REPORT XX ARE AVAILABLE FROM THE URI MARINE ADVISORY SERVICE, NARRAGANSETT BAY CAMPUS, NARRAGANSETT, RHODE ISLAND 02882. COST PER COPY IS $X.00.

This report, the first in a series of two, describes the detailed development of a numerical water quality simulation model and its application to Narragansett Bay, Narragansett, Rhode Island. In the second volume, a user's manual for this model is presented complete with Fortran IV program listings and verification runs. Additional copies of this volume, as well as volume two, can be obtained from the URI Marine Advisory Service, Narragansett Bay Campus, Narragansett, Rhode Island 02882. no longer available

ACKNOWLEDGEMENT

The author wishes to express his appreciation to Professor Frank White, his adviser, and Professors G. Brown and T. Kowalski for their guidance and encouragement during the preparation of this work. Special thanks go to Professor Brown who, as director of the University of Rhode Island's Bay Watch Project has provided invaluable assistance in funding for this work and preparation of the final report.

The staff and operations management for the U.R.I. Computer Laboratory are to be commended for providing the author with the necessary computing services to complete this project.

The research in this report was funded, in part, both by the U.R.I. Sea Grant Program and by a U.R.I. Fellowship which the author held from 1970 through 1972. The laborious typing task has been ably performed by Mrs. Diane Silverman and Miss Meredith Paine.

TABLE OF CONTENTS

TABLE OF CONTENTS (Cont'd)

TABLE OF CONTENTS (Cont'd)

LIST OF ILLUSTRATIONS

LIST OF ILLUSTRATIONS (Cont'd)

LIST OF ILLUSTRATIONS (Cont'd)

LIST OF ILLUSTRATIONS (Cont'd)

LIST OF ILLUSTRATIONS (Cont'd)

LIST OF ILLUSTRATIONS (Cont'd)

LIST OF TABLES

CHAPTER 1

INTRODUCTION

WATER POLLUTION IN ESTUARIES

Since some 60% of the world's population lives in delta and coastal regions (1)*, man has for centuries been using the most economical and convenient means of sewage disposal - discharging it directly into rivers and estuaries. With the ever increasing population and industrial growth, waste loads are increasing at a startling rate and are threatening to turn one of our greatest natural resources into an alarming national problem. This fact is well verified when looking at the progress of water classified as polluted over a period of time. A typical example is Narragansett Bay, as shown in Figs. 1 - 1 through 1 - 6 (2).

* Numbers in parenthesis refer to items in the Bibliography.

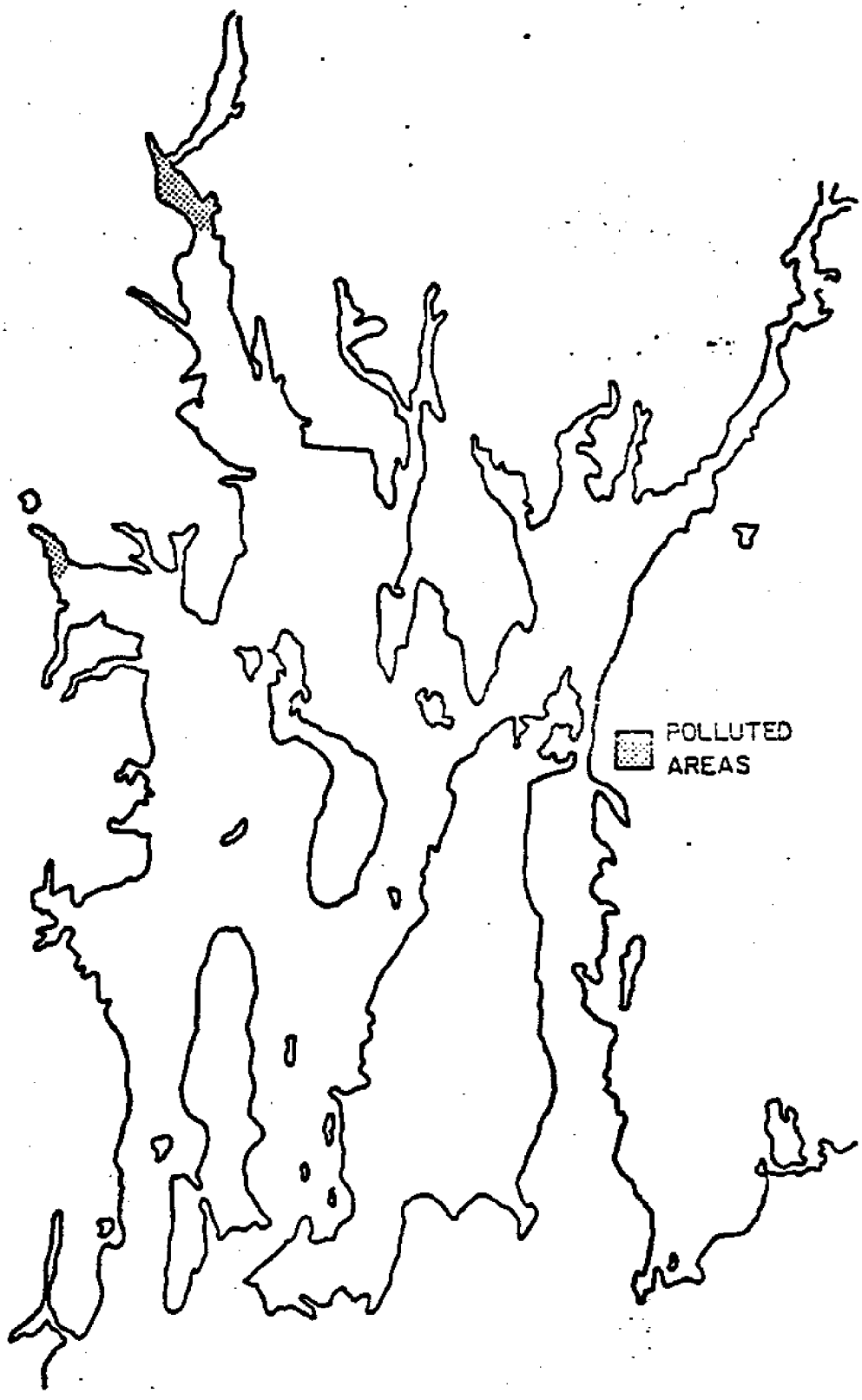

FIG. 1-1 NARRAGANSETT BAY POLLUTION - 1880 (2)

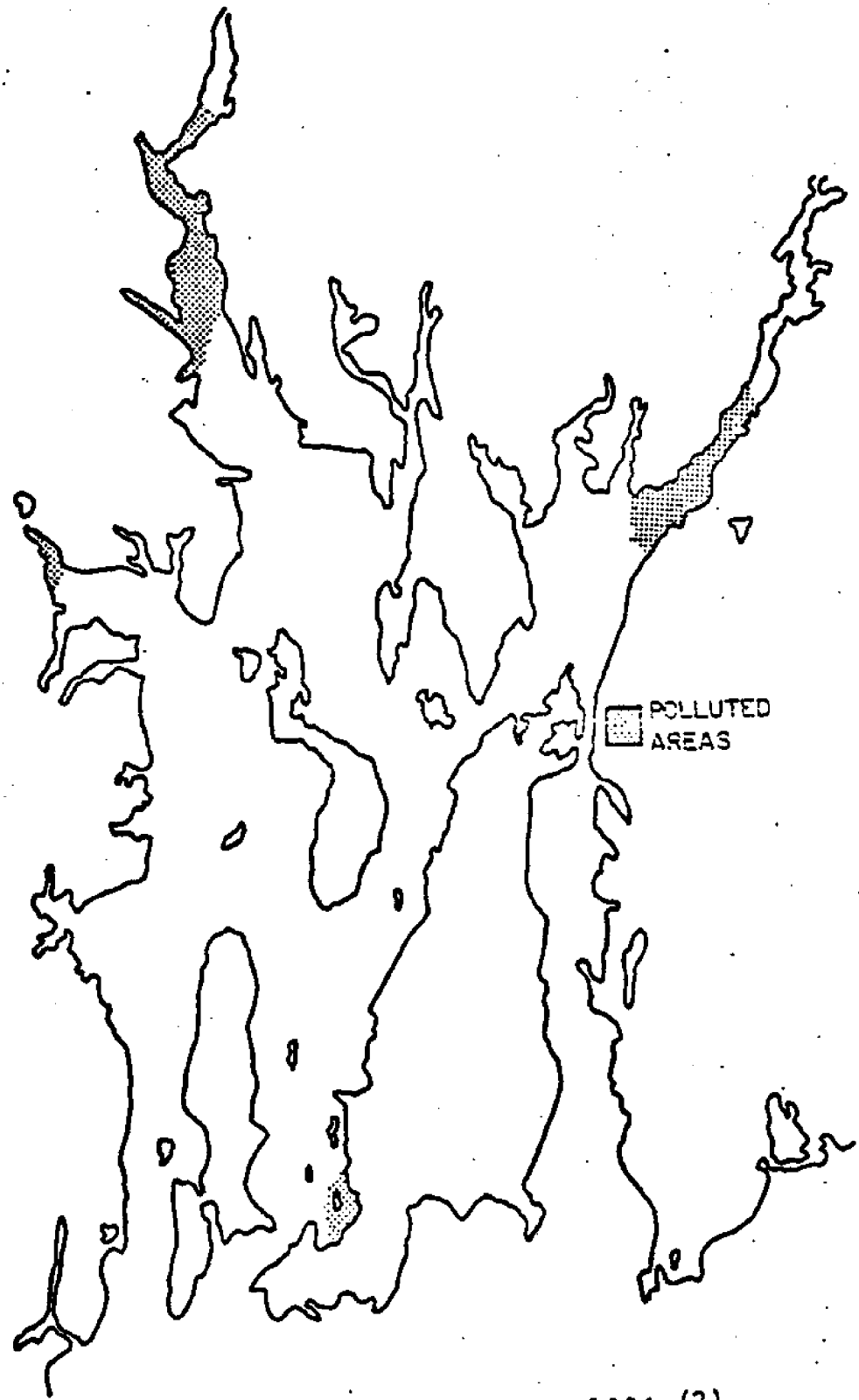

FIG. 1-2 NARRAGANSETT BAY POLLUTION -1904 (2)

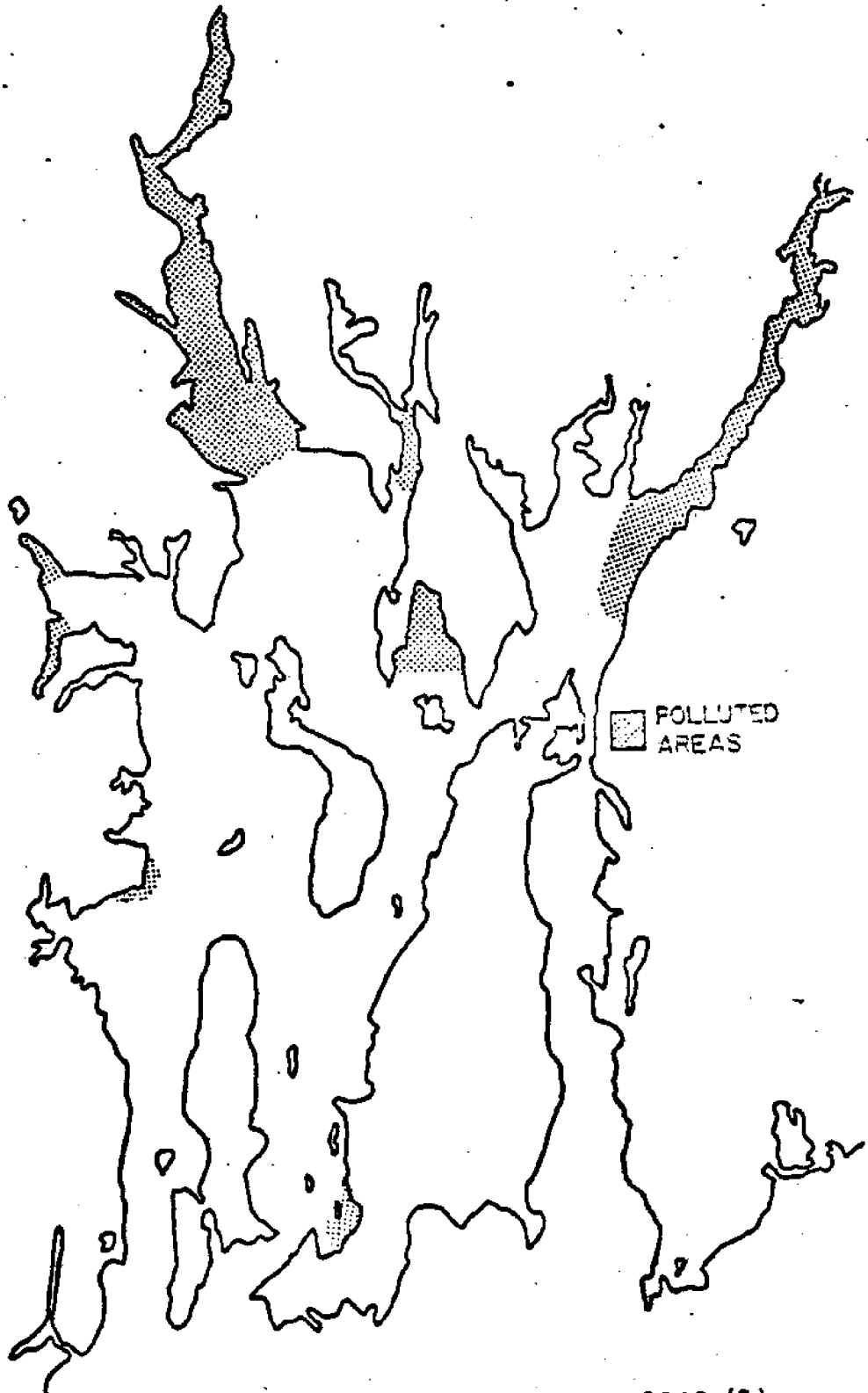

FIGURE 1-3 NARRAGANSETT BAY POLLUTION - 1940 (2)

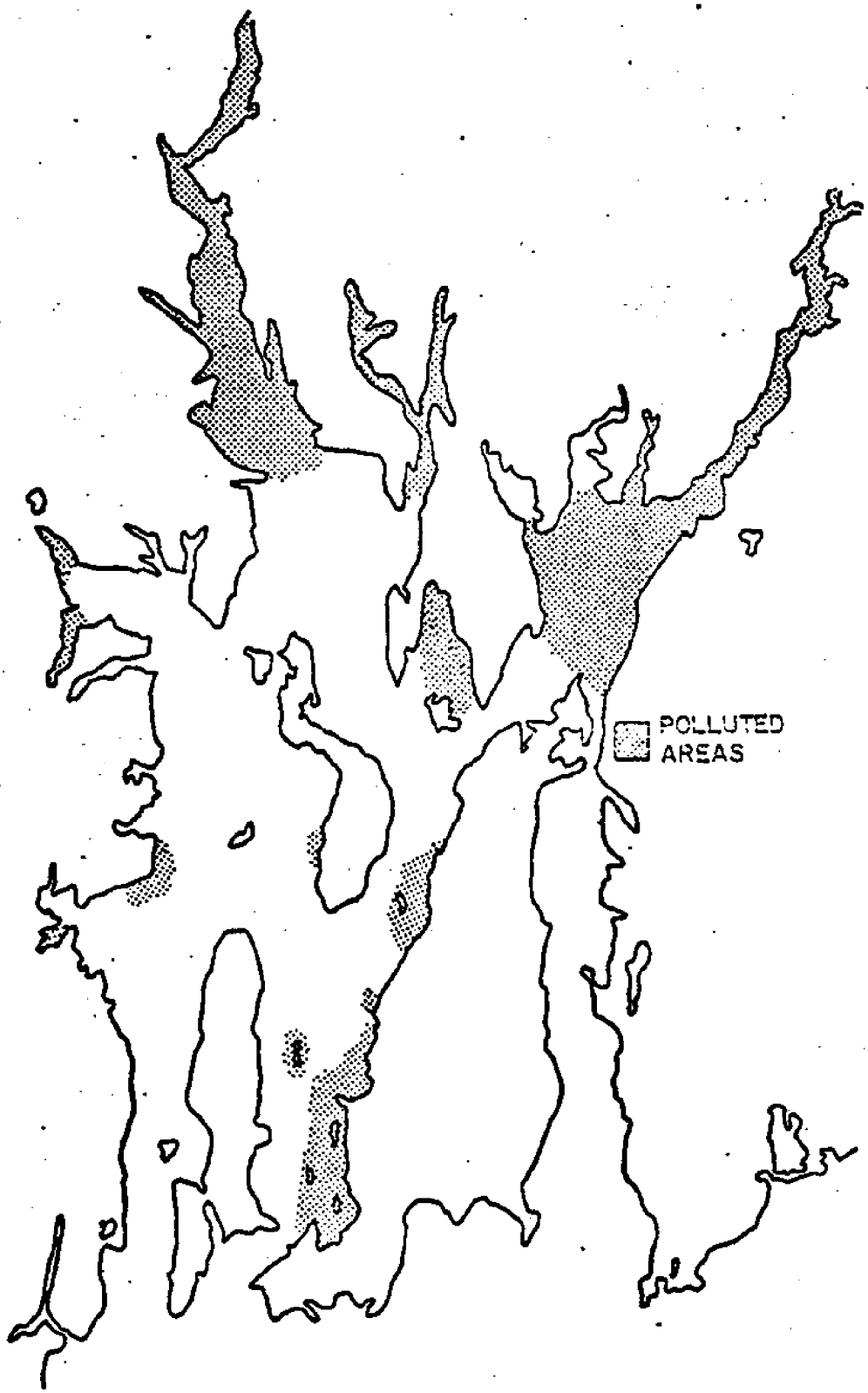

FIG. 1-4 NARRAGANSETT BAY POLLUTION - 1947 (2)

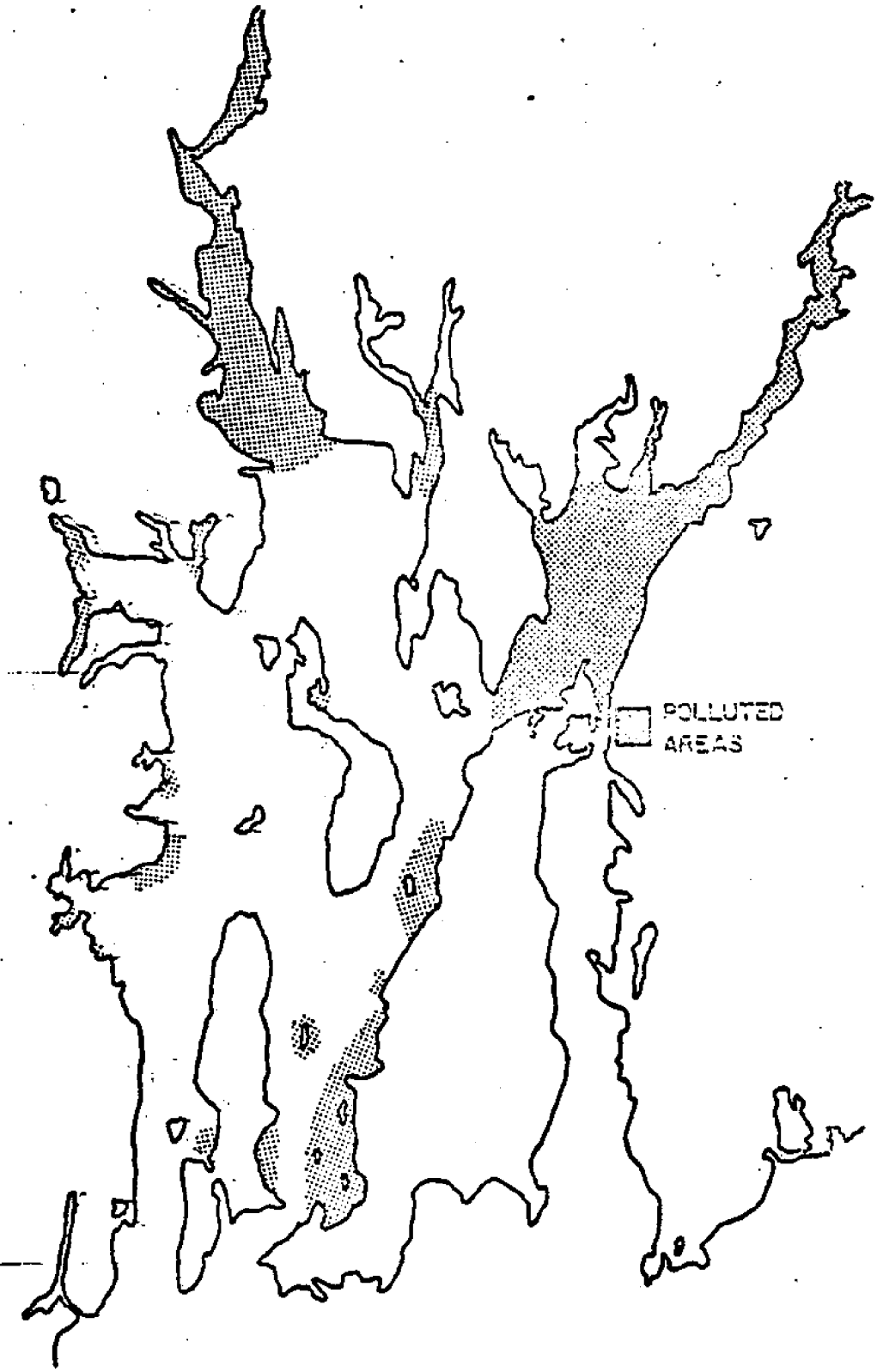

FIG. 1-5 NARRAGANSETT BAY POLLUTION - 1961 (2)

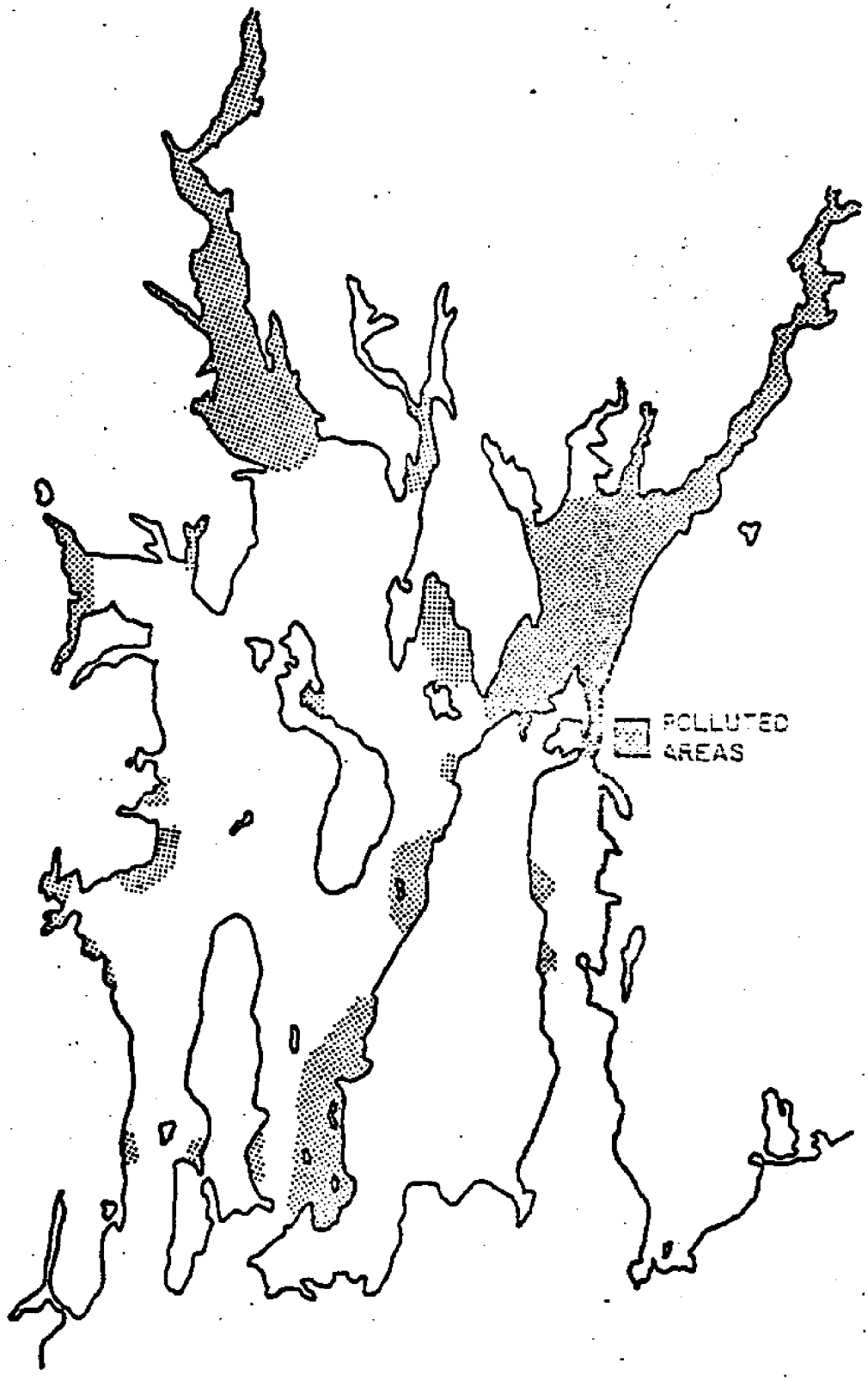

FIG. 1-6 NARRAGANSETT BAY POLLUTION -1969 (2)

The ecosystem of an estuary is a delicate balance of chemical, physical, and ecological factors. A natural system such as this may tolerate a limited amount of human interference by discharging treated and untreated wastes into its waters. This ability is commonly referred to as the assimulative capacity or self-purification capacity of an estuary. Within this extent, the ecological balance of the system will tend to be restored to an equilibrium position with no detrimental effects to the ecology of the estuary. However, if interfered with beyond this limit a new system balance will be achieved which leads to loss of wildlife and fish, overgrowth of some undesirable aquatic and benthic life and other consequences which have long-range effects and have not even been fully determined. The subsequent loss of valuable estuary resources such as fishery, wildlife, and minerals, summarized by Di Luzio (3), shows that continued estuary pollution and its consequent changes of the ecosystem are a threat to the quality and even continuance of man's existence in

these areas both for the immediate present and future generations of mankind.

Estuary pollution can usually be divided into three general categories - bottom, surface, and liquid wastes. Bottom wastes are usually in the form of deposits of inorganic or organic matter which are insoluble. These deposits tend to build up in channels and similar hydrographic features. Their removal is usually accomplished by dredging which often is a very expensive and time-consuming process. Many of these bottom deposits also can exert a considerable oxygen demand on the estuarine water and lead to local eutrophication. On the other hand, surface wastes are usually buoyant materials such as oil which tend to block important surface transport phenomena - such as reareation and heat and light transmission. However, the most important pollution source is that caused by liquid wastes. These are critical since they refer to the majority of the pollution loads discharged into an estuary - i.e. the carbonaceous, nitrogenous, phosphorous, and other soluble organic and

inorganic matters derived from sewage and other waste discharges. The organic matter is of importance since it serves as a food source for bacteria and other organisms whose existence may be detrimental to various water uses. Therefore, this study will deal primarily with the liquid wastes. The others, surface and bottom, only being indirectly considered.

To predict accurately the quality of water requires answers to the following questions (1).

(1) How is a given pollutant from a source transported and distributed through an estuary as a function of time?

(2) How rapidly does the decay or generation by natural processes add or subtract from the water quality parameter being used as an indicator?

The first question is primarily one involving the fluid mechanics of mass transport in the estuary. The processes

involved are advective transport of a constituent due to the mean tidal velocity and dispersive transport produced mainly by turbulent mixing. These values are related solely to the physical hydrodynamical or flow characteristics of the estuary and are both time and space dependent. The second question is chiefly concerned with the chemical and microbiological processes of species generation and decay. These variables tend to be temperature and time dependent and in cases concentration dependent.

Water quality models describing both the hydrodynamic transport and the decay or generation of a specific parameter usually assume the form of a mass transport equation with a specific source-sink or reaction matrix term. Normally the types of models developed can be divided into two general classes, conservative and non-conservative. The non-conservative models can also be further subdivided into one-stage through multi-stage reaction schemes. To aid in visualizing the mathematical structure of these models an example of each is presented.

Example 1 - Conservative Case (Salinity or Chlorinity)

$$\frac{\partial S_a}{\partial t} + u \frac{\partial S_a}{\partial x} + v \frac{\partial S_a}{\partial y} + w \frac{\partial S_a}{\partial z} - \frac{\partial}{\partial x}\left(e_x \frac{\partial S_a}{\partial x}\right) - \frac{\partial}{\partial y}\left(e_y \frac{\partial S_a}{\partial y}\right) - \frac{\partial}{\partial z}\left(e_z \frac{\partial S_a}{\partial z}\right) = 0 \qquad (1.1)$$

S_a - Conservative constituent such as salinity or chlorides

u,v,w, - x,y,z - directed velocity components, respectively

e_x, e_y, e_z - x,y,z - directed diffusion coefficients, respectively

Example 2 - Non-Conservative, Single-Stage Reaction Case (Coliform)

$$\frac{\partial C_o}{\partial t} + u \frac{\partial C_o}{\partial x} + v \frac{\partial C_o}{\partial y} + w \frac{\partial C_o}{\partial z} - \frac{\partial}{\partial x}\left(e_x \frac{\partial C_o}{\partial x}\right) - \frac{\partial}{\partial y}\left(e_y \frac{\partial C_o}{\partial y}\right) - \frac{\partial}{\partial z}\left(e_z \frac{\partial C_o}{\partial z}\right) = - K_{cd} C_o + Co_s \qquad (1.2)$$

C_o - concentration of coliform bacteria (MPN)

K_{cd} - decay constant for coliform bacteria (1/sec)

Co_s - source of coliform bacteria (MPN/sec)

u,v,w - x,y,z - directed velocity components, respectively

e_x, e_y, e_z - x,y,z - directed diffusion coefficients, respectively

Example 3 - Non-Conservative, Two-Stage Reaction Case

(D.O. - B.O.D.)

$$\frac{\partial L}{\partial t} + u\frac{\partial L}{\partial x} + v\frac{\partial L}{\partial y} + w\frac{\partial L}{\partial z} - \frac{\partial}{\partial x}\left(e_x \frac{\partial L}{\partial x}\right) - \frac{\partial}{\partial y}\left(e_y \frac{\partial L}{\partial y}\right) - \frac{\partial}{\partial z}\left(e_z \frac{\partial L}{\partial z}\right) = -K_D L + J \qquad (1.3)$$

(B.O.D.) equation

$$\frac{\partial c}{\partial t} + u\frac{\partial c}{\partial x} + v\frac{\partial c}{\partial y} + w\frac{\partial c}{\partial z} - \frac{\partial}{\partial x}\left(e_x \frac{\partial c}{\partial x}\right) - \frac{\partial}{\partial y}\left(e_y \frac{\partial c}{\partial y}\right) - \frac{\partial}{\partial z}\left(e_z \frac{\partial c}{\partial z}\right) = -K_D L + K_A (c_{SAT} - c) + S_{DO}$$

(D.O. equation)

L - biochemical oxygen demand (B.O.D.) concentration (mg/l)

u,v,w-x,y,z - directed velocity components, respectively

e_x, e_y, e_z - x,y,z - directed diffusion coefficients, respectively.

K_D - B.O.D. decay coefficients (1/sec)

J - point load of B.O.D. (mg/l of B.O.D./sec.)

K_A - reareation coefficient for dissolved oxygen (1/sec).

c_{SAT} - saturation level for dissolved oxygen (mg/l)

c - concentration of dissolved oxygen (D.O.) (mg/l)

S_{DO} - source or sink for D.O. (mg/l sec)

Higher order reaction schemes such as that for the nitrogen cycle have not been shown but follow a similar pattern. A careful survey of the reaction schemes presented shows a common mass transport equation with varying reaction terms. Hence, the development in this work will be based on the basic mass transport equation with indications as to how multi-stage reaction mechanisms may be added.

The ability to predict the actions of these systems on the estuary is then the chief concern of a well constructed water quality model. This model thus provides a method to study the technical alternatives to various

political, legal and administrative decisions, and should aid in managerial approaches to control pollution in an estuary.

PRESENT STUDY

Work in estuary water quality has progressed rather rapidly in recent years with the development of mathematical models for the one-dimensional (1,4,5) and vertically-averaged, two dimensional (6) mass-transport equations. An excellent summary of the current status of research in this area is provided in a report published by the TRACOR Corporation (7).

In all these models, however, no account has been taken of the vertical structure which is found in many estuaries. A typical example of this structure can be seen in regions of partial mixing and stratification such as at the head of Narragansett Bay. Here, there

appears a 30% variation in the dissolved oxygen content between the surface and bottom water layers (8). Other partially mixed and stratified estuary reaches undoubtedly show similar vertical structure in water quality parameters.

The present study will develop a two-dimensional, laterally or cross-stream averaged, mass-transport equation such that vertical structure will be incorporated into the model. Then using an A.D.I. (Alternating Direction Implicit) finite-difference technique to approximate the original parabolic, partial differential, mass-transport equation, the two-dimensional concentration fields will be predicted as a function of time.

To adequately model all situations for vertical structure a non-dimensional and dimensional vertical (z) axis model will be developed. The dimensional model is best suited to regions where variations in tidal height are insignificant and depth changes are small such as in the upper reaches of rivers. In contrast, the dimensionless vertical axis model is

generally applicable to the entire estuary since it can handle variations in depth due to tidal height and significant hydrographical changes in an area.

In order to assure that the model predictions are valid, an analysis of the mass-transport equation both for stability and dissipative and dispersive effects will be performed. In addition, the computer-model transport equations will be checked to assure that the mass of a conservative substance is indeed conserved.

Since one of the main water quality parameters is the dissolved oxygen - biochemical oxygen demand system, often abbreviated D.O. - B.O.D., the computer model of the mass transport equation will be designed specifically for this parameter with indications on how other reaction schemes may be incorporated. The ability to handle conservative constituents will also be included.

Once developed, the computer model will be used to simulate the simple carbonaceous B.O.D. - D.O.

reaction scheme for Narragansett Bay as well as an accelerated no-load Bay cleanup.

A better perspective of the work to be presented can be obtained by use of a typical environmental model (6). Fig. 1-7 outlines such a model. The present research will attempt only to solve the mass transport equation, leaving the tidal hydrodynamics to be determined from existing models (1,9). Therefore, the solid lines in Fig. 1-7 indicate relations explained by the present model development while dotted lines show relationships that are not taken into account.

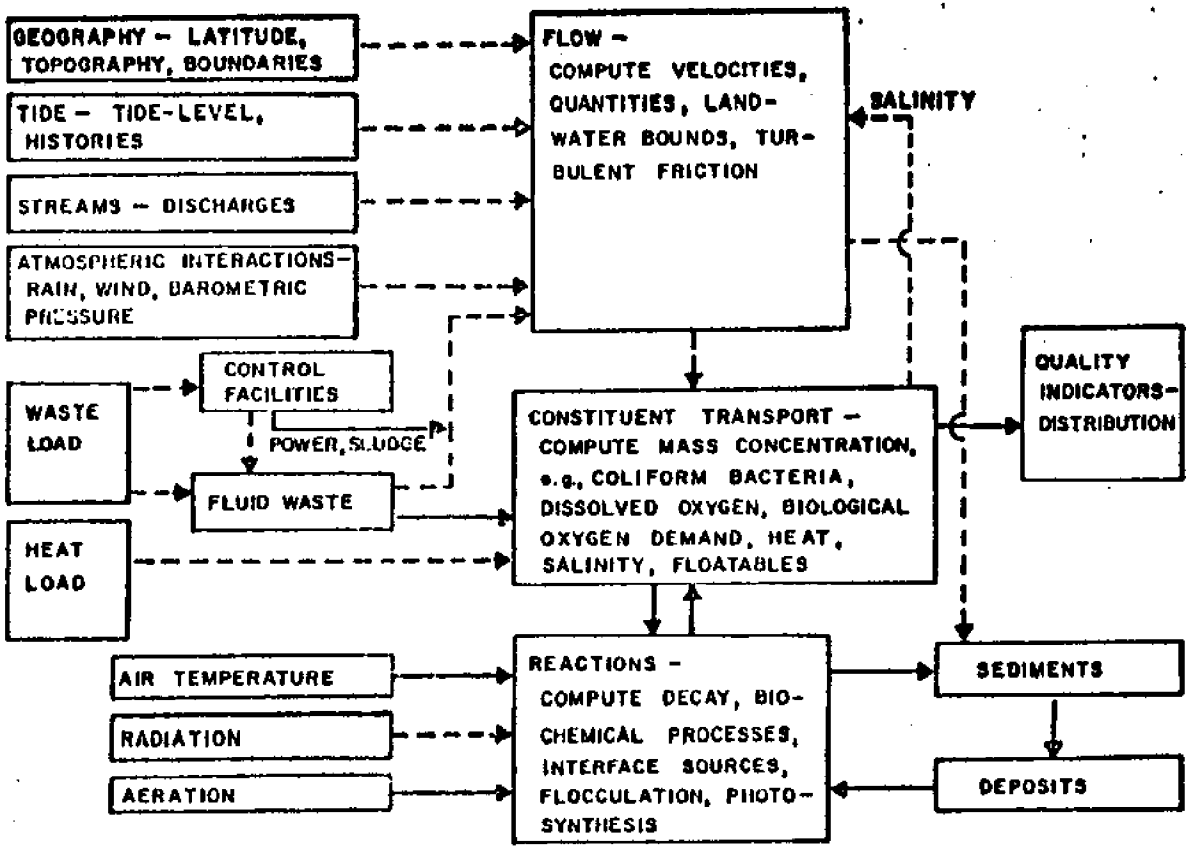

FIG. 1-7 ENVIRONMENTAL WATER QUALITY MODEL FOR LIQUID WASTES (6)

CHAPTER 2

MASS-TRANSPORT MODEL FOR AN ESTUARY

DETAILED DERIVATION OF THE MASS-TRANSPORT EQUATION

In a turbulent medium the mass balance equation may be written according to Bird and al. (10) as

$$\frac{\partial \rho_A}{\partial t} + \frac{\partial \rho_A u}{\partial x} + \frac{\partial \rho_A v}{\partial y} + \frac{\partial \rho_A w}{\partial z} =$$

$$\frac{\partial}{\partial x}\left(e_x \frac{\partial \rho_A}{\partial x} \right) + \frac{\partial}{\partial y}\left(e_y \frac{\partial \rho_A}{\partial y} \right) + \frac{\partial}{\partial z}\left(e_z \frac{\partial \rho_A}{\partial z} \right)$$

$$+ S_A$$

where

ρ_A - mass density of substance A

e_x, e_y and e_z - turbulent diffusion coefficients

S_A - source and sink terms of substance A

u,v,w - time-mean velocity over short sampling times in the x,y, and z directions, respectively.

In this rather fundamental form several approximations have already been made. Molecular diffusion has been neglected in anticipation of the fact that in most estuarine system processes it is several orders of magnitude smaller than the turbulent eddy diffusivity. The diffusion terms are obtained by assuming that the turbulent flux terms, $u'\rho_A'$ etc. can be adequately represented by the product of an eddy diffusion coefficient and the ensemble mean concentration gradient. Thus the coefficients e_x, e_y and e_z are the eddy diffusivities for the parameter ρ_A.

In addition, it has also been assumed that no diffusive transports are caused by thermal or pressure gradients within the system. All these approximations have been shown to be applicable to estuarine environments (1,11).

It was indicated that the velocities in Eq. (2.1) were time-mean velocities over short sampling periods. By this, it is meant that the time-averaging process occurs over intervals of time much smaller than the time for a tidal cycle, i.e. 1 minute periods. This procedure

then sucessfully eliminates the stochastic variation in mass density.

For a better understanding of the elements or terms of the mass transport equation Fig. 2-1 shows the major transporting mechanisms. In most estuaries the lateral and longitudinal advective and vertical dispersive transports are of primary importance.

Since in its generalized three-dimensional form Eq. (2.1) at best is extremely difficult to solve even in the simplest of cases, the standard approach is to integrate over one of the spatial variables or time to, in effect, reduce the dimensionality of the equation. For the case at present we note that our aim is to laterally integrate Eq. (2.1) to achieve a model with vertical structure while simultaneously eliminating the lateral structure.

It must be remembered in interpreting the results that we have laterally integrated the equation and not just dropped one of the spatial directions, in this case the cross-sectional direction.

The intepretation of the mass d ensity is now an average

$$\underbrace{\frac{\partial \rho_A}{\partial t}}_{\text{TEMPORAL CHANGE OF MASS DENSITY}} + \underbrace{\frac{\partial \rho_A u}{\partial x} + \frac{\partial \rho_A v}{\partial y} + \frac{\partial \rho_A w}{\partial z}}_{\text{ADVECTIVE TRANSPORT}} = \underbrace{\frac{\partial}{\partial x}\left(e_x \frac{\partial \rho_A}{\partial x}\right) + \frac{\partial}{\partial y}\left(e_y \frac{\partial \rho_A}{\partial y}\right) + \frac{\partial}{\partial z}\left(e_z \frac{\partial \rho_A}{\partial z}\right)}_{\text{TURBULENT OR DIFFUSIVE TRANSPORT}} + \underbrace{S_A}_{\text{SOURCES AND SINKS}}$$

MASS TRANSPORT MODEL

FIG. 2-1 MASS TRANSPORT MODEL (1)

over a lateral cross section. Similarly, diffusion terms now become not only representative of the turbulent fluctuations but also the dispersive effect of lateral variations in ρ_A and lateral shear in the current, therefore when incorporating these other effects they will be called dispersive or dispersion terms rather than diffusive terms.

As a first step toward determining the laterally-integrated, mass-transport equation the coordinate system must be defined. The x axis is fixed to the mean sea level plane for the dimensional model or varies with the tide height for the non-dimensional z axis model pointing in the direction of the estuary mouth and having its origin at the most upstream point where the model is to be employed. The x axis, therefore will be approximately in the same direction as the mean flood or ebb tidal flow. The y axis is perpendicular to the x and in the same plane as the mean sea level or tidal plane. The z axis is then vertically upward or opposite the direction of gravity and perpendicular to the x,y plane. Figure 2-2 shows the orientation for a typical estuary.

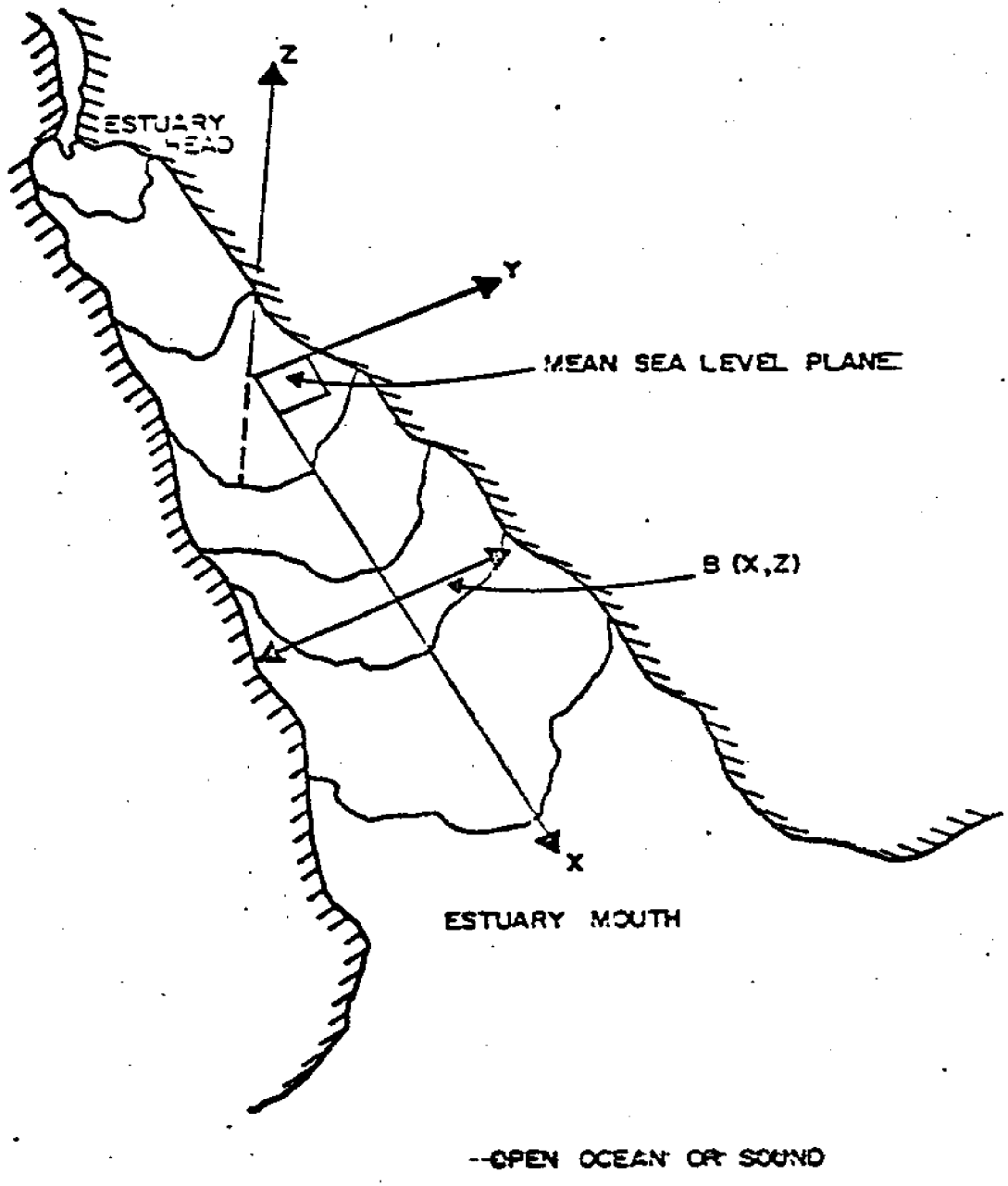

FIG. 2-2 COORDINATE SYSTEM ORIENTATION

Proceeding with the lateral integration of Eq. (2.1) we need to introduce the following notation:

$$PB = \int_0^B \rho A \, dy \tag{2.2}$$

$$UB = \int_0^B u \, dy \tag{2.3}$$

$$WB = \int_0^B w \, dy \tag{2.4}$$

where B is the estuary width and P,U,W represent the laterally averaged values of ρ_A, u and w respectively. Now, assuming a distribution of mass density according to:

$$\rho_A(y) = P \, [\, 1 + \rho_A'(y)] \tag{2.5}$$

and similarly assuming a distribution of velocities according to:

$$u(y) = U[1 + u'(y) \,] \tag{2.6}$$

$$w(y) = W[1 + w'(y) \,] \tag{2.7}$$

The definitions of the laterally integrated variables are completed.

In view of these definitions then:

$$\int_0^B \rho_A' (y)\ dy = 0 \qquad (2.8)$$

$$\int_0^B u'(y)\ dy = 0 \qquad (2.9)$$

$$\int_0^B w'(y)\ dy = 0 \qquad (2.10)$$

These relationships show that ρ_A', u', and w' are essentially distribution functions of ρ_A, u, and w respectively.

Equation (2.1) can be laterally integrated, but first we need Leibnitz's rule which states that:

$$\left\langle \frac{\partial [f_g (x,y,z,t]}{\partial t} \right\rangle = \frac{\partial \langle f_g (x,y,z,t) \rangle}{\partial t} - f_g (x,B,z,t) \frac{\partial B}{\partial t} \tag{2.11}$$

where the notation

$$\langle \quad \rangle = \int_0^B (\quad) \, dy \tag{2.12}$$

has been used for convenience. A similar procedure can be employed when the derivative of f_g is taken with respect to some spatial coordinate.

Proceeding term by term to laterally integrate Eq. (2.1) and employing Eqs. (2.2) through (2.12), for the temporal change term we find:

$$\int_0^B \frac{\partial \rho_A}{\partial t} \, dy = \frac{\partial}{\partial t} (BP) - \rho_A(B) \frac{\partial B}{\partial t} \tag{2.13}$$

Noting that B, the estuary width is usually a function of x, and z only, and not time, then $\partial/\partial t\ (B) \longrightarrow 0$, however, for generality, assume B = B(t) for the present and note that if we have no lateral inflows $\rho_A(B) = 0$, then:

$$\int_0^B \frac{\partial \rho_A}{\partial t}\, dy = \frac{\partial}{\partial t}\ (BP) \qquad (2.14)$$

For the convective terms:

$$\int_0^B \frac{\partial \rho_A u}{\partial x}\, dy = \frac{\partial}{\partial x} \int_0^B \rho_A u dy - \rho_A(B)\ u\ (B)\ \frac{\partial B}{\partial x} \qquad (2.15)$$

Substituting for ρ_A and u from Eqs. (2.5) and (2.6) respectively, expanding and employing Eqs. (2.8) and (2.9) results in:

$$\int_0^B \frac{\partial \rho_A u}{\partial x}\, dy = \frac{\partial}{\partial x}\ [\ PU\ (\langle 1 + \rho_A' u' \rangle)\ ] \qquad (2.16)$$

where $\rho_A(B)$ or u(B) have been assumed equal to zero, under the assumption of no lateral inflows. A similar approach can be used to obtain:

$$\int_0^B \frac{\partial \rho_A w}{\partial z}\, dy = \frac{\partial}{\partial z}\left[PW\left(\left\langle 1 + \rho_A' w'\right\rangle\right)\right] \qquad (2.17)$$

where Eqs. (2.5), (2.7), (2.8) and (2.10) have been used. For the diffusion terms, laterally integrating we find:

$$\int_0^B \frac{\partial}{\partial x}\left(e_x \frac{\partial \rho_A}{\partial x}\right) dy = \frac{\partial}{\partial x} \int_0^B e_x \frac{\partial \rho_A}{\partial x}\, dy - e_x(B) \frac{\partial \rho_A(B)}{\partial x} \frac{\partial B}{\partial x} \qquad (2.18)$$

assuming that $e_x(B) = 0.0$ by noting that we have no lateral inflows and making use of the notation in Eq. (2.12) results in:

$$\int_0^B \frac{\partial}{\partial x}\left(e_x \frac{\partial \rho_A}{\partial x}\right) dy = \frac{\partial}{\partial x}\left\langle e_x \frac{\partial \rho_A}{\partial x}\right\rangle \qquad (2.19)$$

Similarly for the vertically (z) directed diffusion term:

$$\int_0^B \frac{\partial}{\partial z}\left(e_z \frac{\partial \rho_A}{\partial z}\right) dy = \frac{\partial}{\partial z}\left\langle e_z \frac{\partial \rho_A}{\partial z}\right\rangle \qquad (2.20)$$

Substituting Eqs. (2.14), (2.16), (2.17), (2.19) and (2.20) into Eq. (2.1) results in:

$$\frac{\partial}{\partial t}(BP) + \frac{\partial \left[\left\langle 1 + \rho_A' u' \right\rangle\right] UP}{\partial x} +$$

$$+ \frac{\partial \left[\left\langle 1 + \rho_A' w' \right\rangle\right] WP}{\partial x} - \frac{\partial \left\langle e_x \frac{\partial \rho_A}{\partial x} \right\rangle}{\partial x} \tag{2.21}$$

$$- \frac{\partial \left\langle e_z \frac{\partial \rho_A}{\partial z} \right\rangle}{\partial z} = SB$$

where $$S = \frac{1}{B} \int_0^B S_A \, dy \tag{2.22}$$

Now if we assume that the density variations in the y, or lateral direction, are small, i.e., lateral homogeneity, then

$$\rho_A'(y) = 0 \tag{2.23}$$

The mass balance equation using the assumption in Eq. (2.23) becomes:

$$\frac{\partial}{\partial t}(BP) + \frac{\partial UBP}{\partial x} + \frac{\partial WBP}{\partial z} - \frac{\partial \left\langle e_x \frac{\partial \rho_A}{\partial x} \right\rangle}{\partial x}$$

$$- \frac{\partial \left\langle e_z \frac{\partial \rho_A}{\partial z} \right\rangle}{\partial z} = SB \tag{2.34}$$

Looking at the turbulent dispersion terms, they can be expanded to,

$$\int_0^B e_x \frac{\partial \rho_A}{\partial x} \, dy = BD_x \frac{\partial P}{\partial x} \tag{2.25}$$

and

$$\int_0^B e_z \frac{\partial \rho_A}{\partial z} \, dy = BD_z \frac{\partial P}{\partial z} \tag{2.26}$$

where D_x and D_z represent the laterally-averaged dispersion coefficients in the x and z directions, respectively.

Using Eqs. (2.26) and (2.25) in Eq. (2.24) gives the final form of the laterally-integrated mass-transport equation for mass concentration P :

$$\frac{\partial BP}{\partial t} + \frac{\partial UBP}{\partial x} + \frac{\partial WBP}{\partial z} - \frac{\partial}{\partial x}\left(BD_x \frac{\partial P}{\partial x}\right) - \frac{\partial}{\partial z}\left(BD_z \frac{\partial P}{\partial z}\right) = SB \tag{2.27}$$

where S has been taken to represent a generalized laterally integrated source-sink term.

This development has shown how the ordinary mass-transport model can be laterally averaged to neglect lateral structure in its formulation. Indications of how this model may be adjusted to both the dimensional and dimensionless (z) vertical axis cases will be provided in the sections on the development of the computational model.

DISPERSION IN TWO-DIMENSIONAL COMPUTATIONS

With the lateral integration of the mass-balance or transport equation we have introduced dispersion coefficients which incorporate both the normal turbulent mass fluctuation terms, $u' \rho_A'$, and in addition the variations in the velocity profile in the cross stream direction. In order to develop relations to express adequately these dispersive terms a general look at the mechanism of dispersion will be attempted in this section followed by a specific formulation for the problem of interest.

Dispersion of a pollutant can be caused by the following mechanism as described by Fisher (12). The flow in various parts of an estuary taken perpendicular to the mean flow show differences in velocity. Due to these variations portions of a "field" of pollution constituent will move more rapidly than the mean flow and other portions more slowly, hence dispersing the pollutant in the direction of the flow. This variation causes cross-sectional differences in the mass concentration and leads to a

cross-sectional turbulent diffusion which tends to transfer constituents from the parts with higher concentration to those with lower concentration. A similar explanation can be employed for the contribution of the variations in the vertical and lateral structure of the mean tidal velocity, u.

Obviously, from the description above, the magnitude of the dispersion coefficients employed in any computational scheme can vary widely, since they are dependent on the variations in constituent concentrations and velocity within each section. For instance, if the lateral deviations of the mean tidal velocity are small, then the grid or section sizes may be increased without effecting the solution. However, if the variations are large, grid size changes can determine the dispersive transport.

Using Taylor's concept (13), and work based on I.E. Thomas' (14) doctoral dissertation, Elder (15) determined the longitudinal and lateral dispersion coefficients based on the mean velocity, depth, and bottom roughness for a one-dimensional steady flow. Elder found the longitudinal dispersion coefficient, D_x to be:

$$D_x = 5.93\ Hu^* \qquad (2.28)$$

where u^* - friction velocity or shear stress velocity

H - the average section depth

The shear stress velocity is related to the mean velocity by the relation:

$$u^* = \left(\frac{\tau_x}{\rho} \right)^{1/2} = \bar{u} g^{1/2} C_z^{-1} \qquad (2.29)$$

where

τ_x - bed shear stress

$\bar{u}$ - uniform flow speed

g - gravity

C_z - Chezy coefficient

ρ - density

Now combining Eqs. (2.29) and (2.28) results in:

$$D_x = 5.93\ H\bar{u}\ g^{1/2}\ C_z^{-1} \qquad (2.30)$$

For the lateral turbulent dispersion, perpendicular to the mean flow, Elder obtained:

$$\epsilon_y = 0.23\ Hu^* \qquad (2.31)$$

Fisher (12), and Fischer (16) have indicated that Elder's approach was correct for channel flows but showed poor comparison to actual river data, always underestimating the actual longitudinal dispersion coefficients by several orders of magnitude. This they attributed to the fact that Elder's work only included a vertical variation in the mean velocity $\bar{u}$, whereas, in actual stream flows, the lateral variation in mean velocity is usually the more important mechanism in longitudinal dispersion.

Fischer (16) then extended Taylor's analysis to three-dimensional flows and determined that:

$$D_x = -\frac{1}{A}\int_0^B H(y)\ u''(y)\ F_p(y)\ dy \qquad (2.32)$$

in which

A - cross-sectional area

B - width of channel

H(y) - depth of channel at point y

$F_p(y)$ - position function

u"(y) - local depth-averaged velocity deviation

$$u''(y) = \frac{1}{H(y)} \int_{o}^{H(y)} u' \, dz \qquad (2.33)$$

where

$u'(z)$ - vertical deviation of mean velocity

and

$$F_p(y) = \int_{o}^{Y} \frac{1}{\epsilon_y H} dy \int_{o}^{y} \int_{o}^{H} u' \, dzdy \qquad (2.34)$$

Substituting Eq. (2.33) and (2.34) into (2.32) results in:

$$D_x = -\frac{1}{A} \int_{o}^{B} u''(y) \, H(y) \left[\int_{o}^{y} \frac{1}{\epsilon_y H(y)} dy \int_{o}^{y} \int_{o}^{H(y)} u' \, dz \, dy \right] dy \qquad (2.35)$$

in which ϵ_y has been assumed as that obtained by Elder in Eq. (2.31).

Experimental work performed by Fischer (16) has shown that the vertical variations in the mean velocity are small for river flows but can be quite sizeable for estuarine applications.

Since Eq. (2.35) is rather complicated from a computational viewpoint, another prediction method was developed by Fischer (16) based on a Lagrangian time scale,

this method is of a more approximate nature, but more easily applied. The longitudinal dispersion is assumed of the form:

$$D_x = (\bar{u}')^2 \, T_t \qquad (2.36)$$

in which

u' - variation of u from the cross-sectional mean

T_t - the Lagrangian time scale

An adequate expression relating the bulk channel parameters has been found to be

$$T_t = 0.30 \, \frac{l_c^2}{r \, u^*} \qquad (2.37)$$

where

l_c - the characteristics length of the channel, defined as the distance on the surface from the point of maximum velocity to the most distant bank

r - the hydraulic radius

u* - the shear stress velocity as defined in Eq. (2.29)

For slowly time varying conditions such as occur in tidal regions and estuaries, the mechanisms of dispersion described previously would still hold. If there are significant variations in mean tidal velocity in a lateral direction Eq. (2.35) or Eqs. (2.36) and (2.37) should be used, however if the lateral variations are small Eq. (2.30) would then be a proper formulation.

In addition, the longitudinal dispersion is influenced by the wind through a local circulation and wave motion. Wilson and Masch (17) have performed research in this area of a preliminary nature, but do not indicate any general formulation of the wind effect term.

In many estuaries there are regions where only partial mixing or even stratification occur and these effects must be included in any formulation of the vertical dispersion coefficient. Pritchard using an analysis of salt balance data on the James River estuary (18) has introduced a time-averaged vertical dispersion coefficient

based on estuary physical characteristics (19).

The vertical dispersion coefficient can be expressed as a product of a mixing length ϕ and a characteristic velocity, u** which is proportional to the root mean square turbulent velocity fluctuations.

$$D_z = \phi u^{**} \tag{2.38}$$

In a vertically homogeneous medium, the mixing length would be a function of the distance from the boundaries only. Since most estuaries are very much wider than deep, the boundaries may be approximated by two parallel flat plates. Using this analysis Montgomery (20) determined that:

$$\phi = \frac{\chi \, z \, (H-z)}{H} \tag{2.39}$$

where

χ - is a constant $\approx .4$

H - is the depth of the estuary at that point

z - is measured downward from mean sea level

When density increases with depth, more energy is required to move a parcel of water a given distance vertically than in the case of a homogeneous estuary. To account

for this effect Kent and Pritchard (12) modified Eq. (2.39) to obtain

$$\phi = \frac{z\ (H-z)}{H}\ (\ 1 + \beta_p\ R_i)^{-1} \qquad (2.39a)$$

for vertically non-homogeneous estuaries. In which

R_i - Richardson number

$$R_i = \frac{g}{\rho}\ \frac{\partial \rho}{\partial z}\ /\ (0.7\ \frac{\bar{U}}{H}\ )^2 \qquad (2.40)$$

where

β_p - empirical constant

The characteristic velocity u** as shown in Eq. (2.38) is composed of two parts:

(1) "flow induced" turbulence associated with the mean streaming velocity of the free fluid.

(2) random motion induced at the surface by the wind.

The first part is essentially determined by the mean tidal velocity and vertical stability, while the second part is dependent on wind conditions and vertical stability. The wind induced portion can be expected to decrease exponentially with depth and assumed proportional to the orbital wave velocity. Then the characteristic velocity

becomes:

$$u^{**} = \left[U \frac{z(H-z)}{H^2} (1+\beta_p R_i)^{-1} + \alpha_p \pi \frac{WH}{WT} e^{\frac{-2\pi z}{WL}} (1+\beta_p R_i)^{-1}\right] \quad (2.41)$$

where

u^{**}	-	rms turbulent velocity fluctuations
U	-	mean flow velocity
WH	-	wave height
WL	-	wave length
α_p, β_p	-	constants of proportionality
WT	-	wave period

Substituting Eqs. (2.39a) and (2.41) into Eq. (2.38) the vertical dispersion coefficient results in

$$D_z = \eta_p \frac{Uz^2 (H-z)^2}{H^3} (1+\beta_p R_i)^{-2} + \alpha_p \frac{z(H-z)}{H} \frac{WH}{WT} e^{\frac{-2\pi z}{WL}} (1+\beta_p R_i)^{-2} \quad (2.42)$$

where

$\eta_p, \beta_p, \alpha_p$	-	constants for a particular estuary

For the James River Estuary during the period of study (summer) the constants assumed the following values (19)

$$\eta_p = .00859$$
$$\beta_p = .276 \qquad (2.43)$$
$$\alpha_p = .00957$$

Pritchard when presenting these results states that the formulation has been applied only to long-term movements for the James River Estuary and therefore has questionable value when employed in short term time-varying situations or to other estuaries. However, lacking any better overall representation at this time, Pritchard's results will be used for the development of this model and the results interpreted accordingly.

In order to develop an estimate of how this formulation behaves under typical estuary conditions, a brief numerical experiment was conducted. Figures 2-3, 2-4 and 2-5 display the variations caused by wind for a constant density field. Increasing wave length and wave

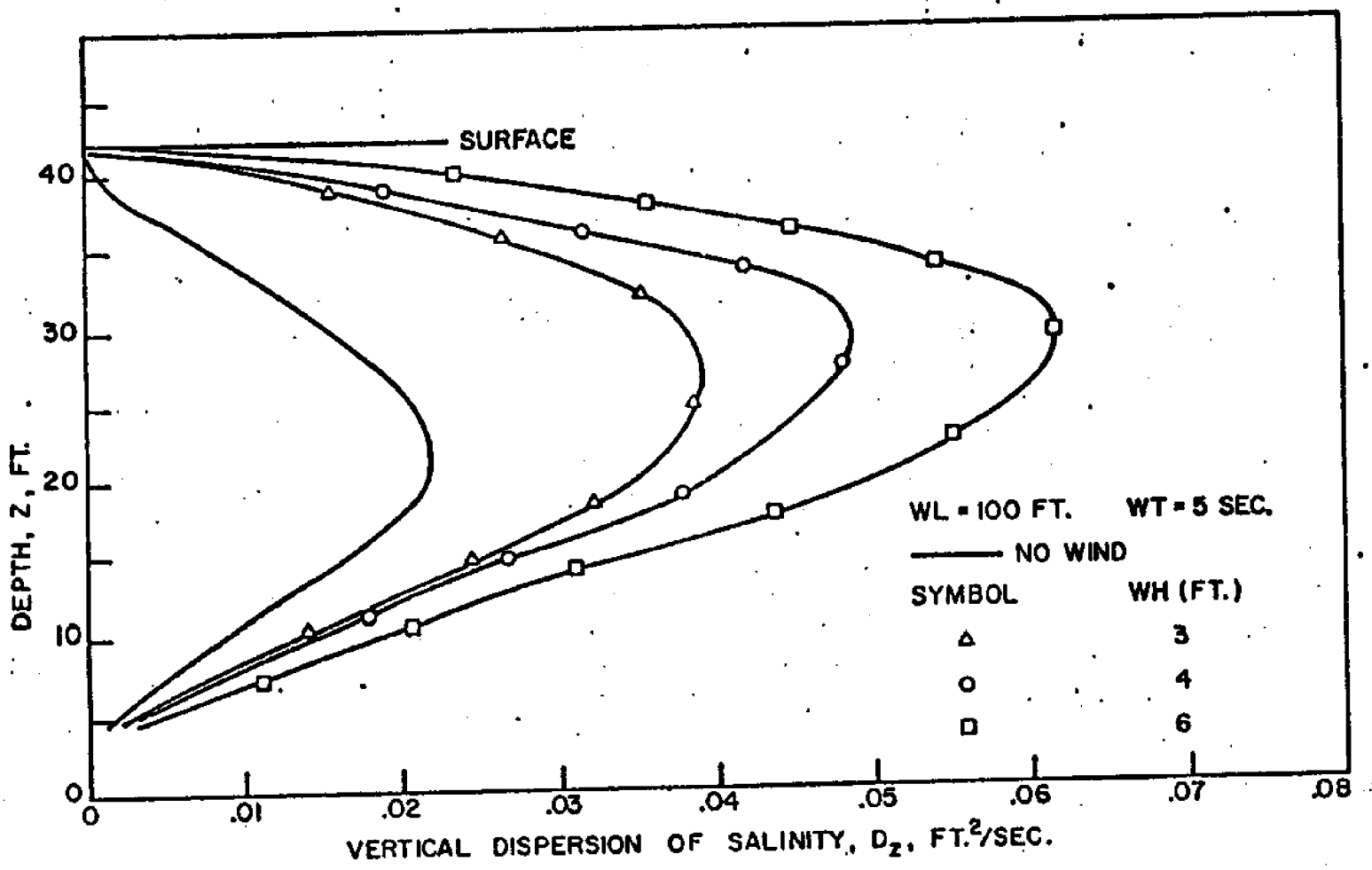

FIG. 2-3 EFFECT OF VARIATION IN WAVE PERIOD ON VERTICAL DISPERSION COEFFICIENT FOR A CONSTANT DENSITY PROFILE

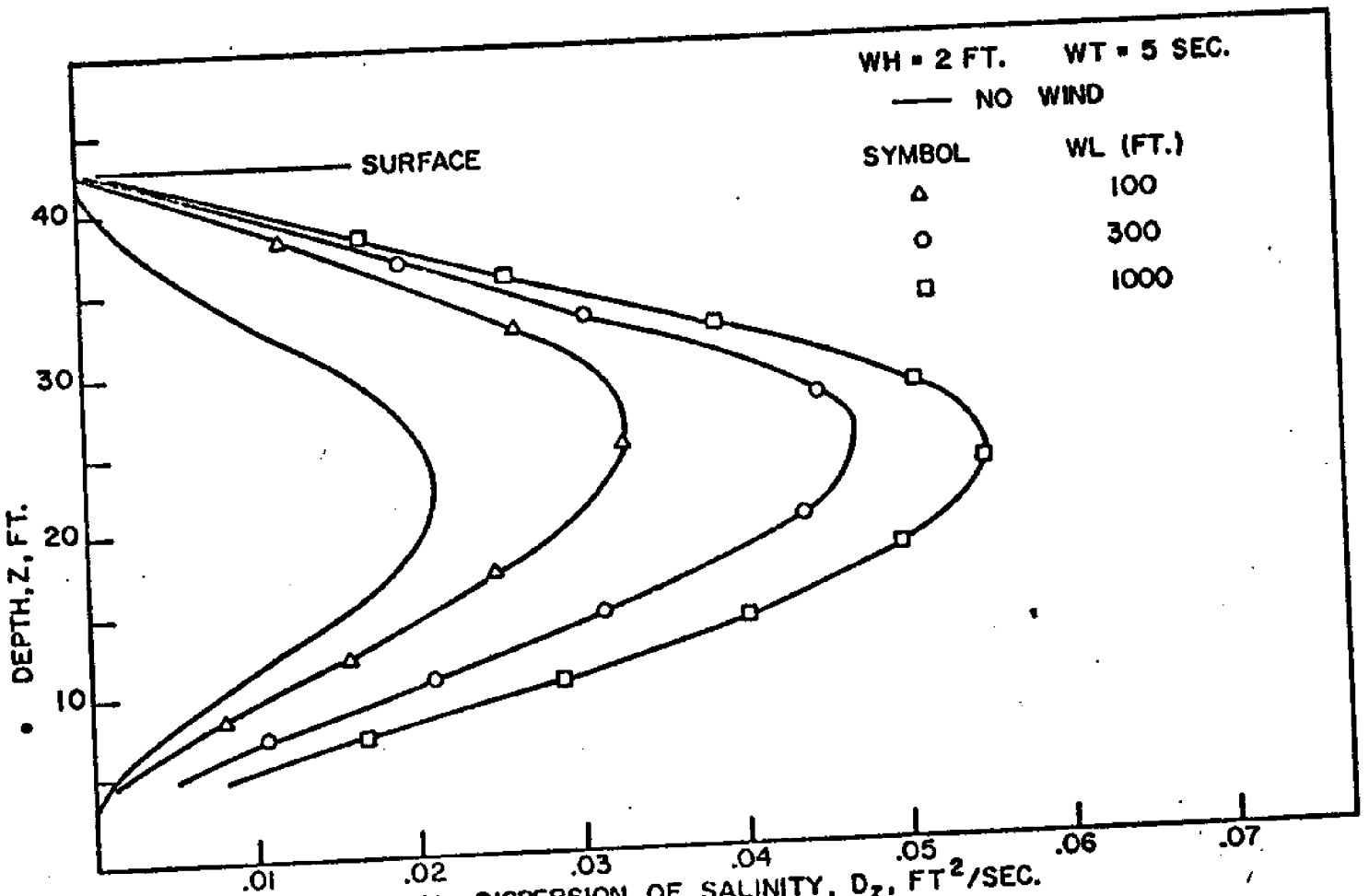

FIG. 2-4 EFFECT OF VARIATION IN WAVELENGTH ON VERTICAL DISPERSION COEFFICIENT FOR A CONSTANT DENSITY PROFILE

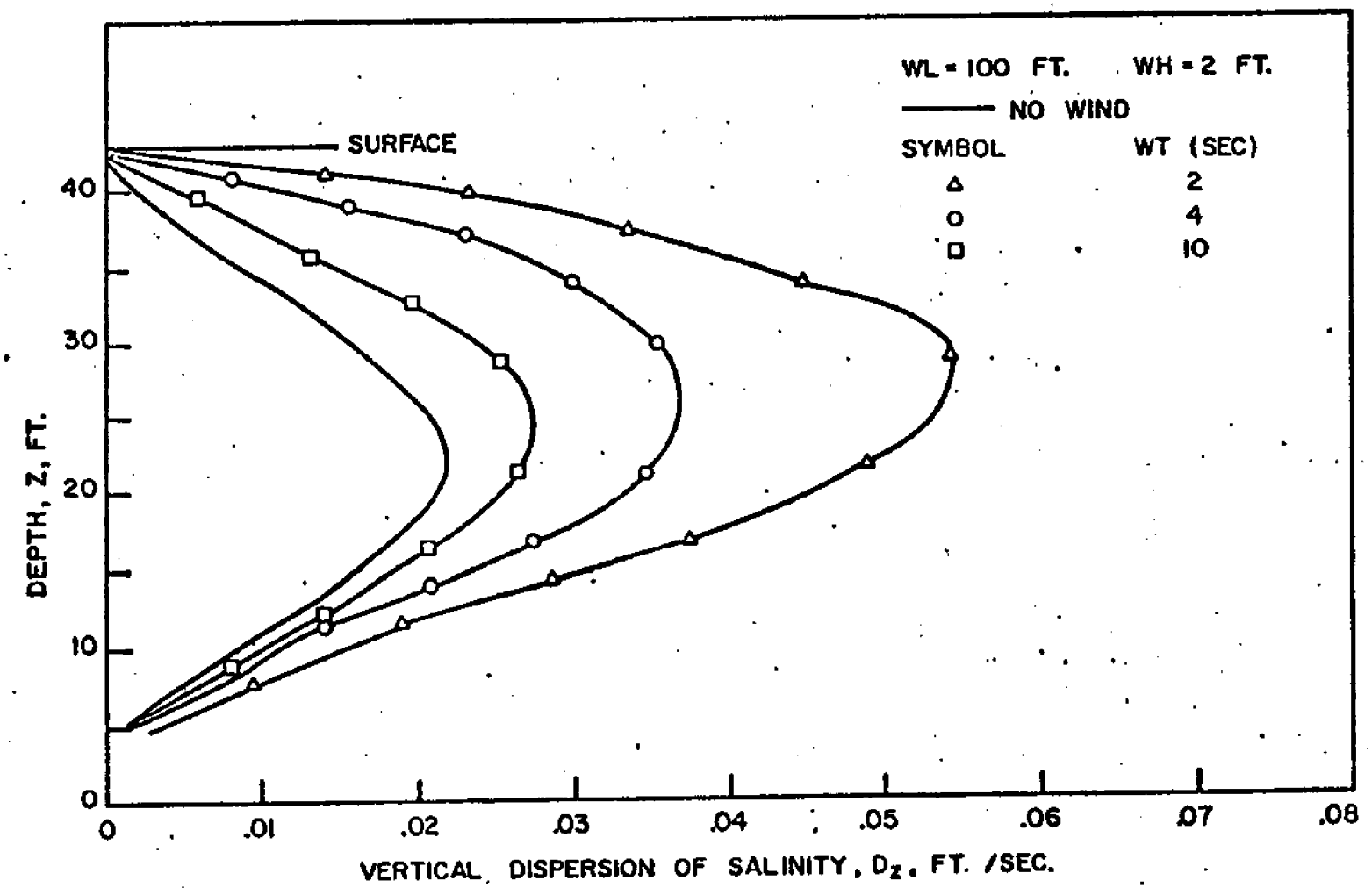

FIG. 2-5 EFFECT OF VARIATION IN WAVE HEIGHT ON VERTICAL DISPERSION COEFFICIENT FOR A CONSTNAT DENSITY PROFILE

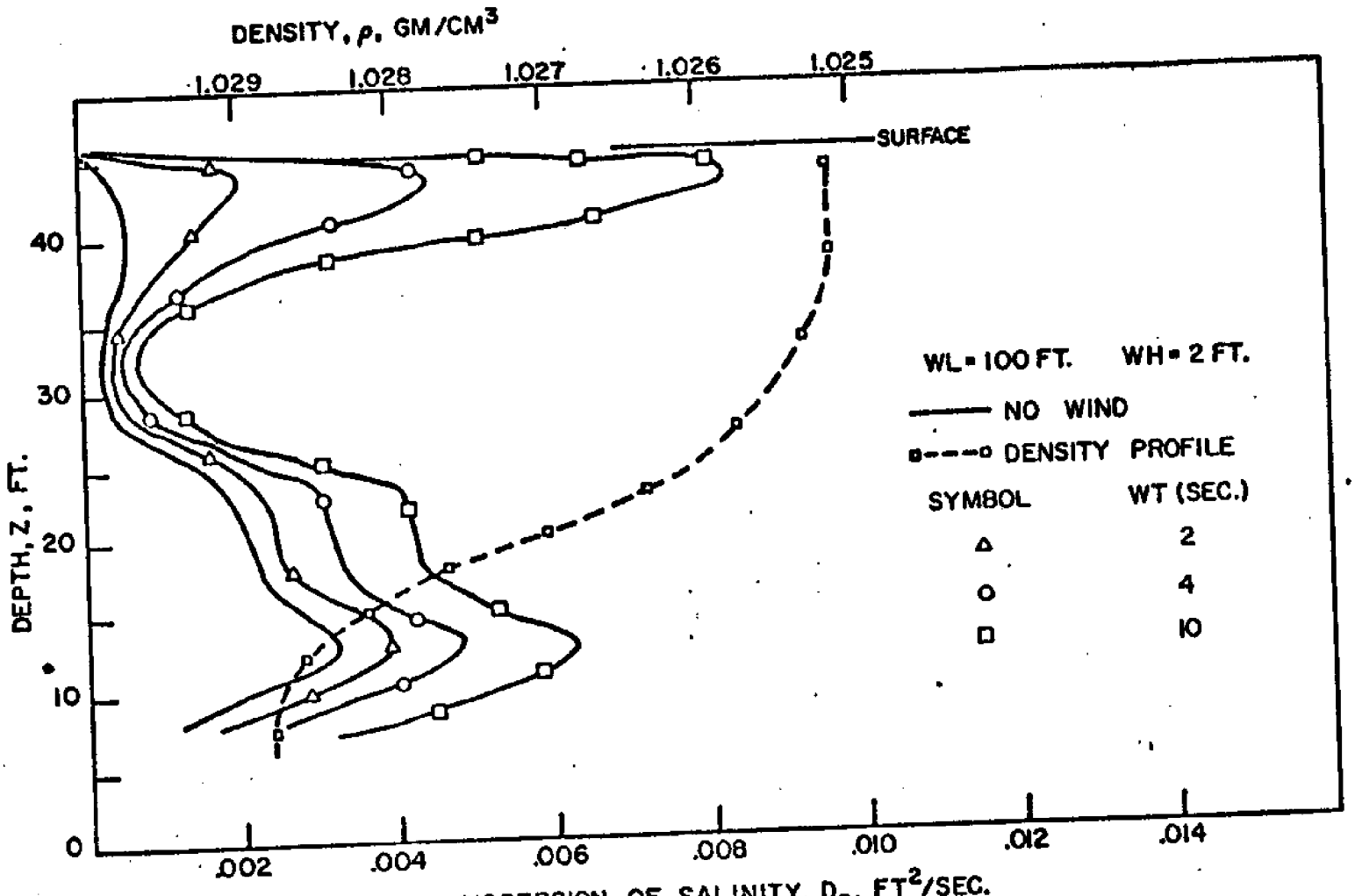

FIG. 2-6 EFFECT OF VARIATION IN WAVE PERIOD ON VERTICAL DISPERSION COEFFICIENT FOR A VARIABLE DENSITY PROFILE

height; and decreasing wave period cause increases in the vertical diffusivity. Figure 2-6 shows a vertical diffusivity profile for a variable density profile typical of stratified conditions. A series of profiles similar to those of Figs. 2-3 to 2-5 could have been displayed for the variable density profile but show no new results, and therefore have been omitted. An important point to notice in comparing the vertical dispersion values for a constant density profile and those for a variable density profile is the difference in their relative magnitudes. According to Pritchard's formulation the stratification profile inhibits vertical mixing and therefore sharply reduces the vertical dispersion.

Comparison of the longitudinal and vertical dispersion coefficients show that the former is always at least several orders of magnitude greater than the latter for estuarine environments. This fact complicates the modeling effort since dispersion becomes anisotropic, and the dispersive term of Eq. (2.27) should include cross product terms such as:

$$\frac{\partial \left[\left(D_{xx} \frac{\partial P}{\partial x} + D_{xz} \frac{\partial P}{\partial z}\right) B\right]}{\partial x} + \frac{\partial \left[\left(D_{zx} \frac{\partial P}{\partial z} + D_{zz} \frac{\partial P}{\partial x}\right) B\right]}{\partial z} \tag{2.44}$$

where the dispersion coefficients D_{xx}, D_{xz}, D_{zx} and D_{zz} are dependent on the current magnitude and direction. From a computational approach the use of Eq. (2.44) is very unwieldy, hence another method should be found.

Holley (22) made a comparison of the mass transport caused by longitudinal dispersion and advection.

$$R = \frac{BD_x \frac{\partial P}{\partial x}}{BuP} = \frac{D_x}{u} \frac{\partial \ln P}{\partial x} \tag{2.45}$$

By comparing these quantities, he found that the advective transport was much larger than that due to the dispersive mechanism, therefore, Holley concluded that except in regions of discharge of constituents where dispersive transports are large, the advective transport is most important.

Based on this argument it can be stated that the anisotropic dispersion effects may be replaced by an isotropic approximation in each direction, and that the

cross products of dispersion appearing in Eq. (2.44) can be assumed negligible. Also if it is further assumed that the lateral profile of the tidal velocity is approximately constant, then Eq. (2.28) can be used to represent the longitudinal dispersion since small variations in D_x caused by this approximation have little effect on the ratio of the dispersive transport to the advective transport. Numerical experiments on the model confirm this conclusion.

In the present model development a modified version of Eq. (2.28) has been used to represent the laterally-averaged dispersive coefficient and Eq. (2.42) employed for the laterally-averaged vertical dispersive coefficient. Another approach for obtaining these values is to use experimentally determined quantities, but this method is time consuming and expensive.

CHAPTER 3

COMPUTATIONAL MODEL

DERIVATION OF FINITE-DIFFERENCE EQUATION

The mass-transport equation as developed in Eq. (2.27) permits a large number of finite difference approximations. For each approach an analysis of the convergence, and stability characteristics has to be performed, such that some assurance is gained that the difference approximations will actually represent the solution to the proposed equation. Theoretical literature of the behavior of finite-difference approximations for parabolic equations such as the mass transport equation is extensive (23) however, few large computational models exist to serve as a guide in designing a good model, a notable exception is Leendertse's two-dimensional vertically-averaged models (6,24,25).

The computational model presented here for the transport model is based upon methods developed by Peaceman and Rachford (26) and Douglas and Gunn (27) and

is called an A.D.I. method standing for Alternating Direction Implicit.

Following work by Leendertse (6) a space staggered grid system is used to locate the discrete values of the variables. Figure 3-1 shows the location of the variables on the grid system. The values of tidal height ζ and mass concentration P are defined on integer values of M and N where M is the x directed index and N is the z directed index, while D_z, W and D_x, U are located at integer values of M and half integer values of N and integer values of N and half integer values of M respectively. The estuary width B and depth H are both defined at half integer values of M and N. With this staggering system a computational cell is then defined as noted in Fig. 3-1. For a typical cell then the variables are defined in blocks having sides between each integer values of M and the next half integer value and between integer values of N and the next half integer value.

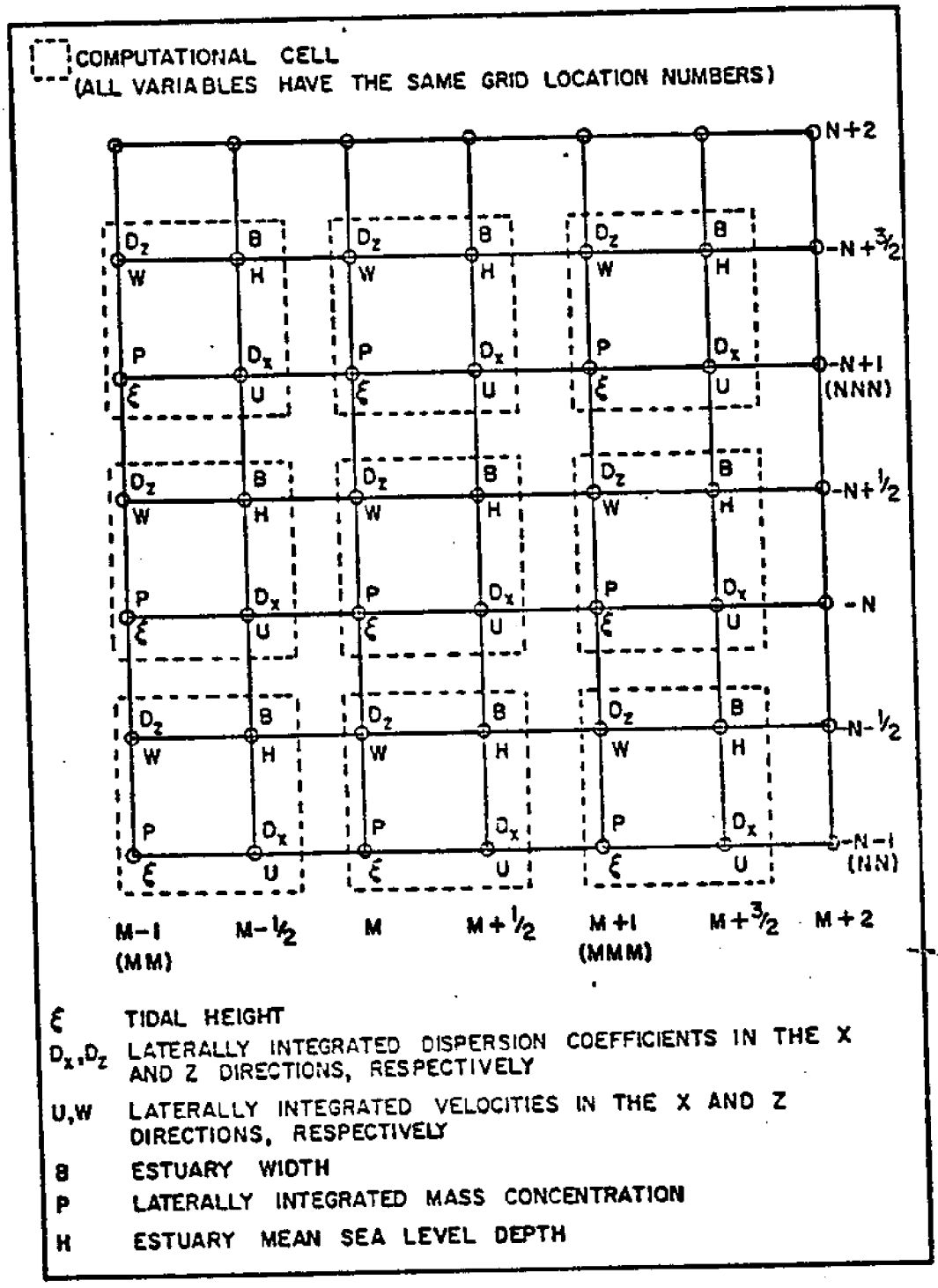

FIG. 3-1 LOCATION OF VARIABLES IN A STAGGERED GRID SYSTEM

The major advantage of this grid system formulation is that there exists a centrally located spatial derivative in time and space for the linear terms. More comments will be made on the advantages of the central location of these linear terms in Chapter 4 - Effects of Computational Model Approximation.

The laterally-averaged parabolic equation for the dimensional mass transport equation from Chapter 2 is

$$B\frac{\partial P}{\partial t} = \frac{\partial}{\partial x}\left(BD_x\frac{\partial P}{\partial x}\right) + \frac{\partial}{\partial z}\left(BD_z\frac{\partial P}{\partial z}\right) - \frac{\partial}{\partial x}(UBP) - \frac{\partial}{\partial z}(WBP) + BS \qquad (2.27)$$

where the variables have been previously defined. For the purposes of the derivation of the finite-difference equation it will be assumed that no generalized source or sink (BS term) terms are present. This approximation has no effect on the general finite-difference formulation for the mass-balance equation and therefore neglecting it should have no effect on the computational model for a conservative case. Indications for inclusion of the

reaction schemes will be outlined later in this chapter.

Using an approach presented by Mitchell (28) the finite-difference approximations to Eq. (2.27) will now be derived. If we rearrange Eq. (2.27) one can obtain:

$$\frac{\partial P}{\partial t} = \frac{1}{B} \left[\frac{\partial}{\partial x} \left(BD_x \frac{\partial P}{\partial x} \right) + \frac{\partial}{\partial z} \left(BD_z \frac{\partial P}{\partial z} \right) - \frac{\partial}{\partial x} (UBP) \right.$$

$$\left. - \frac{\partial}{\partial z} (WBP) \right] \qquad (3.1)$$

In general this can be represented in the form

$$\frac{\partial P}{\partial t} = \frac{1}{B_o} L_o \left\{ P \right\} \qquad (3.2)$$

where

B_o - some spatial or temporal averaging of the estuary width

L_o - linear operator defined as:

$$L_o \equiv D_1 (BD_x D_1) + D_2 (BD_z D_2) - D_1 UB - D_2 WB \qquad (3.3)$$

where $D_1 \equiv \partial/\partial x$ and $D_2 \equiv \partial/\partial z$

We can now let:

$$x = m\Delta x$$
$$z = n\Delta z \qquad (3.4)$$
$$t = \ell\,\Delta t$$

where

m,n,ℓ - are integers and

$\Delta x, \Delta z$ - are the spatial grid sizes

Δt - is the temporal grid spacing

Difference formulas involving two adjacent time levels and called two-level schemes are obtained employing a Taylor expansion. Expanding P(x,z,t) about zero gives:

$$P(x,z,t+\Delta t) = \left(1 + \Delta t \frac{\partial}{\partial t} + \frac{1}{2!}(\Delta t)^2 \frac{\partial^2}{\partial t^2} + \frac{1}{3!}\right. \qquad (3.5)$$

$$\left.(\Delta t)^3 \frac{\partial 3}{\partial t^3} + \ldots.\right) P(x,z,t)$$

and making use of:

$$e^x = 1 + x + \frac{x^2}{2} + \frac{x^3}{3!} + \ldots. \qquad (3.6)$$

then results in:

$$P\ (x,z,t+\Delta t) = \exp\ (\Delta t \frac{\partial}{\partial t})\ P\ (x,z,t) \qquad (3.7)$$

and using the following notation:

$$P(x,z,t) = P(m\Delta x,\ n\Delta z,\ \ell\Delta t) = P^{\ell}_{m,n} \qquad (3.8)$$

$$P(x,z,t+\Delta t) = P(m\Delta x,\ n\Delta z,\ (\ell+1)\Delta t) = P^{\ell+1}_{m,n} \qquad (3.9)$$

and after employing Eqs, (3.2), (3.7),(3.8) and (3.9) we find that:

$$P^{\ell+1}_{m,n} = \exp\ (\frac{\Delta t}{B_o}\ L_o)\ P^{\ell}_{m,n} \qquad (3.10)$$

Now, we need to incorporate several definitional relationships which will be useful before proceeding. An exact formula derived by Hildebrand (29) connecting D_1 and D_2, the exact formulae, to δ_x and δ_z, the central difference operators is:

$$D_1 = \frac{2}{\Delta x} \sinh^{-1} \frac{\delta_x}{2} = \frac{1}{\Delta x} \left[\delta_x - \frac{1^2}{2^2 3!} \delta_x^3 + \right.$$

$$\left. + \frac{1^2 3^2}{2^4 5!} \delta_x^5 + \ldots \right] \tag{3.11}$$

and:

$$D_2 = \frac{2}{\Delta z} \sinh^{-1} \frac{\delta_z}{2} = \frac{1}{\Delta z} \left[\delta_z - \frac{1^2}{2^2 3!} \delta_z^3 + \right.$$

$$\left. + \frac{1^2 3^2}{2^4 5!} \delta_z^5 + \ldots \right] \tag{3.12}$$

where:

$$\delta_x P^{\ell}_{m,n} = P^{\ell}_{m+1/2,n} - P^{\ell}_{m-1/2,n} \tag{3.13}$$

$$\delta_x^2 P^{\ell}_{m,n} = P^{\ell}_{m+1,n} - 2P^{\ell}_{m,n} + P^{\ell}_{m-1,n} \tag{3.14}$$

and similarily:

$$\delta_z P^{\ell}_{m,n} = P^{\ell}_{m,n+1/2} - P^{\ell}_{m,n-1/2} \tag{3.15}$$

$$\delta_z^2 P^{\ell}_{m,n} = P^{\ell}_{m,n+1} - 2P^{\ell}_{m,n} + P^{\ell}_{m,n-1} \tag{3.16}$$

With these definitions complete we may proceed with the remainder of the derivation.

Separating the exponential term in Eq. (3.10) gives:

$$\exp\left[\left(-\frac{1}{2}\,\frac{\Delta t}{B_o}\,L_o\right)\right] P_{m,n}^{\ell+1} = \exp\left[\left(\frac{1}{2}\,\frac{\Delta t}{B_o}\,L_o\right)\right] P_{m,n}^{\ell} \tag{3.17}$$

Now substituting for the linear operator, L_o from Eq. (3.3) into Eq. (3.17) gives:

$$\exp\left[-\frac{\Delta t}{2B_o}\left\{D_1(BD_xD_1) + D_2(BD_zD_2) - D_1UB - D_2WB\right\}\right] P_{m,n}^{\ell+1} = \exp\left[\frac{\Delta t}{2B_o}\left\{D_1(BD_xD_1) + D_2(BD_zD_2) - D_1UB - D_2WB\right\}\right] P_{m,n}^{\ell} \tag{3.18}$$

Expanding Eq. (3.18) substituting Eqs. (3.11) and (3.12) to the first order in δ_x and δ_z, respectively, and combining constants as in Eq. (3.19)

$$\begin{aligned} r_1 &= \frac{\Delta t}{\Delta x} \\ r_2 &= \frac{\Delta t}{\Delta z} \\ r_{11} &\equiv \frac{\Delta t}{(\Delta x)^2} = \frac{r_1}{\Delta x} \\ r_{22} &\equiv \frac{\Delta t}{(\Delta z)^2} = \frac{r_2}{\Delta z} \end{aligned} \tag{3.19}$$

gives:

$$\left[1 - \frac{r_{11}}{2B_o} \delta_x (BD_x \delta_x) \right] \left[1 - \frac{r_{22}}{2B_o} \delta_z (BD_z \delta_z) \right]$$

$$\left[1 + \frac{r_1}{2B_o} \delta_x (UB) \right] \left[1 + \frac{r_2}{2B_o} \delta_z (WB) \right] P_{m,n}^{\ell+1} =$$

$$\left[1 + \frac{r_{11}}{2B_o} \delta_x (BD_x \delta_x) \right] \left[1 + \frac{r_{22}}{2B_o} \delta_z (BD_z \delta_z) \right]$$

$$\left[1 - \frac{r_1}{2B_o} \delta_x (UB) \right] \left[1 - \frac{r_2}{2B_o} \delta_z (WB) \right] P_{m,n}^{\ell} \qquad (3.20)$$

Making use of a Peaceman-Rachford splitting technique, a finite-difference approximation for the first half and second half of the time step is presented. The notation $P_{m,n}^{\ell+1/2}$ indicates the laterally-averaged mass density at the end of the first-half time step, and $P_{m,n}^{\ell+1}$ indicates the laterally-averaged mass density at the end of the second-half time step or the end of the

first whole time step. Further information on how these splitting techniques work can be obtained from any of the finite difference references on the A.D.I. methods (26,27,28). For the first half time step, going from time level ℓ to $\ell + \frac{1}{2}$:

$$\left[1 - \frac{r_{11}}{2B_o} \delta_x (BD_x \delta_x) \right] \left[1 + \frac{r_1}{2B_o} \delta_x (UB) \right] P_{m,n}^{\ell + \frac{1}{2}}$$

$$= \left[1 + \frac{r_{22}}{2B_o} \delta_z (BD_z \delta_z) \right] \left[1 - \frac{r_2}{2B_o} \delta_z (WB) \right] P_{m,n}^{\ell} \qquad (3.21)$$

and for the second half time step proceeding from time level $\ell + \frac{1}{2}$ to $\ell + 1$.

$$\left[1 - \frac{r_{22}}{2B_o} \delta_z (BD_z \delta_z) \right] \left[1 + \frac{r_2}{2B_o} \delta_z (WB) \right] P_{m,n}^{\ell + 1}$$

$$= \left[1 + \frac{r_{11}}{2B_o} \delta_x (BD_x \delta_x) \right] \left[1 - \frac{r_1}{2B_o} \delta_x (UB) \right] P_{m,n}^{\ell + \frac{1}{2}} \qquad (3.22)$$

Equations (3.21) and (3.22) form the fundamental basis for the dimensional vertical axis computational model. Other splitting techniques are available as noted by Mitchell (28) but will not be considered here.

Equations (3.21) and (3.22) need to be expanded to present the finite-difference approximations in a more useable form. Multiplying the terms in Eqs. (3.21) and (3.22) and neglecting terms of order:

$$\frac{r_1 r_{11}}{4B_o} \delta_x (BD_x \delta_x) \delta_x (UB) \tag{3.23}$$

and:

$$\frac{r_2 r_{22}}{4B_o} \delta_z (BD_z \delta_z) \delta_z (WB) \tag{3.24}$$

while replacing the notation δ_x and δ_z by their appropriate values as defined in Eqs. (3.13) and (3.15), respectively, results in the following for the first half of the time step, from time level ℓ to time level $\ell + 1/2$:

$$B_o P^{\ell+1/2}_{m,n} - \frac{r_{11}}{2} B_{m+1/2,n} Dx^{\ell+1/2}_{m+1/2,n} (P^{\ell+1/2}_{m+1,n} - P^{\ell+1/2}_{m,n})$$

$$+ \frac{r_{11}}{2} B_{m-1/2,n} Dx^{\ell+1/2}_{m-1/2,n} (P^{\ell+1/2}_{m,n} - P^{\ell+1/2}_{m-1,n}) + \frac{r_1}{2} U^{\ell+1/2}_{m+1/2,n}$$

$$B_{m+1/2,n} P^{\ell+1/2}_{m+1/2,n} - \frac{r_1}{2} U^{\ell+1/2}_{m-1/2,n} B_{m-1/2,n} P^{\ell+1/2}_{m-1/2,n} =$$

$$B_o P^{\ell}_{m,n} + \frac{r_{22}}{2} B_{m,n+1/2} Dz^{\ell}_{m,n+1/2} (P^{\ell}_{m,n+1} - P^{\ell}_{m,n})$$

$$- \frac{r_{22}}{2} B_{m,n-1/2} Dz^{\ell}_{m,n-1/2} (P^{\ell}_{m,n} - P^{\ell}_{m,n-1}) -$$

$$\frac{r_2}{2} W^{\ell}_{m,n+1/2} B_{m,n+1/2} P^{\ell}_{m,n+1/2} + \frac{r_2}{2} W^{\ell}_{m,n-1/2} B_{m,n-1/2} P^{\ell}_{m,n-1/2}$$

(3.25)

and for the second half of the time step from time level $\ell + 1/2$ to time level $\ell + 1$:

$$B_o P^{\ell+1}_{m,n} - \frac{r_{22}}{2} B_{m,n+1/2} D_{z}{}^{\ell+1}_{m,n+1/2} (P^{\ell+1}_{m,n+1} - P^{\ell+1}_{m,n})$$

$$+ \frac{r_{22}}{2} B_{m,n-1/2} D_{z}{}^{\ell+1}_{m,n-1/2} (P^{\ell+1}_{m,n} - P^{\ell+1}_{m,n-1})$$

$$+ \frac{r_2}{2} W^{\ell+1}_{m,n+1/2} B_{m,n+1/2} P^{\ell+1}_{m,n+1/2} - \frac{r_2}{2} W^{\ell+1}_{m,n-1/2} B_{m,n-1/2} P^{\ell+1}_{m,n-1/2} =$$

$$B_o P^{\ell+1/2}_{m,n} + \frac{r_{11}}{2} B_{m+1/2,n} D_{x}{}^{\ell+1/2}_{m+1/2,n} (P^{\ell+1/2}_{m+1,n} - P^{\ell+1/2}_{m,n})$$

$$- \frac{r_{11}}{2} B_{m-1/2,n} D_{x}{}^{\ell+1/2}_{m-1/2,n} (P^{\ell+1/2}_{m,n} - P^{\ell+1/2}_{m-1,n}) -$$

$$\frac{r_1}{2} U^{\ell+1/2}_{m+1/2,n} B_{m+1/2,n} P^{\ell+1/2}_{m+1/2,n} +$$

$$\frac{r_1}{2} U^{\ell+1/2}_{m-1/2,n} B_{m-1/2,n} P^{\ell+1/2}_{m-1/2,n}$$

(3.26)

Close observation of Eqs. (3.25) and (3.26) reveals that all the variables presented do not conform to the space-staggered grid system of Fig. 3-1, in particular the mass densities in the convective term and the estuary widths in all terms. To force these variables to conform to this grid system and at the same time maintaining a spatially-centered convective term which is important for stability considerations, as will be seen, the following changes have been employed:

$$B_{m,n+1/2} \longrightarrow (B_{m+1/2,n+1/2}+B_{m-1/2,n+1/2})\ \frac{1}{2} \tag{3.27}$$

$$B_{m,n-1/2} \longrightarrow (B_{m+1/2,n-1/2}+B_{m-1/2,n-1/2})\ \frac{1}{2} \tag{3.28}$$

$$B_{m+1/2,n} \longrightarrow (B_{m+1/2,n+1/2}+B_{m+1/2,n-1/2})\ \frac{1}{2} \tag{3.29}$$

$$B_{m-1/2,\ n} \longrightarrow (B_{m-1/2,n+1/2} + B_{m-1/2,n-1/2})\ \frac{1}{2} \tag{3.30}$$

$$B_{o} \longrightarrow (B_{m-1/2,n+1/2} + B_{m-1/2,n-1/2} + B_{m+1/2,n-1/2} + B_{m+1/2,n+1/2})\ \frac{1}{4} \tag{3.31}$$

$$P_{m+1/2,n} \longrightarrow P_{m,n} \tag{3.32}$$

$$P_{m-1/2,n} \longrightarrow P_{m-1,n} \tag{3.33}$$

$$P_{m,n+1/2} \longrightarrow P_{m,n} \tag{3.34}$$

$$P_{m,n-1/2} \longrightarrow P_{m,n-1} \tag{3.35}$$

Since substitution of Eqs. (3.27) through (3.35) into Eqs. (3.25) and (3.26) becomes a tedious exercise in writing and prone to error, a notational scheme will be developed in the next paragraph so as to present the difference equations in an abbreviated and physically intuitive form.

The following notation, as presented by Leenderste (6) is used as an approximation of the differential equation by a system of difference equations.

$$F(m\,\Delta x,\ n\,\Delta z,\ \ell\,\Delta t)$$

where

$$(x,z,t) = (m\,\Delta x,\ n\,\Delta z,\ \ell\,\Delta t)$$

and

$$m,n,\ell = 0,\ \pm\ \frac{1}{2}\ ,\ \pm\ 1,\ \pm\ \frac{3}{2}$$

The symbols used for differencing and averaging are listed below. Only equations for x are shown but similar results for z and t are also valid.

$$\bar{F}^{x} = \frac{1}{2}\left\{F\ [\ (m+\tfrac{1}{2})\,\Delta x,\ n\,\Delta z,\ \ell\,\Delta t] + F[\ (m-\tfrac{1}{2})\,\Delta x,\ n\,\Delta z,\ \ell\,\Delta t]\right\} \tag{3.36}$$

$$\delta_x F = \frac{1}{\Delta x}\left\{F\left[\left(m+\frac{1}{2}\right)\Delta x,\ n\Delta z,\ \ell\Delta t\right] - F\left[\left(m-\frac{1}{2}\right)\Delta x,\ n\Delta z,\ \ell\Delta t\right]\right\} \tag{3.37}$$

$$F = \frac{1}{4}\left\{F\left[\left(m+\frac{1}{2}\right)\Delta x,\ \left(n+\frac{1}{2}\right)\Delta z,\ \ell\Delta t\right] +\right.$$

$$+ F\left[\left(m+\frac{1}{2}\right)\Delta x,\ \left(n-\frac{1}{2}\right)\Delta z,\ \ell\Delta t\right] +$$

$$+ F\left[\left(m-\frac{1}{2}\right)\Delta x,\ \left(n+\frac{1}{2}\right)\Delta z,\ \ell\Delta t\right] +$$

$$\left. + F\left[\left(m-\frac{1}{2}\right)\Delta x,\ \left(n-\frac{1}{2}\right)\Delta z,\ \ell\Delta t\right]\right\} \tag{3.38}$$

A special notation used to indicate a shifted time level is:

$$\delta_{+\frac{1}{2}t} F = \frac{2}{\Delta t}\left\{F\left[m\Delta x,\ n\Delta z,\ \left(\ell+\frac{1}{2}\right)\Delta t\right]\right.$$

$$\left. - F\left[m\Delta x,\ n\Delta z,\ \ell\Delta t\right]\right\} \tag{3.39}$$

$$F_+ = F\left[m\Delta x,\ n\Delta z,\ \left(\ell+\frac{1}{2}\right)\Delta t\right] \tag{3.40}$$

The set of difference equations will now be presented in order of their use and employing the notation of Eqs. (3.36), (3.37), (3.38), (3.39) and (3.40). For the first half time step, going from time level ℓ to time level $\ell + \frac{1}{2}$.

$$\delta_{+\frac{1}{2}t} [P\bar{\bar{B}}] + \delta_x [\bar{B}^z U_+ \overset{-x}{P_+}] + \delta_z [\bar{B}^x W \bar{P}^z]$$

$$- \delta_x [\bar{B}^z D_{x_+} \delta_x P_+] - \delta_z [\bar{B}^x D_z \delta_z P] + S\bar{\bar{B}} = 0 \qquad (3.41)$$

(at point (m,n,ℓ))

For the second half of the time step, going from time level $\ell + \frac{1}{2}$ to time level $\ell + 1$:

$$\delta_{+\frac{1}{2}t} [P \bar{\bar{B}}] + \delta_x [\bar{B}^z U \bar{P}^x] + \delta_z [\bar{B}^x W_+ \bar{P}^z_+]$$

$$- \delta_x [\bar{B}^z D_x \delta_x P] - \delta_z [\bar{B}^x D_{z_+} \delta_z P_+] + \bar{\bar{B}} S = 0$$

(3.42)

(at point $(m,n,\ell+\frac{1}{2})$)

In many estuaries the use of a dimensional model as just derived limits the definition of the vertical structure in the regions in which that structure is most important - shallow areas near the head of the tide, and also fails to account for tidal height variations. To circumvent this problem and also eliminate many troublesome boundary conditions at the estuary bottom, the non-dimensional z, (vertical) axis model of the mass-transport equation will be outlined in the following paragraphs. The derivation of the finite-difference approximations is analogous to that just obtained for the dimensional z axis model and therefore will not be repeated, only the final difference approximation being shown.

Using the depth of the estuary, mean sea level depth plus instantaneous tidal height, the z axis of the mass-transport equation given by Eq. (2.27) can be nondimensionalized and a dimensionless z axis laterally-averaged mass-transport equation found to be:

$$B \quad \frac{\partial HP}{\delta t} + \frac{\delta}{\delta x}(H_\tau UBP) + \frac{\partial}{\partial \eta}(W_\eta BP) - \frac{\delta}{\delta x}(H_\tau BD_x \frac{\delta P}{\delta x})$$

$$- \frac{\partial}{\partial \eta}\left(\frac{BD_z}{H_\tau} \frac{\partial P}{\partial \eta}\right) + BH_\tau S = 0 \qquad (2.27a)$$

where

H_τ - estuary depth mean sea level depth plus tidal height, $(H + \xi)$

$\eta = z/H$

$W = W_\eta + \eta \frac{\delta H}{\delta t} + u\eta \frac{\delta H}{\delta x}$

W_η - product of the dimension less vertical velocity (ω) and depth (H) or ωH

$\frac{\delta}{\delta t}$, $\frac{\delta}{\delta x}$ - derivatives of time and space in the (x, η, t) coordinate system.

and other variables remain as previously defined. Higher order expressions resulting from the transformation of the dispersion terms, order $\frac{\delta}{\delta x}\left(\frac{\delta H}{\delta x} D_x B \frac{\partial P}{\partial \eta}\right)$, have been neglected based on a comparison of the relative importance of the dispersion and advection processes (22).

In finite-difference approximation and using the notational scheme as outlined in Eqs. (3.36) through (3.40) results in:

For the first half time step from time level ℓ to time level $\ell + \frac{1}{2}$

$$\delta_{+\frac{1}{2}t}\left[P\,(\bar{\bar{B}})\,(\bar{\bar{H}} + \xi)\right] + \delta_x\left[(\bar{H}^z + \bar{\xi}^x)\, U_+\, \bar{P}^x{}_+\, \bar{B}^z\right]$$

$$+ \delta_\eta[\bar{P}^z W_\eta \bar{B}^x] - \delta_x [(\bar{H}^z + \bar{\xi}^x_+) D_{x_+} \bar{B}^z \delta_x P_+]$$

$$- \delta_\eta[\frac{D_z \bar{B}^x}{(\bar{H} + \xi)} \delta_\eta P] + \bar{\bar{B}} (\bar{\bar{H}} + \xi) S = 0 \qquad (3.41a)$$

For the second half time step from time level $\ell + \frac{1}{2}$ to $\ell + 1$:

$$\delta_+ \frac{1}{2} t [P (\bar{\bar{B}}) (\bar{\bar{H}} + \xi)] + \delta_x [\bar{H}^z + \bar{\xi}^x) \bar{B}^z UP^x]$$

$$+ \delta_\eta [\bar{B}^x W_{+_\eta} \bar{P}^z_+] - \delta_x [(\bar{H}^z + \bar{\xi}^x) \bar{B}^z D_x \delta_x P]$$

$$- \delta_\eta [\frac{D_z + \bar{B}^x}{(\bar{H}^x + \xi_+)} \delta_\eta P_+] + \bar{\bar{B}} (\bar{\bar{H}} + \xi) S = 0 \qquad (3.42a)$$

In the discussion following, the dimensional difference equations will be used as the model to present the solution algorithms but a similar approach can also be employed for the dimensionless z axis model and therefore no difficulty should be encountered.

SOLUTION ALGORITHM

In solving A.D.I. type problems the approach is to solve Eq. (3.41) or (3.41a) in the x direction or on a given column N from time level ℓ to $\ell+\frac{1}{2}$ and then with these results for mass density to solve Eq. (3.42) or (3.42a) in the z direction or along a given row M from time level $\ell+\frac{1}{2}$ to $\ell+1$. In order to understand clearly how this approach is employed Eqs. (3.41) and (3.42) will be expanded and the positions of their terms in the staggered grid system noted.

Using the notational definitions from Eqs. (3.36), (3.37), (3.38), (3.39) and (3.40) and expanding Eq. (3.41) results in:

For the first half time step from time level ℓ to time level $\ell+1/2$.

$$\frac{2}{\Delta t}\left(\frac{B_{m+1/2,n+1/2}+B_{m+1/2,n-1/2}+B_{m-1/2,n+1/2}+B_{m-1/2,n-1/2}}{4}\right)P^{\ell+1/2}_{m,n}$$

$$-\frac{2}{\Delta t}\left(\frac{B_{m+1/2,n+1/2}+B_{m+1/2,n-1/2}+B_{m-1/2,n+1/2}+B_{m-1/2,n-1/2}}{4}\right)P^{\ell}_{m,n}$$

$$+\frac{1}{4\,\Delta x}\left(B_{m+1/2,n+1/2}+B_{m+1/2,n-1/2}\right)U^{\ell+1/2}_{m+1/2,n}P^{\ell+1/2}_{m+1,\,n}+$$

$$\frac{1}{4\,\Delta x}\left(B_{m+1/2,n+1/2}+B_{m+1/2,n-1/2}\right)U^{\ell+1/2}_{m+1/2,n}P^{\ell+1/2}_{m,n}$$

$$-\frac{1}{4\,\Delta x}\left(B_{m-1/2,n+1/2}+B_{m-1/2,n-1/2}\right)U^{\ell+1/2}_{m-1/2,n}P^{\ell+1/2}_{m,n}$$

$$-\frac{1}{4\,\Delta x}\left(B_{m-1/2,n+1/2}+B_{m-1/2,n-1/2}\right)U^{\ell+1/2}_{m-1/2,n}P^{\ell+1/2}_{m-1,n}$$

$$+\frac{1}{4\,\Delta z}\left(B_{m+1/2,n+1/2}+B_{m-1/2,n+1/2}\right)W^{\ell}_{m,n+1/2}P^{\ell}_{m,n+1}$$

$$+\frac{1}{4\,\Delta z}\left(B_{m+1/2,n+1/2}+B_{m-1/2,n+1/2}\right)W^{\ell}_{m,n+1/2}P^{\ell}_{m,n}$$

$$-\frac{1}{4\,\Delta z}\left(B_{m+1/2,n-1/2}+B_{m-1/2,n-1/2}\right)W^{\ell}_{m,n-1/2}P^{\ell}_{m,n}$$

$$-\frac{1}{4\,\Delta z}\left(B_{m+1/2,n-1/2}+B_{m-1/2,n-1/2}\right)W^{\ell}_{m,n-1/2}P^{\ell}_{m,n-1}$$

$$-\frac{1}{2(\Delta x)^2}\left[\left(B_{m+1/2,n+1/2}+B_{m+1/2,n-1/2}\right)D_{x}{}^{\ell+1/2}_{m+1/2,n}P^{\ell+1/2}_{m+1,n}\right]$$

$$+\frac{1}{2(\Delta x)^2}\left[B_{m+1/2,n+1/2}+B_{m+1/2,n-1/2}\right)D_{x}{}^{\ell+1/2}_{m+1/2,n}P^{\ell+1/2}_{m,n}\right]$$

$$+\frac{1}{2(\Delta x)^2}\left[B_{m-1/2,n+1/2}+B_{m-1/2,n-1/2}\right) D_{x_{m-1/2,n}}^{\ell+1/2} P_{m,n}^{\ell+1/2}]$$

$$-\frac{1}{2(\Delta x)^2}\left[B_{m-1/2,n+1/2}+B_{m-1/2,n-1/2}\right) D_{x_{m-1/2,n}}^{\ell+1/2} P_{m-1,n}^{\ell+1/2}]$$

$$-\frac{1}{2(\Delta z)^2}\left[(B_{m+1/2,n+1/2}+B_{m-1/2,n+1/2}\right) D_{z_{m,n+1/2}}^{\ell} P_{m,n+1}^{\ell}]$$

$$+\frac{1}{2(\Delta z)^2}\left[B_{m+1/2,n-1/2}+B_{m-1/2,n-1/2}\right) D_{z_{m,n-1/2}}^{\ell} P_{m,n}^{\ell}]$$

$$+\frac{1}{2(\Delta z)^2}\left[(B_{m+1/2,n+1/2}+B_{m-1/2,n+1/2}\right) D_{z_{m,n+1/2}}^{\ell} P_{m,n}^{\ell}]$$

$$-\frac{1}{2(\Delta z)^2}\left[B_{m+1/2,n-1/2}+B_{m-1/2,n-1/2}\right) D_{z_{m,n-1/2}}^{\ell} P_{m,n-1}^{\ell}]$$

$$+\frac{1}{4}\left(B_{m+1/2,n+1/2}+B_{m-1/2,n-1/2}+B_{m+1/2,n-1/2}+B_{m-1/2,n+1/2}\right) S \qquad (3.43)$$

Similarly expanding Eq. (3.42) but combining terms with similar coefficients for writing convenience:

For the second half time step from time level $\ell + 1/2$ to time level $\ell + 1$:

$$\frac{2}{\Delta t}[(\frac{B_{m+1/2,n+1/2}+B_{m+1/2,n-1/2}+B_{m-1/2,n+1/2}+B_{m-1/2,n-1/2}}{4}) (P_{m,n}^{\ell+1}-P_{m,}^{\ell+}$$

$$+\frac{1}{4\Delta x}\left[\left(B_{m+1/2,n+1/2}+B_{m+1/2,n-1/2}\right) U_{m+1/2,n}^{\ell+1/2}\left(P_{m+1,n}^{\ell+1/2}+P_{m,n}^{\ell+1/2}\right)\right.$$

$$- \frac{1}{4\Delta x}\left[B_{m-1/2,n+1/2}+B_{m-1/2,n-1/2}\right) U^{\ell+1/2}_{m-1/2,n}\left(P^{\ell+1/2}_{m,n}+P^{\ell+1/2}_{m-1,n}\right)$$

$$+ \frac{1}{4\Delta z}\left[\left(B_{m+1/2,n+1/2}+B_{m-1/2,n+1/2}\right) W^{\ell+1}_{m,n+1/2}\left(P^{\ell+1}_{m,n+1}+P^{\ell+1}_{m,n}\right)\right.$$

$$- \frac{1}{4\Delta z}\left[\left(B_{m+1/2,n-1/2}+B_{m-1/2,n-1/2}\right) W^{\ell+1}_{m,n-1/2}\left(P^{\ell+1}_{m,n}+P^{\ell+1}_{m,n-1}\right)\right.$$

$$- \frac{1}{2(\Delta x)^2}\left[\left(B_{m+1/2,n+1/2}+B_{m+1/2,n-1/2}\right) D_{x}{}^{\ell+1/2}_{m+1/2,n}\left(P^{\ell+1/2}_{m+1,n}-P^{\ell+1/2}_{m,n}\right)\right.$$

$$+ \frac{1}{2(\Delta x)^2}\left[B_{m-1/2,n+1/2}+B_{m-1/2,n-1/2}\right) D_{x}{}^{\ell+1/2}_{m-1/2,n}\left(P^{\ell+1/2}_{m,n}-P^{\ell+1/2}_{m-1,n}\right)$$

$$- \frac{1}{2(\Delta z)^2}\left[\left(B_{m+1/2,n+1/2}+B_{m-1/2,n+1/2}\right) D_{z}{}^{\ell+1}_{m,n+1/2}\left(P^{\ell+1}_{m,n+1}-P^{\ell+1}_{m,n}\right)\right.$$

$$+ \frac{1}{2(\Delta z)^2}\left[\left(B_{m+1/2,n-1/2}+B_{m-1/2,n-1/2}\right) D_{z}{}^{\ell+1}_{m,n-1/2}\left(P^{\ell+1}_{m,n}-P^{\ell+1}_{m,n-1}\right)\right.$$

$$+ \frac{1}{4}\left(B_{m+1/2,n+1/2}+B_{m+1/2,n-1/2}+B_{m-1/2,n-1/2}+B_{m-1/2,n+1/2}\right) S \qquad (3.44)$$

A close examination of Eq. (3.43) shows that it can be written in the form

$$a_m P^{\ell+1/2}_{m-1,n} + b_m P^{\ell+1/2}_{m,n} + c_m P^{\ell+1/2}_{m+1,n} = d_m \tag{3.45}$$

This can be accomplished by multiplying Eq. (3.43) by $\tau = \Delta t/2$ and collecting similar type terms. It is to be noted that this equation involves only grid points on a given column N. The values of a_m, b_m, c_m and d_m are then given by:

$$a_m = -\frac{\tau}{4\Delta x}(B1)U^{\ell+1/2}_{m-1/2,n} - \frac{\tau}{2(\Delta x)^2}(B1)\, D_x{}^{\ell+1/2}_{m-1/2,n} \tag{3.46}$$

$$b_m = BO - \frac{\tau}{4\Delta x}(B1)\, U^{\ell+1/2}_{m-1/2,n} + \frac{\tau}{4\Delta x}(B2)\, U^{\ell+1/2}_{m+1/2,n}$$

$$+ \frac{\tau}{2(\Delta x)^2}(B2)\, D_x{}^{\ell+1/2}_{m+1/2,n} + \frac{\tau}{2(\Delta x)^2}(B1)\, D_x{}^{\ell+1/2}_{m-1/2,n} \tag{3.47}$$

$$c_m = \frac{-\tau}{2(\Delta x)^2}(B2)\, D_x{}^{\ell+1/2}_{m+1/2,n} + \frac{\tau}{4\Delta x}(B2)\, U^{\ell+1/2}_{m+1/2,n}$$

and

$$d_m = P_{m,n}\ (B0) - \frac{\tau}{4\,\Delta z}\ (B4)\ W^{\ell}_{m,n+1/2}\,(P^{\ell}_{m,n} + P^{\ell}_{m,n+1})$$

$$+ \frac{\tau}{4\,\Delta z}\ (B3)\ W^{\ell}_{m,n-1/2}\ (P^{\ell}_{m,n} + P^{\ell}_{m,n-1})$$

$$+ \frac{\tau}{2(\Delta z)^2}\ (B4)\ D_z{}^{\ell}_{m,n+1/2}\ (P^{\ell}_{m,n+1} - P^{\ell}_{m,n})$$

$$+ \frac{\tau}{2(\Delta z)^2}\ (B3)\ D_z{}^{\ell}_{m,n-1/2}\,(P^{\ell}_{m,n-1} - P^{\ell}_{m,n}) - (B0)\ S \qquad (3.49)$$

in which for notational expediency:

$$B0 = \frac{1}{4}\ [\ B_{m+1/2,n+1/2} + B_{m-1/2,n+1/2} + B_{m+1/2,n-1/2} + B_{m-1/2,n-1/2}\ ]$$

$$\begin{aligned} B1 &= B_{m-1/2,n+1/2} + B_{m-1/2,n-1/2} \\ B2 &= B_{m+1/2,n+1/2} + B_{m+1/2,n-1/2} \\ B3 &= B_{m+1/2,n-1/2} + B_{m-1/2,n-1/2} \\ B4 &= B_{m+1/2,n+1/2} + B_{m-1/2,n+1/2} \end{aligned} \qquad (3.50)$$

Using a similar approach as shown above, Eq. (3.44) can be written in the form:

$$a_n P^{\ell+1}_{m,n-1} + b_n P^{\ell+1}_{m,n} + c_n P^{\ell+1}_{m,n+1} = d_n \tag{3.51}$$

Noting also that Eq. (3.51) involves only grid points on a given row M. The values for the coefficients a_n, b_n, c_n and d_n are given below using the notations in Eq. (3.50)

$$a_n = -\frac{\tau}{4\Delta z}(B3)\, W^{\ell+1}_{m,n-1/2} - \frac{\tau}{4(\Delta z)^2}(B3)\, D_z{}^{\ell+1}_{m,n-1/2} \tag{3.52}$$

$$b_n = \frac{\tau}{4\Delta z}(B4)\, W^{\ell+1}_{m,n+1/2} + BO - \frac{\tau}{4\Delta z}(B3)\, W^{\ell+1}_{m,n-1/2} \tag{3.53}$$

$$+ \frac{\tau}{2(\Delta z)^2}(B4)\, D_z{}^{\ell+1}_{m,n+1/2} + \frac{\tau}{2(\Delta z)^2}(B3)\, D_z{}^{\ell+1}_{m,n-1/2}$$

$$c_n = \frac{\tau}{4\Delta z}(B4)\, W^{\ell+1}_{m,n+1/2} - \frac{\tau}{2(\Delta z)^2}(B4)\, D_z{}^{\ell+1}_{m,n+1/2} \tag{3.54}$$

and:

$$d_n = P^{\ell+1/2}_{m,n} BO - \frac{\tau}{4\Delta x}(B2)\, U^{\ell+1/2}_{m+1/2,n} \left(P^{\ell+1/2}_{m,n} + P^{\ell+1/2}_{m+1,n}\right)$$

$$+ \frac{\gamma}{4\,\Delta x}(B1)\; U^{\ell+1/2}_{m-1/2,n}\left(P^{\ell+1/2}_{m,n}+P^{\ell+1/2}_{m-1,n}\right) + \frac{\gamma}{2(\Delta x)^2}(B2)$$

$$Dx^{\ell+1/2}_{m+1/2,n}\left(P^{\ell+1/2}_{m+1,n} - P^{\ell+1/2}_{m,n}\right) - \frac{\gamma}{2(\Delta x)^2}(B1)\; Dx^{\ell+1/2}_{m-1/2,n}$$

$$\left(P^{\ell+1/2}_{m,n} - P^{\ell+1/2}_{m-1,n}\right) - \gamma(BO)\; S \qquad (3.55)$$

In the above equation S has been used to represent a generalized source and sink term combination. In a generalized approach for a reaction scheme as presented by Leenderste (24) S becomes the combination of a reaction matrix and a source-sink term which will be presented later in this chapter.

It will be instructive at this time to note the positions of the various components of Eqs. (3.46) through (3.49) and Eqs. (3.52) through (3.55). First however, Fig. 3-2 shows the position of the various widths in the computational system. Close examination shows that the widths chosen for any particular term such as U,W,D_x, and D_z are always chosen so as to be spatially centered around these variables. This approach alleviates any possible computational waves from being generated by discontinuities in the width values between adjacent grids.

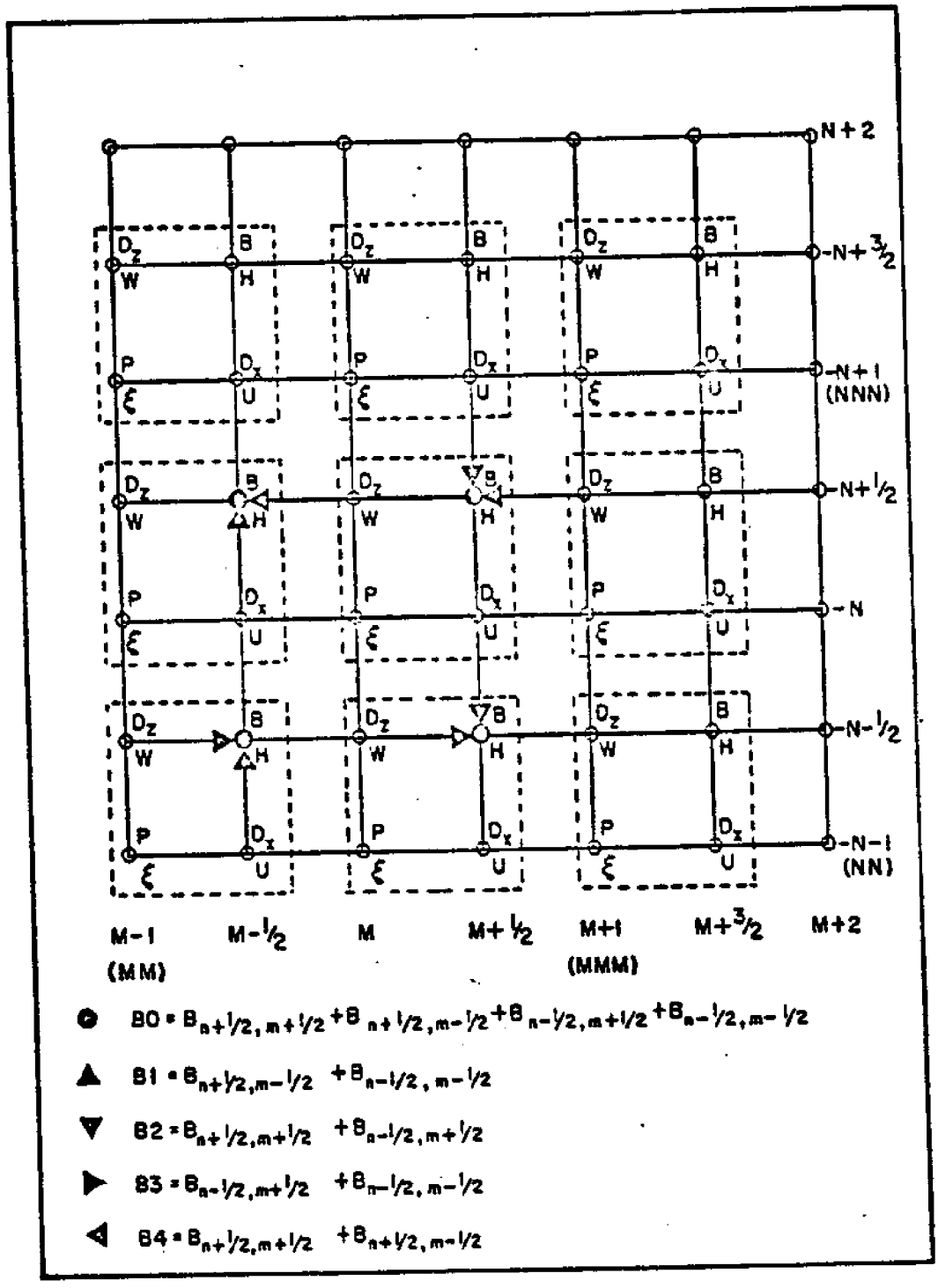

FIG. 3-2 LOCATION OF WIDTH PARAMETERS IN GRID SYSTEM

Figures 3-3 and 3-4 show the grid positions of the terms given by Eq. (3.46) through (3.49). Similarly Figs. 3-5 and 3-6 show the grid positions of the terms given by Eqs. (3.52) through (3.55). Observation of these figures displays that the location of terms in the grid system used for the coefficients a,b,c, and d occur in a direction perpendicular to the computation direction, thus showing the alternating direction characteristics of the method.

Figure 3-7 presents the combination of the first and second half of the time step and verifies the fact that this solution approach is also centered in time as well as in spatial coordinates.

Much comment has been made concerning the desirability to have variables centered in time and space in this section. The reason for this concern will become apparent when the dissipative and dispersive effects of this solution approach are consequently studied in Chapter 4 - Effects of Computational Model Approximation.

To solve Eqs. (3.45) and (3.51) for the mass densities requires the identical solution approach only employed in a different direction. Therefore:

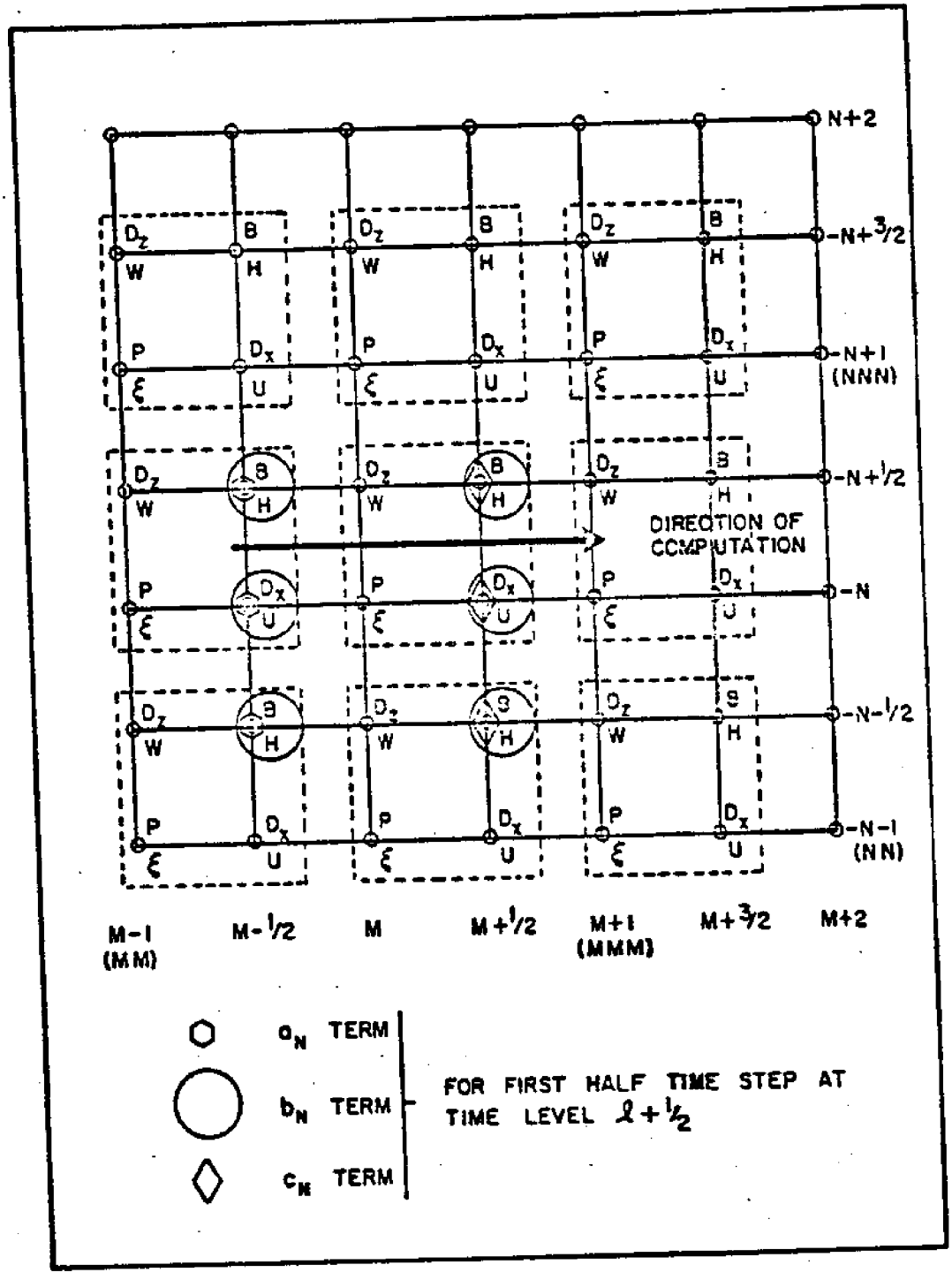

FIG. 3-3 GRID POSITION FOR TERMS a_N, b_N, and c_N FOR THE FIRST HALF TIME STEP

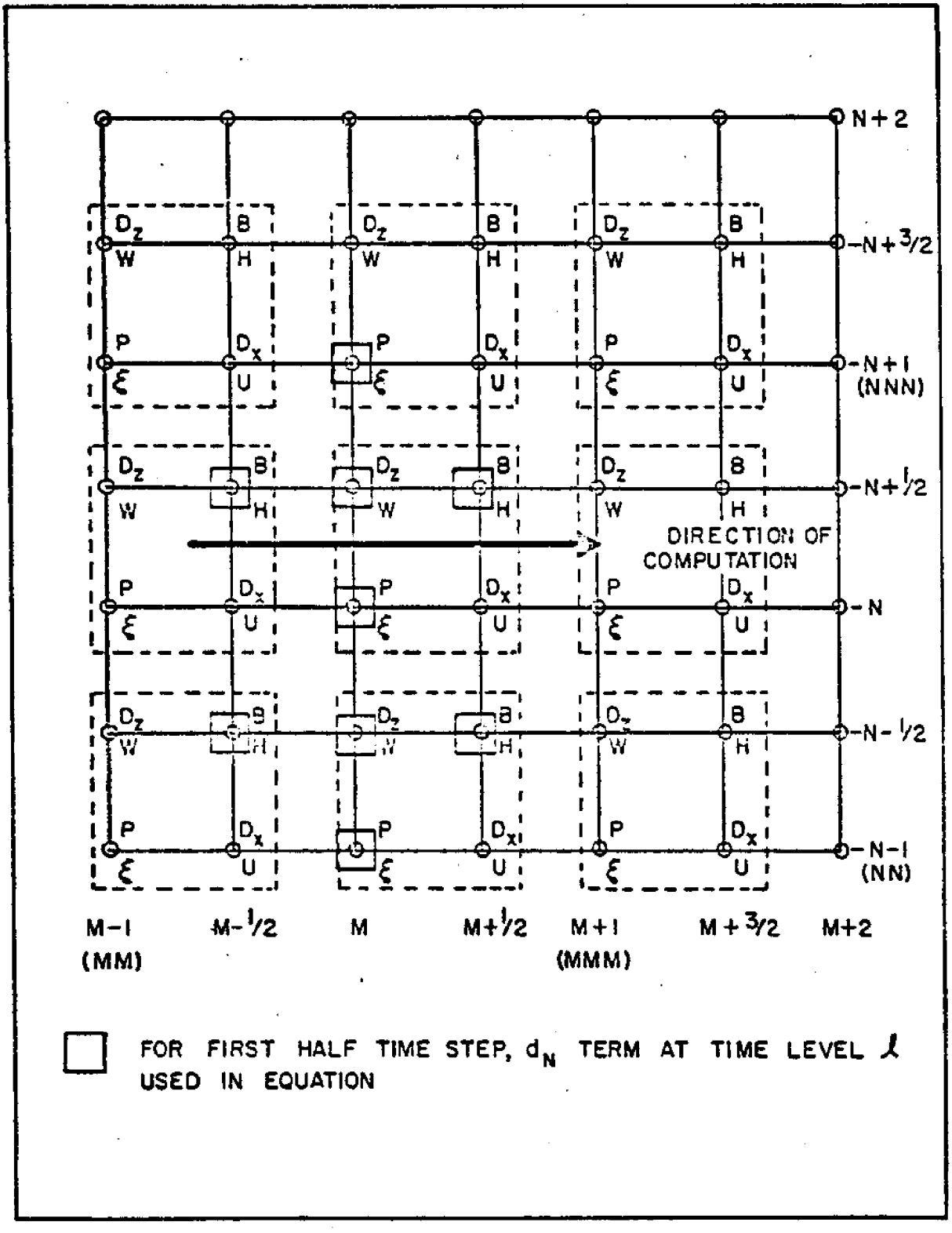

FIG. 3-4 GRID POSITIONS FOR TERM d_N FOR FIRST HALF TIME STEP

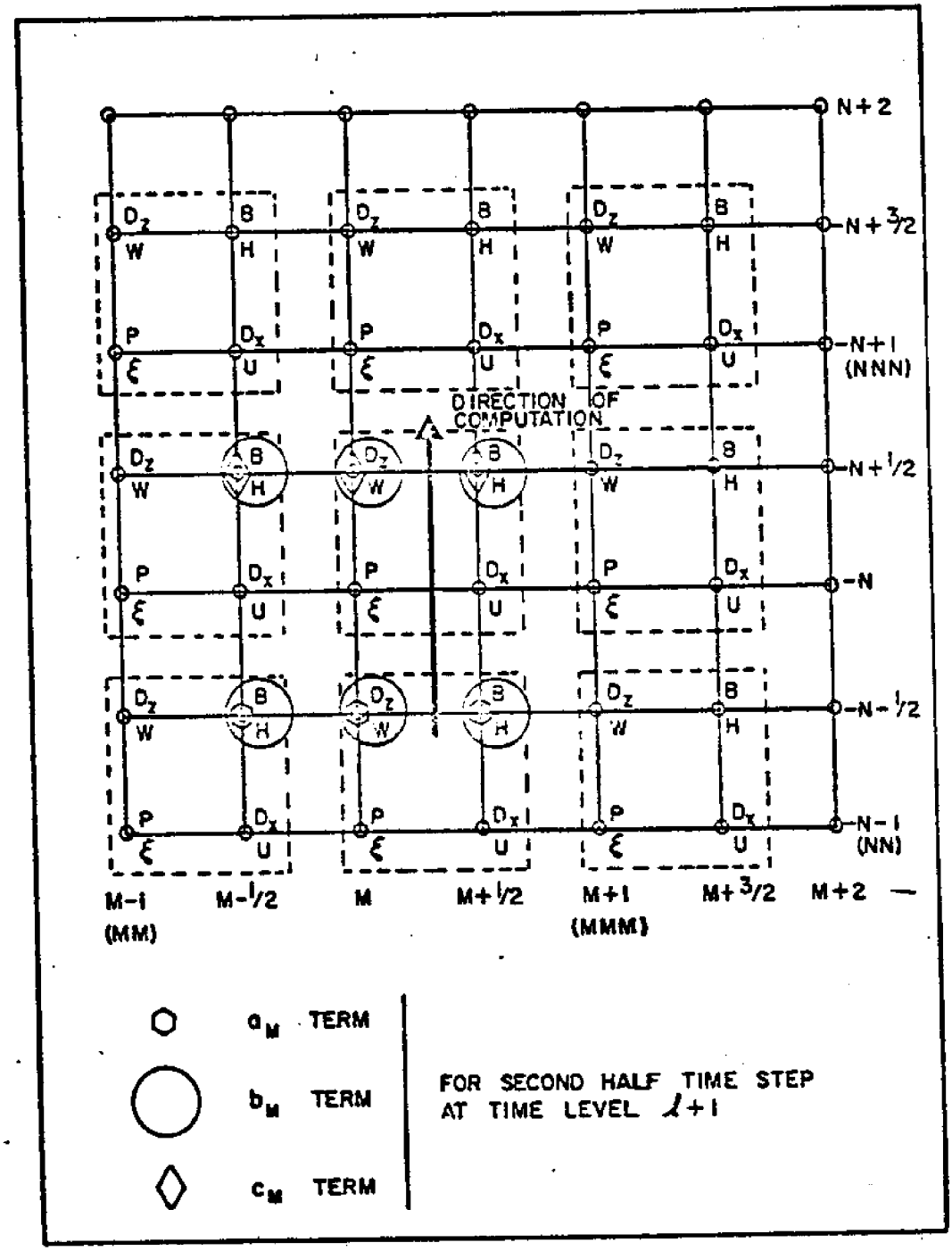

FIG. 3-5 GRID POSITIONS FOR TERMS a_M, b_M, and c_M, FOR SECOND HALF TIME STEP

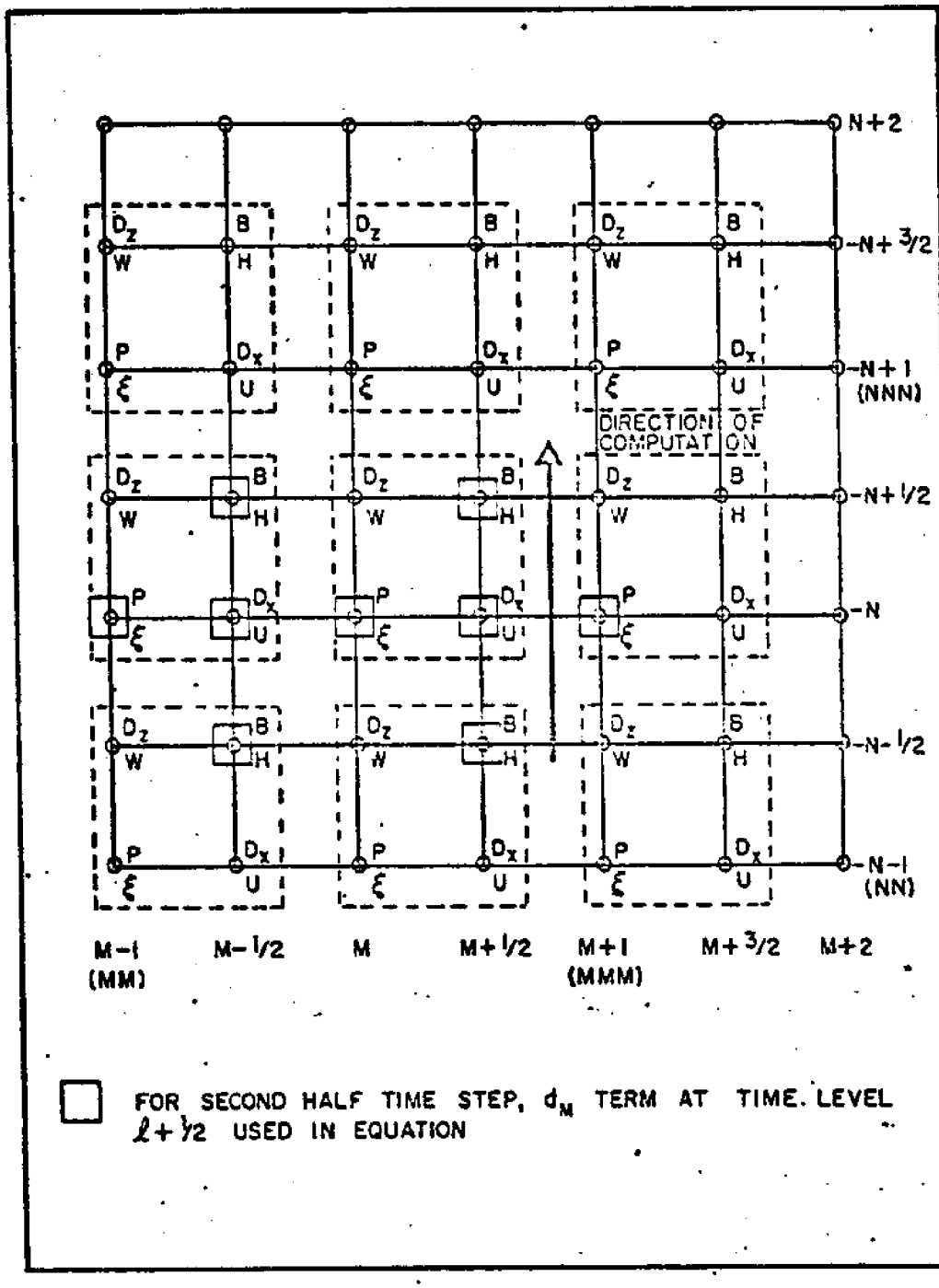

FIG. 3-6 GRID POSITIONS FOR TERM d_M FOR SECOND HALF TIME STEP

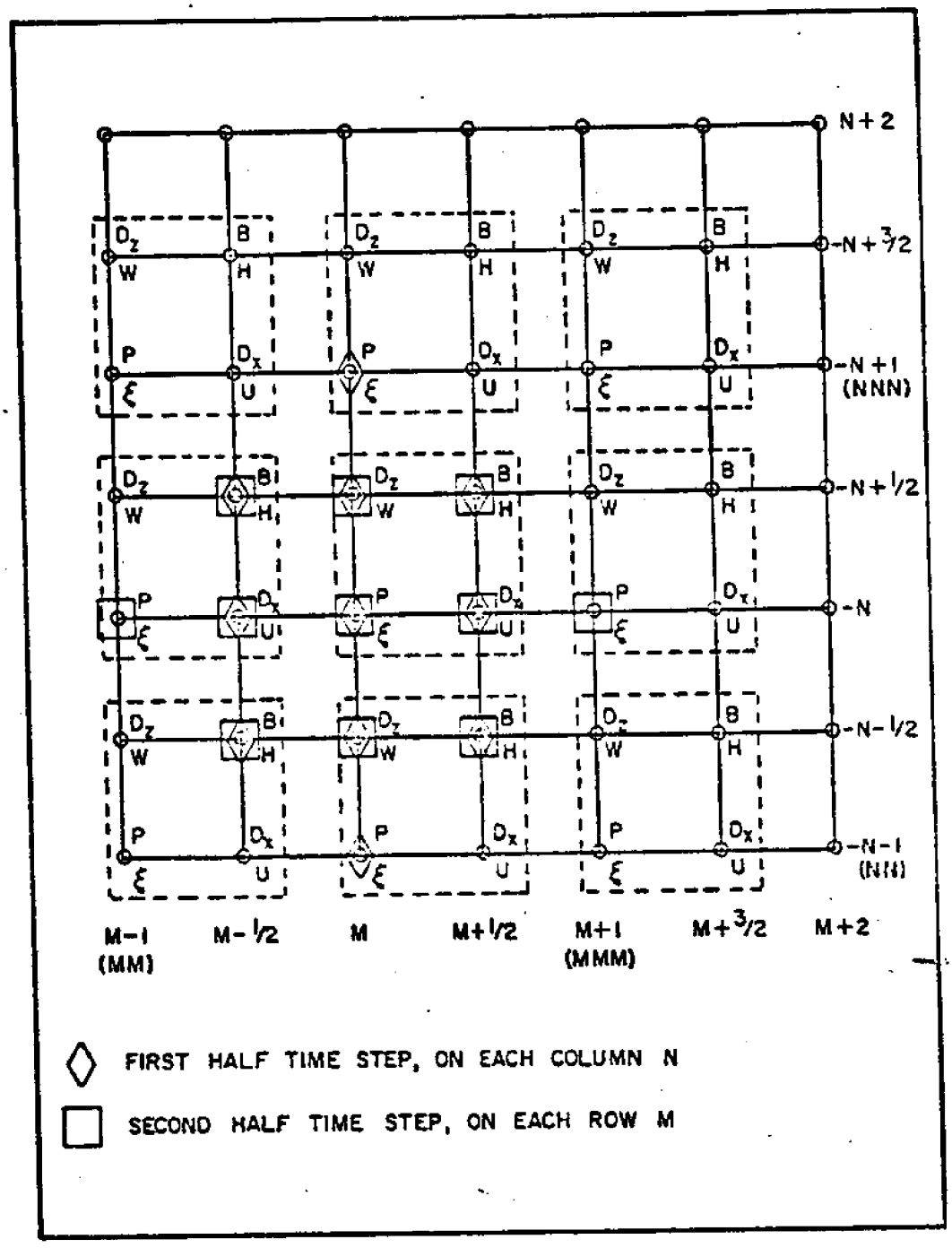

FIG. 3-7 GRID POSITIONS FOR BOTH THE FIRST AND SECOND HALF TIME STEPS

$$a_m P^{\ell+1/2}_{m-1,\,n} + b_m P^{\ell+1/2}_{m,n} + c_m P^{\ell+1/2}_{m+1,n} = d_m \qquad (3.45)$$

will be used for the purposes of explanation. Dropping the time notation $\ell + 1/2$ and the z direction grid number (N), since they remain unchanged, results in:

$$a_m P_{m-1} + b_m P_m + c_m P_{m+1} = d_m \qquad (3.56)$$

Assume that we have a closed left hand boundary, as shown in Fig. 3-8.

Then the advective and diffusive transport from grid M-1 to M is zero, or equivalently $a_m = 0$. Now Eq. (3.56) becomes:

$$b_m P_m + c_m P_{m+1} = d_m \qquad (3.57)$$

For the next point (M+1) we have:

$$a_{m+1} P_m + b_{m+1} P_{m+1} + c_{m+1} P_{m+2} = d_{m+1} \qquad (3.58)$$

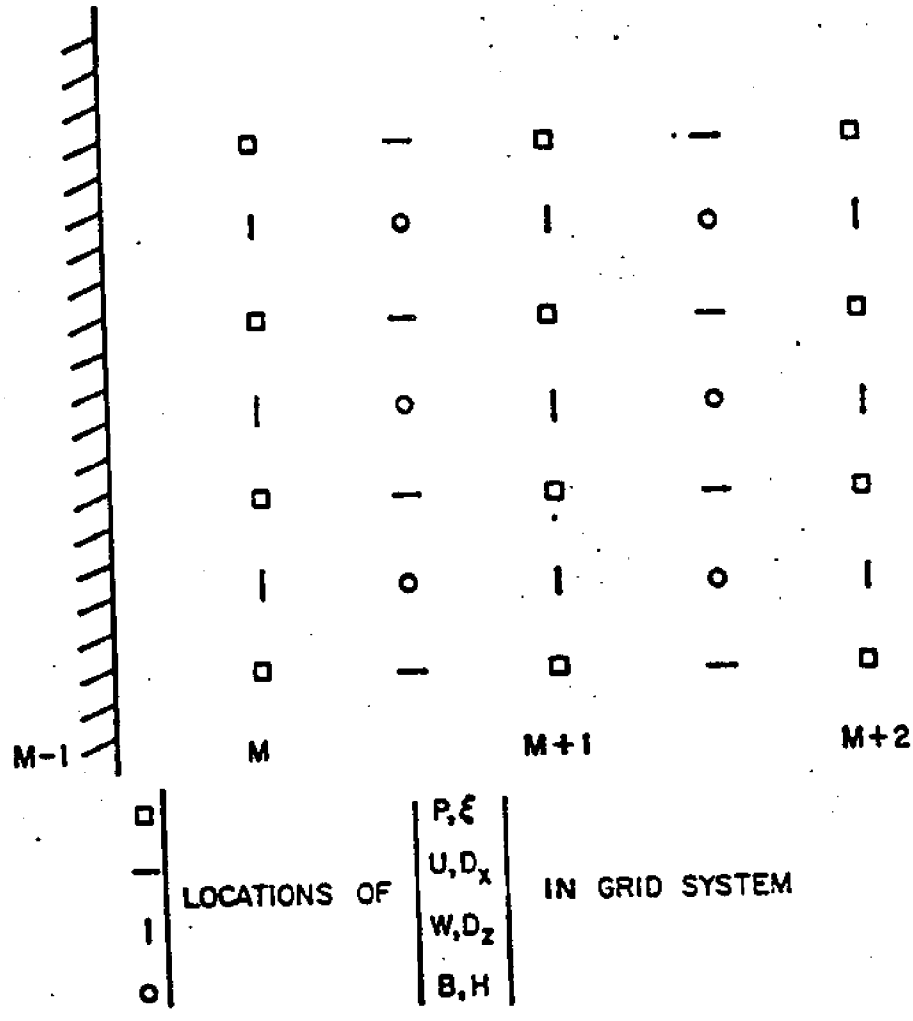

FIG. 3-8 GRID SYSTEM FOR CLOSED LEFT HAND BOUNDARY ON A GIVEN COLUMN N

Solving Eq. (3.57) for P_m results in:

$$P_m = \frac{d_m}{b_m} - \frac{c_m}{b_m} P_{m+1} \tag{3.59}$$

or rearranging:

$$P_m = Q_{m+1} + E_{m+1} P_{m+1} \tag{3.60}$$

where:

$$Q_{m+1} = \frac{d_m}{b_m} \tag{3.61}$$

$$E_{m+1} = - \frac{c_m}{b_m} \tag{3.62}$$

To solve for P_{m+1} we substitute Eq. (3.60) into Eq. (3.58) and obtain:

$$P_{m+1} = \frac{d_{m+1} - a_{m+1} Q_{m+1}}{E_{m+1} a_{m+1} + b_{m+1}} - \frac{c_{m+1}}{E_{m+1} a_{m+1} + b_{m+1}} P_{m+2} \tag{3.63}$$

or letting:

$$E_{m+2} = - \frac{c_{m+1}}{E_{m+1} a_{m+1} + b_{m+1}} \tag{3.64}$$

and:

$$Q_{m+2} = \frac{d_{m+1} - a_{m+1} Q_{m+1}}{E_{m+1} a_{m+1} + b_{m+1}} \tag{3.65}$$

obtain:

$$P_{m+1} = Q_{m+2} + E_{m+2} P_{m+2} \qquad (3.66)$$

Equations (3.64), (3.65) and (3.66) represent the general form of the recursion relations to be solved. If the right hand boundary is closed as shown in Fig. 3-9, then the transport due to advection and dispersion from grid M to grid M + 1 is zero, and $c_m = 0$. Now the resulting equation is:

$$a_m P_{m-1} + b_m P_m = d_m \qquad (3.67)$$

Taking the general relation developed in Eq. (3.64) and letting $c_m = 0$ results in $E_{m+1} = 0$. Therefore, for this closed right hand boundary

$$P_m = Q_{m+1} \qquad (3.68)$$

and

$$E_{m+1} = 0.0 \qquad (3.69)$$

To account for open boundaries the appropriate E value is set equal to zero and the Q value set equal to the mass density at the open boundary. For an open left-hand boundary:

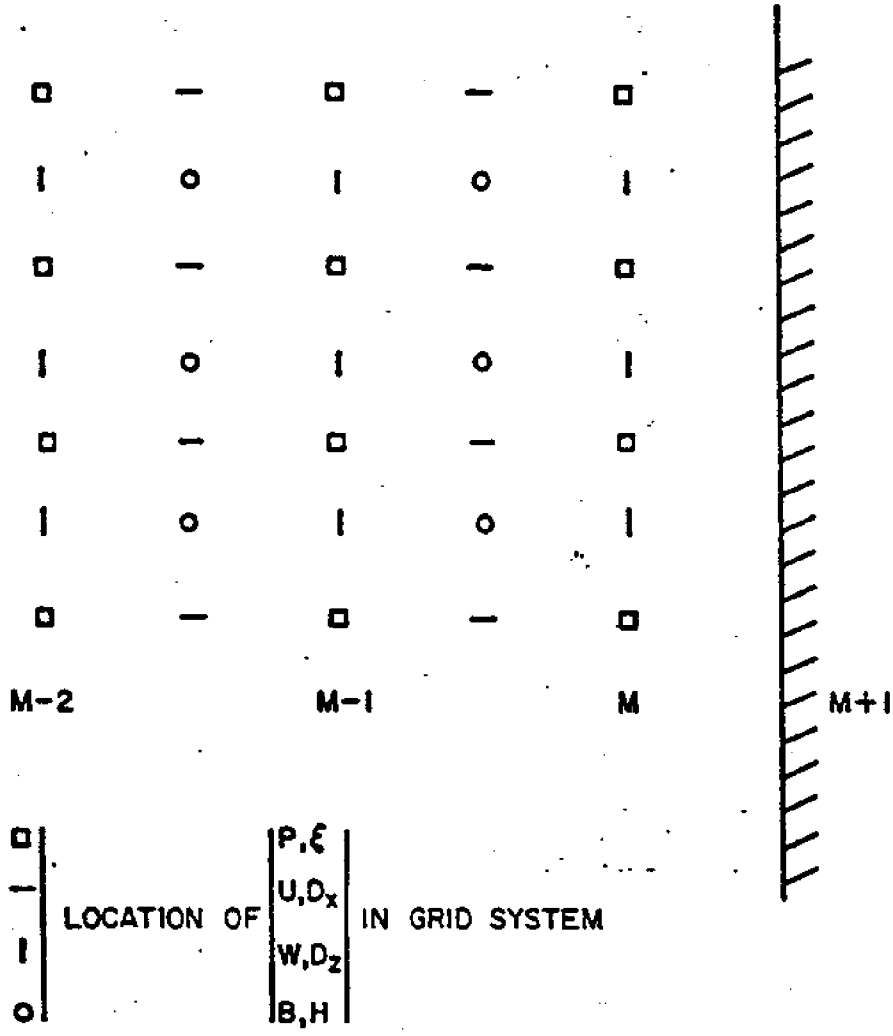

FIG. 3-9 GRID SYSTEM FOR CLOSED RIGHT HAND BOUNDARY ON A GIVEN COLUMN N

$$Q_{m+1} = P_{m-1}$$

$$E_{m+1} = 0.0 \qquad (3.70)$$

Therefore:

$$P_m = Q_{m+1} = P_{m-1} \qquad (3.71)$$

For an open right-hand boundary:

$$Q_{m+1} = P_{m+1} \qquad (3.72)$$

$$E_{m+1} = 0.0$$

Therefore:

$$P_m = Q_{m+1} = P_{m+1} \qquad (3.73)$$

With these basic recursion relations developed, any combination of open and closed boundaries may be achieved. The solution approach, after deciding the boundary conditions, is to calculate the E and Q values in ascending order, and then use Eq. (3.66) in descending order to compute the mass densities. Table 3-1 presents the various boundary cases that may be encountered and the equations used to find their solutions.

CLOSED-OPEN BOUNDARIES

GRID LOCATION	CONDITIONS	DETERMINATION OF E BY EQ.	DETERMINATION OF Q BY EQ.
//// M	CLOSED BOUNDARY BETWEEN M-1 AND M	(3.62)	(3.61)
M+ 1 M+ 2 M+ 3 M+ 4	GENERAL MID-FIELD	(3.64)	(3.65)
M+ 5 *	OPEN BOUNDARY BETWEEN M+5 AND M+6	0	(3.72)

CLOSED-CLOSED BOUNDARIES

GRID LOCATION	CONDITIONS	DETERMINATION OF E BY EQ.	DETERMINATION OF Q BY EQ.
//// M	CLOSED BOUNDARY BETWEEN M-1 AND M	(3.62)	(3.61)
M+ 1 M+ 2 M+ 3 M+ 4	GENERAL MID-FIELD	(3.64)	(3.65)
M+ 5 ////	CLOSED BOUNDARY BETWEEN M+5 AND M+6	0	(3.68)

//// - CLOSED BOUNDARY

* - OPEN BOUNDARY

TABLE 3-1 BOUNDARY CONDITION SOLUTION ALGORITHMS

OPEN-CLOSED BOUNDARIES

GRID LOCATION	CONDITIONS	DETERMINATION OF E BY EQ.	DETERMINATION OF Q BY EQ.
*	OPEN BOUNDARY BETWEEN M-1 AND M	0	(3.70)
M			
M + 1	GENERAL MID-FIELD	(3.64)	(3.65)
M + 2			
M + 3			
M + 4			
M + 5	CLOSED BOUNDARY BETWEEN M+5 AND M+6	0	(3.68)
////			

OPEN-OPEN BOUNDARIES

GRID LOCATION	CONDITIONS	DETERMINATION OF E BY EQ.	DETERMINATION OF Q BY EQ.
*	OPEN BOUNDARY BETWEEN M-1 AND M	0	(3.70)
M			
M + 1	GENERAL MID-FIELD	(3.64)	(3.65)
M + 2			
M + 3			
M + 4			
M + 5	OPEN BOUNDARY BETWEEN M+5 and M+6	0	(3.72)
*			

TABLE 3-1 (CONT'D) BOUNDARY CONDITION SOLUTION ALGORITHMS

Another approach that can be used to determine the open boundary conditions is to calculate the concentration from values extrapolated from the computational field during the outflow and using some preset concentration during inflow across the boundary. Normally an approximation of this nature for outflows can be made by simply regarding the convective outflows based on the arguments in Chapter 2.

EXTENSION OF FINITE-DIFFERENCE MODEL TO INCLUDE REACTIONS

As indicated previously the generalized source and sink term of the mass-balance equation, Eqs. (2.27) or (2.27a) can be employed to simulate a reaction mechanism for some water quality parameter or system of parameters. To present this extension of the basic finite-difference model for the mass-balance equation, the non-dimensional model will be employed, due to its general applicability, and the structural development as presented by Leenderste (24).

The generalized source-sink term as noted in Eq. (2.27a)

can be divided into a source (sink) vector $\vec{S}$ and a reaction matrix [K], or in equation form:

$$BH_T S = BH_T [K] \vec{P} + H_T B\vec{S} \tag{3.74}$$

where P now becomes a mass concentration vector containing constituents and H_T is the instantaneous water depth as previously noted.

In its general form this scheme allows for nonlinear transports of constituents. Decay rates dependent on any particular species concentration and coupling between individual species can all be handled via this reaction matrix scheme.

For example, consider modeling of total coliform bacteria for three independent groups of sources. The reaction matrix for this model and the mass concentration vector then becomes:

$$[K] = \begin{bmatrix} K_{11} & 0 & 0 \\ 0 & K_{22} & 0 \\ 0 & 0 & K_{33} \end{bmatrix} \qquad \vec{P} = \begin{bmatrix} P_1 \\ P_2 \\ P_3 \end{bmatrix} \qquad \vec{S} = 0 \tag{3.75}$$

where

$K_{11}, K_{22},$ and K_{33} - the first order decay constants

$P_1, P_2,$ and P_3 - the concentration of coliform bacteria for the first, second, and third source groups respectively.

An example of a two-stage non-conservative reaction model can be shown with the biochemical oxygen demand (B.O.D.) and dissolved oxygen (D.O.) interaction in a fluid. Discharges of organic waste from municipal and industrial outfalls are decomposed by bacteria in the surrounding water column. These bacteria require oxygen to perform this function which they take from the receiving waters. The amount of oxygen utilized in the process is referred to as the B.O.D. Replacement of the dissolved oxygen occurs through reareation at the surface and in certain cases throughout the water body due to photosynthesis due to the growth of algae. Assuming that the B.O.D. can be modeled as a single first-order reaction coefficient and if photosynthesis is neglected then the reaction matrix [K]

and the mass concentration vector $\bar{P}$ can be written:

$$[K] = \begin{bmatrix} K_A & K_D \\ 0 & K_D \end{bmatrix}$$

$$P = \begin{bmatrix} P_1 \\ P_2 \end{bmatrix} \qquad S = \begin{bmatrix} -K_A & C_{SAT} \\ 0 & \end{bmatrix} \tag{3.76}$$

where

K_A - reareation coefficient of oxygen (1/sec)

K_D - first order decay coefficient for B.O.D. (1/sec.)

P_1 - DO concentration (mg/ℓ)

P_2 - BOD concentration (mg/ℓ)

C_{SAT} - Saturation concentration of oxygen (mg/ℓ)

Point sources of BOD and DO such as occur at sewage outfalls or benthic demands are simulated by employing pulse inputs to the source vector, $\vec{S}$, at appropriate spatial points.

Generalization to higher-order reaction schemes such as the nitrogen system follow a similar pattern of development and will not be covered in this work.

Following the work of Leenderste (24) on a two-dimensional vertically-averaged water quality model, a finite-difference approximation for the reaction scheme can be developed. In this presentation the results of his work will simply be altered to apply to the model development employed and the interested reader is referred to Reference (24). The notational scheme follows that previously used to present the finite-difference approximation to the mass balance equation. Then for the first-half time step, going from time level ℓ to time level $\ell+1/2$ we find:

$$\overline{\overline{B}}H_T S = \overline{\overline{B}}\,(\overline{\overline{H}} + \overline{\overline{\rho}})\,S =$$

$$\sum_{j=1}^{i-1} \overline{\overline{B}}(\overline{\overline{H}} + \overline{\overline{\rho}}_+)\,K_{ij}\,P_{j+}\alpha_i + \overline{\overline{(\overline{\overline{H}} + \overline{\overline{\rho}})\,K_{ii}\,P_i}}^{t/2}\,\overline{\overline{B}}$$

$$+ \sum_{j=i+1}^{j_{max}} \overline{\overline{B}}\,(\overline{\overline{H}} + \overline{\overline{\rho}})\,K_{ij}P_j\beta_i + \overline{\overline{B}}\,(\overline{\overline{H}} + \overline{\overline{\rho}})\,S_i \qquad (3.77)$$

for which $\overline{}^{t/2}$ indicates an averaging over the time levels $\ell\Delta t$ and $(\ell + 1/2)\,\Delta t$.

where

$$\alpha_i = \begin{cases} 0 & i = 1 \\ 1 & 1 < i \leq j \text{ max} \end{cases}$$

$$\beta_i = \begin{cases} 0 & i = j \text{ max} \\ 1 & 1 \leq i < j \text{ max} \end{cases}$$

j max - maximum number of constituents

and for the second-half step, going from time level $\ell + 1/2$ to time level $\ell + 1$ results in:

$$\overline{\overline{B}} H_T S = \sum_{j=1}^{i-1} \overline{\overline{B}} \left(\overline{\overline{H}} + \overline{\overline{\zeta}}\right) K_{ij} P_j \alpha_i +$$

$$\frac{}{\overline{\overline{B}} \left(\overline{\overline{H}} + \overline{\overline{\zeta}}\right) K_{ii} P_i + \sum_{j=i+1}^{j\max} \left(\overline{\overline{H}} + \overline{\overline{\zeta}}_+\right) K_{ij} P_j \beta_i} \; t/2$$

$$+ \overline{\overline{B}} \left(\overline{\overline{H}} + \overline{\overline{\zeta}}\right) S_i \qquad (3.78)$$

It is observed now that the constituent concentrations of the previous finite-difference approximation for the mass balance equation now become generalized to P_i where i represents a specific element of the mass concentration vector.

The numerical computational scheme for the reaction matrix is performed by a sequential use of forward and

backward information as shown by Eqs. (3.77) and (3.78). For example, if j_{max} constituents are transported in the fluid for constituent i information in the reaction terms at time level $\ell + 1/2$ is used for all constituents for which a sequence number j is smaller than i. For all constituents which have a sequence number larger than i, information at time level ℓ is employed. The constituents in this step are computed in ascending order from i = 1 to i = j_{max}.

During the second-half step from time level $\ell + 1/2$ to time level $\ell + 1$ the constituents are computed in descending order, i = j_{max} to i = 1. Information on time level $\ell + 1/2$ is employed for all constituents having a sequence number smaller than i and values on the time level $\ell + 1$, are used for all constituents with a number larger than i. The preceeding procedure centers the reaction matrix information over the time interval ℓ to $\ell + 1$, whereas the terms involving the i^{th} constituent are taken centered over each half time step.

MASS BALANCE CHECK

An important part of any transport computational model is to assure that the mass in the system remains conserved for any conservative substance. This procedure assures that the finite-difference equations representing the partial differential equations are correctly formulated and that the boundary conditions have been properly posed.

In fundamental terms the mass balance for the computational model becomes:

Input of substance due to dispersion and advection	-	Output of substance due to dispersion and advection	+	Sources of substance

- Sinks of substance	=	total mass in the field

This relation should hold for the time domain of the computation.

In addition to conserving mass over each time step, the computational scheme must show that cumulative error in th

mass balance must also stay within acceptable limits, for large fields (16 X 50) to $\pm$ 1 %. Also if a constant field concentration is set in the computational grids and the same value is used for the boundary conditions then for mass to be conserved in each grid the concentration of that grid cannot change with time as the model is run.

For both the dimensionless z axis model and the dimensional model of the finite-difference equations, numerical modeling experiments show that mass is conserved to within $\pm$ .15 % cumulative mass error for a 16 X 50 grid system with initial field concentration of 4.0 mg/ℓ and a typical conservative tidal velocity field. Program runs consisting of over a thousand time steps indicate that the concentration of each grid square remain unchanged. With these conditions satisfied it has been verified that the model and boundary conditions have been correctly approximated in regards to conservation of constituent mass.

If however, the values of dispersion become excessively large in either model, a loss of mass will occur near complicated geometry or boundary conditions. These problems

can be overcome by suitably altering the dispersion in these areas or locally smoothing the geometrical representation of the estuary at that particular point.

CHAPTER 4

EFFECTS OF COMPUTATIONAL MODEL APPROXI

DISSIPATIVE AND DISPERSIVE ASPECTS

When a properly designed computational method using finite-difference approximations of partial differential equations is used, a decrease in grid size will cause the numerical and analytical solutions of the differential equations to converge. Therefore, before proceeding with the solution to any such set of equations an analysis or analytical determination of the computational effects of grid discreteness should be performed on the proposed finite-difference model. This however, is often not a convenient approach to use on the full set of equations due to limitations in computer size, memory and speed.

To overcome these difficulties an analysis can be performed on a simpler but similar equation. This procedure will be used in the following discussion having

been originally outlined by Leenderste (6).

At any instant in time, the spatial variation of mass density in the area of computation can be considered to consist of a superposition of Fourier series with differing spatial frequencies. The computational effects of importance are dissipative and dispersive. By dissipative it is meant that the components of the Fourier series decay without any physical reason, whereas dispersive refers to the difference in propagation speed of components in the computational model and those in the analytical or prototype solution.

These effects, dispersive and dissipative, are therefore to be avoided in a computational model since we would be unable to separate physical processes such as diffusion, decay of waste components, etc. from computational effects. This difference would also result in a mass-transport model which would be incapable of conserving mass.

To study these dispersive and dissipative aspects a one-dimensional mass transport equation with constant velocity, estuary width, and dispersion coefficients will be used. The equation has the form:

$$\frac{\partial P}{\partial t} + u \frac{\partial P}{\partial x} - D_x \frac{\partial^2 P}{\partial x^2} = 0 \qquad (4.1)$$

Using a multioperation scheme for this equation similar to that used for the two-dimensional scheme in Chapter 3, the following equations are obtained:

$$P_m^{\ell+1} - P_m^{\ell} + \frac{\Delta t}{2\Delta x} u \left[(1+\alpha) P_{m+1}^{\ell+1} - 2\alpha P_m^{\ell+1} + (1-\alpha) P_{m-1}^{\ell+1} \right]$$

$$- D_x \frac{\Delta t}{(\Delta x)^2} \left(P_{m+1}^{\ell+1} - 2P_m^{\ell+1} + P_{m-1}^{\ell+1} \right) = 0 \qquad (4.2)$$

and:

$$P_m^{\ell+2} - P_m^{\ell+1} + \frac{\Delta t}{2\Delta x} u \left[(1+\alpha) P_{m+1}^{\ell+1} - 2\alpha P_m^{\ell+1} + (1-\alpha) P_{m-1}^{\ell+1} \right]$$

$$- D_x \frac{\Delta t}{(\Delta x)^2} \left[P_{m+1}^{\ell+1} - 2P_m^{\ell+1} + P_{m-1}^{\ell+1} \right) = 0 \qquad (4.3)$$

where the following notation has been employed

$P_m^{\ell} = P(m\Delta x, \ell \Delta t)$

Δx = grid size for x spatial direction

Δt = time step size

α = -1,0,1 (indicating weighting factors i.e. backward, central, and forward difference schemes).

The solution of the finite difference equations can be expressed by a Fourier series. For this equation then:

$$P(x,t) = \sum_j P_j^* \exp.\ [\, i\ (\sigma_j x + \omega_j t)] \qquad (4.4)$$

where

ω_j = frequency

σ_j = wave number

j = $1,2,3,\ldots\ \infty$

P^*_j = complex amplitude

Now since the equation is linear, only one term of Eq. (4.4) needs to be considered in the analysis. Substituting the first term of Eq. (4.4) into Eq. (4.2) results in:

$$P_m^{*\,\ell+1} = P_m^{*\,\ell} \Big/ \Big[\, 1 + \frac{\Delta t}{\Delta x}\, i\, u \sin(\sigma \Delta x) -$$

$$\frac{2\,\Delta t}{\Delta x} \propto u \sin^2\left(\frac{\sigma \Delta x}{2}\right) + 4\, D_x \frac{\Delta t}{(\Delta x)^2} \sin^2\left(\frac{\sigma \Delta x}{2}\right) \Big] \qquad (4.5)$$

or

$$P_m^{*\,\ell+1} = \lambda_i P_m^{*\,\ell} \qquad (4.6)$$

where:

$$\lambda_1 = \frac{1}{1+\frac{\Delta t}{\Delta x} i\, u \sin(\sigma\Delta x) - \frac{2\Delta t}{\Delta x}\alpha u \sin^2\left(\frac{\sigma\Delta x}{2}\right) + 4D_x \frac{\frac{\Delta t}{2}}{(\Delta x)^2} \sin^2\left(\frac{\sigma\Delta x}{2}\right)} \tag{4.7}$$

Using a similar procedure for Eq. (4.3) :

$$P_m^{*\,\ell+2} = \lambda_2 P_m^{*\,\ell+1} \tag{4.8}$$

where

$$\lambda_2 = 1 - \frac{\Delta t}{\Delta x} i\, u \sin(\sigma\Delta x) + \frac{2\Delta t}{\Delta x}\alpha i \sin^2\left(\frac{\sigma\Delta x}{2}\right) - \frac{4D_x\Delta t}{(\Delta x)^2} \sin^2\left(\frac{\sigma\Delta x}{2}\right) \tag{4.9}$$

Using Eqs. (4.6) and (4.8) :

$$P_m^{*\,\ell+2} = g_a(\Delta t, \sigma)\, P_m^{*\,\ell} \tag{4.10}$$

where:

$$g_a(\Delta t, \sigma) = \lambda_1 \lambda_2 \tag{4.11}$$

$g_a(\Delta t, \sigma)$ is called the amplification matrix and since it has only one element, its value is also its eigenvalue (λ).

The eignvalues of the amplification matrix provide

important information on the computational scheme. For stability, according to the Neumann condition (23), which is explained in greater detail in the convergence and stability section of this chapter, the criterion is

$$|\lambda| \leq 1 + 0(\Delta t) \tag{4.12}$$

The validity of this condition should hold for all wave numbers σ. Numerical experimentations show that this condition is always satisfied for space centered spatial differences ($\alpha = 0$) but are <u>not always satisfied</u> for off centered differences ($\alpha = 1, -1$). Therefore, the remainder of the analysis will be completed for spatially centered differences. Now one can see why care was taken in the derivation of the finite-difference representation to assure central spacing.

Employing the concept of the complex propagation factor (6) the eignvalues can also be used to study the dispersive and dissipative aspects of computational schemes. This factor indicates one component of the constituent field with a wavelength L_w. A wave will be designated as the periodic variation of the constituent. To represent the field, finite differences are used in spatial coordinates,

and the progress of the wave is followed over the wavelength. Numerical computations however show changes of wave amplitude and propagation speed from those that actually occur in the prototype as represented by the parabolic partial differential equations.

To study these differences the propagation factor will be employed, expressed as a function of σl or $L_w/\Delta x$, which is the number of finite differences per wavelength. The propagation factor then is defined as the complex ratio of the computed wave in amplitude and phase to the prototype wave after an interval in which the prototype wave has traveled over its wavelength. Therefore, the modulus of the propagation factor is a measure of the amplitude decay during the computation, while the factor's argument is a measure of the phase shift. Consequently, it can be expressed as:

$$T\left(\frac{L_w}{\Delta x}\right) = \frac{\exp\left[i\left(\omega' t + \sigma x\right)\right]}{\exp\left[i\left(\omega t + \sigma x\right)\right]} \qquad (4.13)$$

where

$$x = \frac{2\pi}{\sigma} = L_w$$

and

$$t = \frac{2\pi}{\omega}$$

also

ω' = frequency of the computed wave

ω = frequency of the prototype wave

Figure (4 - 1) shows the difference between the prototype and computed waves. The dissipative and dispersive effects are easily noted. The modulus [T (^{Lw} / x)] is the ratio of the amplitudes of the computed wave to the physical wave after time L_w / u and therefore represents the dissipative effects of the computational procedure. This quantity is noted as A" B" / A' B' in Fig. - 4 - 1. To show the phase lag of the computational scheme a comparison is made between the wavelengths of the computed and physical waves. The ratio of these two quantities, noted as B B" / B B' in Fig. 4 - 1, is indicative of the dispersive effects of the computational procedure.

For the first portion of this analysis the behavior of the physical or prototype wave will be considered.

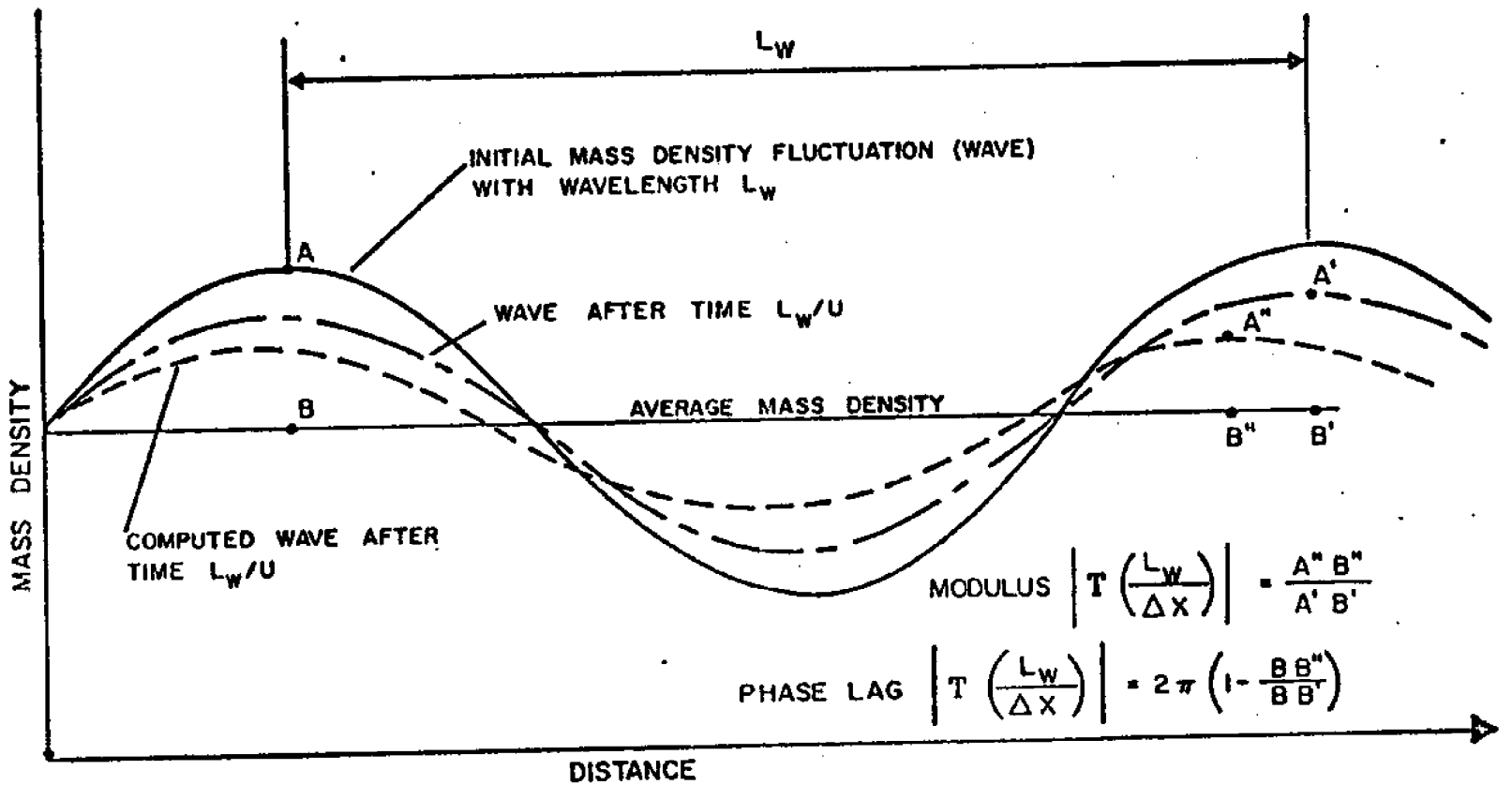

FIG. 4-1 MASS CONCENTRATION WAVES SHOWING DISSIPATIVE AND DISPERSIVE COMPUTATIONAL EFFECTS

The general solution of Eq. (4.1) is:

$$P(x,t) = P^* \exp (i (\sigma x + \omega t)) \qquad (4.14)$$

Now introducing Eq. (4.13) into Eq. (4.1) results in:

$$\omega + \sigma u - i D_x \sigma^2 = 0 \qquad (4.15)$$

or rearranging:

$$\omega = \sigma(-u + i \sigma D_x) \qquad (4.16)$$

which is the relation between wave number and frequency for the prototype wave.

Examining Eq. (4.16) it is found that if a periodic spatial wave is used for the initial condition, that it will decay with time. For a spatial wave of unit amplitude and after a time Δt, the amplitude will decay as $\exp (- \sigma^2 D_x \Delta t)$ and the wave will have propagated a distance $u \Delta t$. This can be seen by substituting Eq. (4.16) into (4.14) then:

$$P(x,t) = P^* \exp (\sigma i (x - u \Delta t + i \sigma D_x \Delta t)$$

Now letting:

$$P^* = 1$$

$$x = u \Delta t$$

then it follows that:

$$P(x,t) = \exp\ (- \sigma^2 D_x \Delta t) \qquad (4.17)$$

However in a computational scheme a different relation between frequency and wave number probably exists. Introducing Eq. (4.13) into Eq. (4.2) and using the spatially-centered difference scheme ($\alpha = 0$) the following is obtained:

$$e^{i \omega_1' t} = \frac{1}{1 + i A + B} = \lambda_1 \qquad (4.18)$$

where ω_1' is the frequency of the implicit step computational method and:

$$A = \frac{\Delta t}{\Delta x} u \sin (\sigma \Delta x)$$

$$B = 4 D_x \frac{\Delta t}{(\Delta x)^2} \sin^2 \left(\frac{\sigma \Delta x}{2} \right) \qquad (4.19)$$

During time interval Δt, the computed wave of this step decays as the modulus of λ_1:

$$\left| \lambda_1 \right| = \frac{1}{\sqrt{(1 + B)^2 + A^2}} \qquad (4.20)$$

The number of operations to be used at a time step Δt for the physical wave to propagate over its wavelength is

$$n = \frac{L_w}{\Delta t u} = \frac{2\pi}{u \Delta t \sigma} \tag{4.21}$$

and the modulus of the propagation factor for this step becomes:

$$T \left({}^{L_w}/_{\Delta x} \right) = \left\{ \frac{[(1 + B)^2 + A^2]^{-1/2}}{\exp (- \sigma^2 D_x \Delta t)} \right\}^n \tag{4.22}$$

In addition the wave speed of the computational scheme is different than that of the physical wave. To compute the difference take the real part of Eq. (4.7) and obtain:

$$R_e (\omega_1' \Delta t) = - \tan^{-1} \left(\frac{A}{1 + B} \right) \tag{4.23}$$

and the real part of Eq. (4.16) obtaining:

$$R_e (\omega \Delta t) = \Delta t u \sigma \tag{4.24}$$

Thus the ratio of the computed to physical wave speeds becomes:

$$R_1 = \frac{R_e (\omega_1' \Delta t)}{R_e (\omega \Delta t)} = \frac{\tan^{-1} \left(\frac{A}{(1+B)} \right)}{\Delta t u \sigma} \tag{4.25}$$

and the phase angle of the propagation factor is then:

$$\text{Arg}\ [\ T_1\ (\ {}^{L_w}/_{\Delta x})\ ] = 2\pi(R_1 - 1) \qquad (4.26)$$

Proceeding with a similar line of reasoning for the second step using Eq. (4.3) and Eq. (4.9) results in:

$$\left| T\ (\ {}^{L_w}/_{\Delta x}) \right| = \left\{ \frac{\sqrt{(1 - B)^2 + A^2}}{\exp\ (-\sigma^2 D_x \Delta t)} \right\}^n \qquad (4.27)$$

and the computed wave speed to physical wave speed ratio is:

$$R_2 = \frac{\tan^{-1} \left(\frac{A}{(1-B)} \right)}{\Delta t\ \sigma\ u} \qquad (4.28)$$

also:

$$\text{Arg}\ [\ T_2\ (\ {}^{L_w}/_{\Delta x})\ ] = 2\pi(R_2 - 1) \qquad (4.29)$$

In the multioperation scheme described in Eqs. (4.2) and (4.3), each operation is used n/2 times per time step and hence the modulus of the propagation factor for the multioperation scheme becomes:

$$\left| T\left({}^{L_w}/_{\Delta x} \right) \right| = \left\{ \frac{\sqrt{\left[(1-B)^2 + A^2 \right] / \left[(1+B)^2 + A^2 \right]}}{\left[\exp\left(-\sigma^2 D_x \Delta t \right) \right]^2} \right\}^{n/2} \tag{4.30}$$

and the ratio of the computed to physical wave speed is:

$$R = \frac{1}{2} \left(R_1 + R_2 \right) \tag{4.31}$$

Taken separately the first step shows that it is strongly dissipative, while the second step becomes unstable. However, in the multioperation scheme the method proves to be stable and if appropiate values of ${}^{L_w}/_{\Delta x}$ are chosen, neither dispersive nor dissipative.

Figures 4-2, 4-3, 4-4, and 4-5 represent the results of a parametric study using ${}^{u \Delta t}/_{\Delta x}$ and ${}^{D_x \Delta t}/_{(\Delta x)^2}$. From these figures it is clearly evident that a decrease in spatial grid size results in a convergence of the solution of the finite-difference equation to the partial differential equation. This phenomena works in different ways, not only is the spatial discreteness improved but the decreased grid size also permits a lowering of the dispersion coefficient which, as can be seen in Figs. 4-2 and 4-3, gives better results.

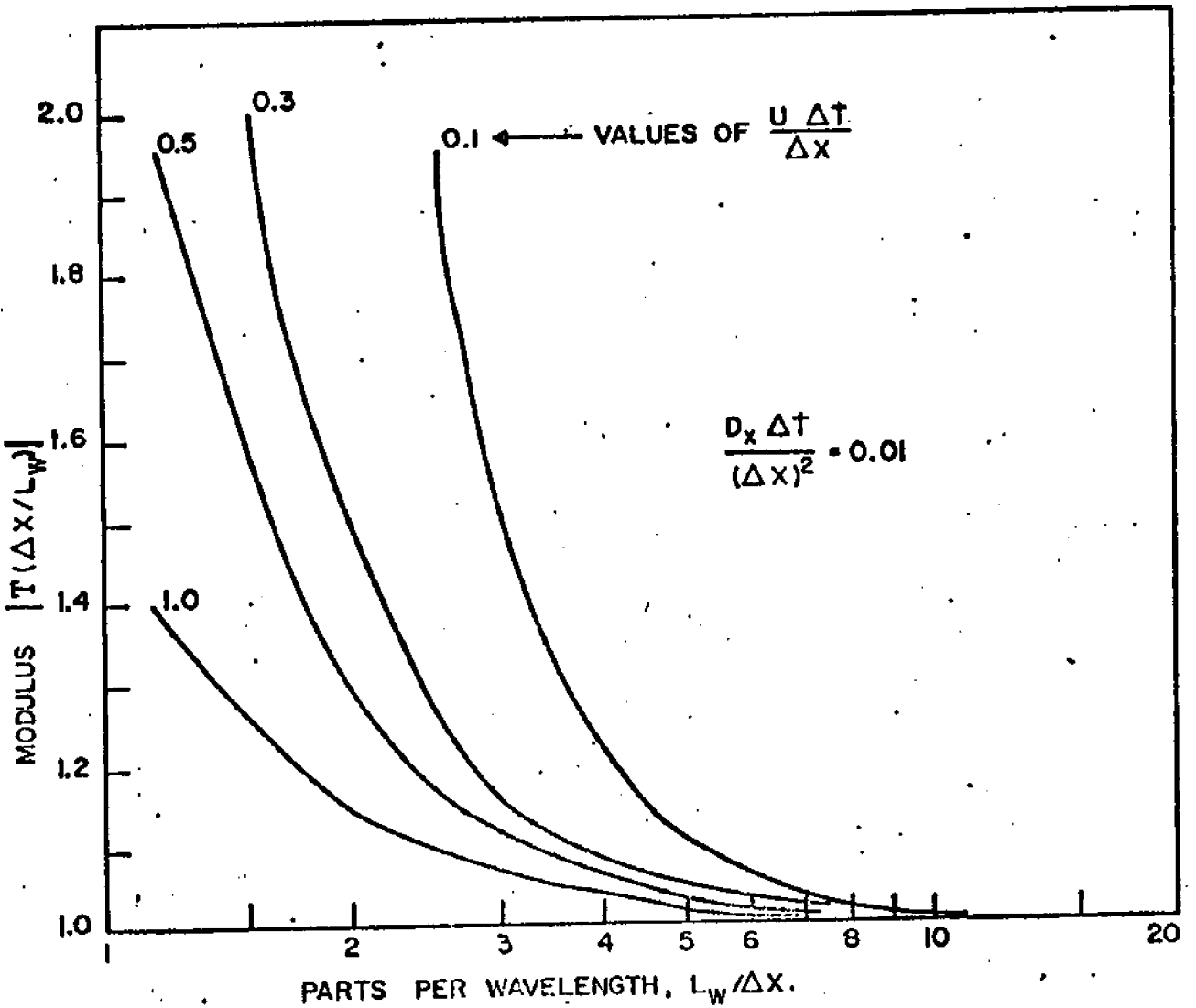

FIG. 4-2 MODULUS OF THE PROPAGATION FACTOR FOR DIFFERENT VALUES OF u $\Delta t/\Delta x$ WITH $D_x \Delta t/(\Delta x)^2 = 0.01$

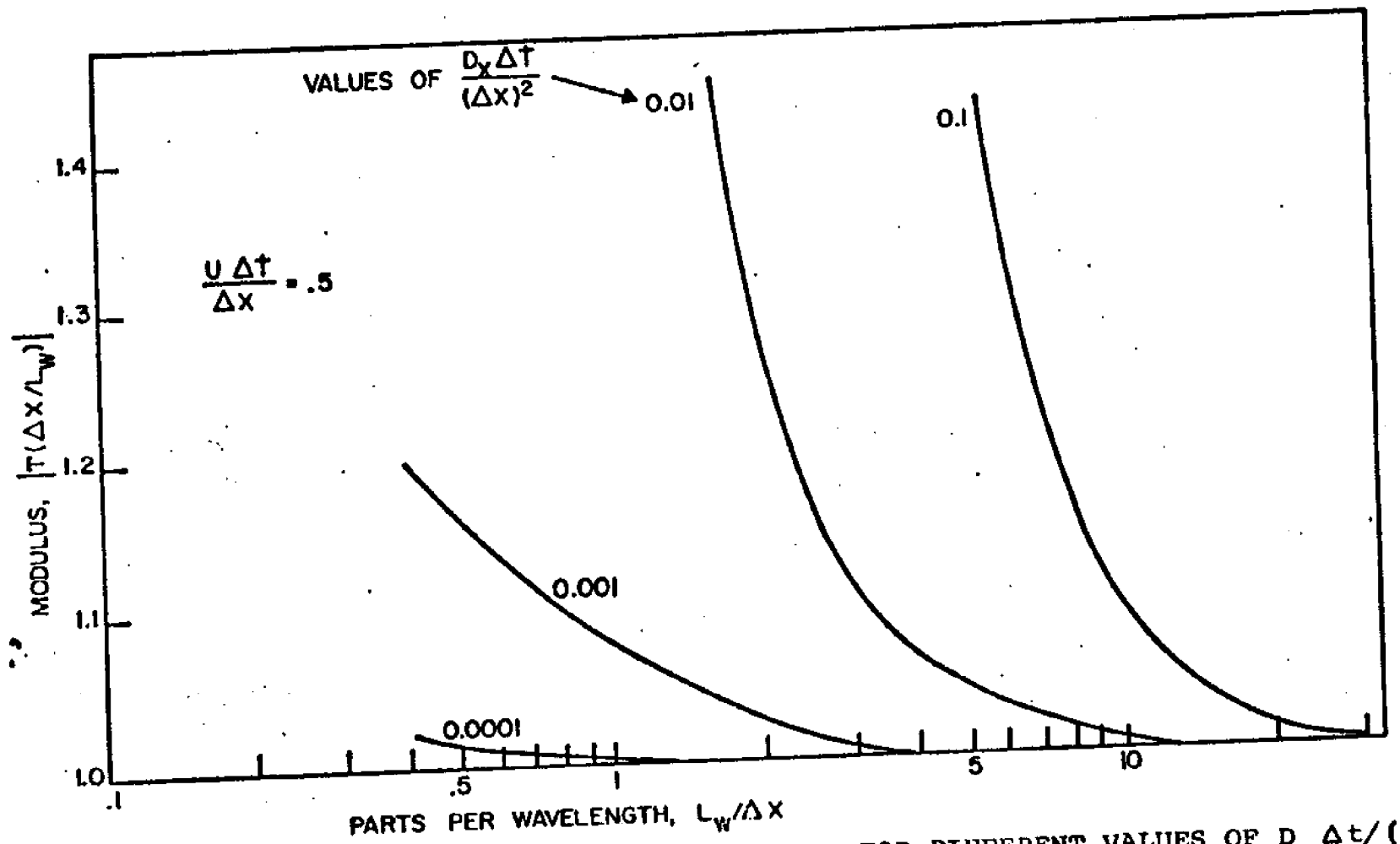

FIG. 4-3 MODULUS OF THE PROPAGATION FACTOR FOR DIFFERENT VALUES OF $D_x \Delta t/(\Delta x)^2$ WITH $u \Delta t/\Delta x = .5$

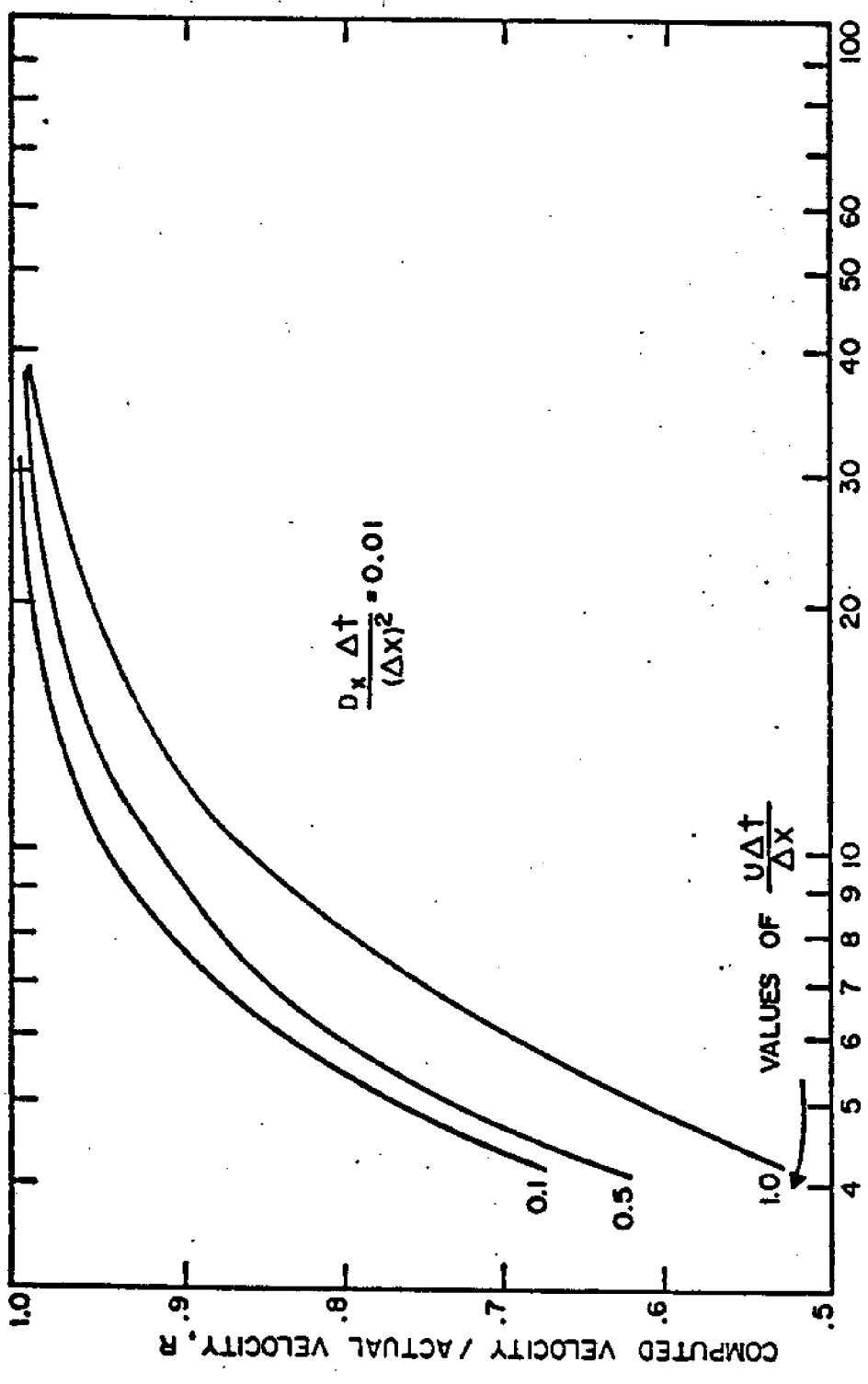

FIG. 4-4 PHASE ANGLE OF THE PROPAGATION FACTOR FOR DIFFERENT VALUES OF $u\,\Delta t/\Delta x$ WITH $D_x\,\Delta t/(\Delta x)^2 = 0.01$

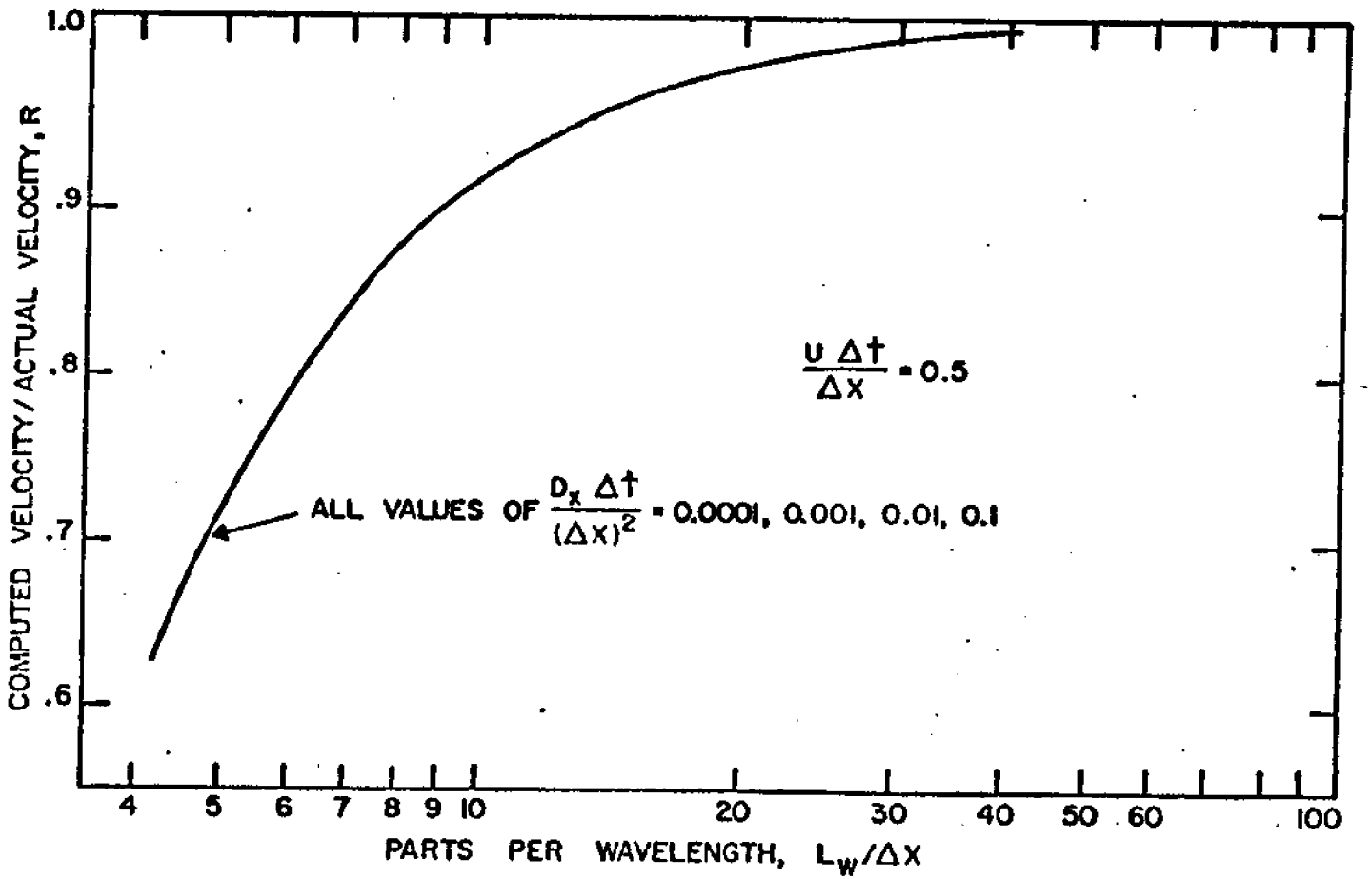

FIG. 4-5 PHASE ANGLE OF THE PROPAGATION FACTOR FOR DIFFERENT VALUES OF $D_x\,\Delta t/(\Delta x)^2$ WITH $u\,\Delta t/\Delta x = 0.5$

In summary then the Figs. 4-2 through 4-5 shpw that:

1. Increasing of $L_w / \Delta x$, grids per wavelength, produce better agreement between the physical and computational models.
2. Decreasing $\frac{D_x \Delta t}{(\Delta x)^2}$ at a constant $\frac{u \Delta t}{\Delta x}$ improves results.
3. Increasing of $\frac{u \Delta t}{\Delta x}$ at constant $\frac{D_x \Delta t}{(\Delta x)^2}$ improves results.
4. In general at least 10 grid spaces per wavelength must be used for an adequate solution.

STABILITY ANALYSIS

In order to better understand of stability for this particular problem the Von Neumann method will be employed again, but in a slightly different manner to show that this finite-difference approximation to the mass transport equation in two dimensions (x,z) is always stable. It must be remembered however, that only when it is shown that the solution is also convergent and satisfies the

dissipative and dispersive requirements is the solution algorithm using these finite-difference approximations a fruitful scheme. The following presentation is similar to Mitchell's approach for two-dimensional stability analysis. For a definition of stability assume that:

$P^{\ell}_{m,n}$ - theoretical solution of the finite-difference equation.

and

$\tilde{P}^{\ell}_{m,n}$ - numerical solution of the finite-difference equation.

where

$$P^{\ell}_{m,n} = P\,(m\Delta x,\ n\Delta z,\ \ell\Delta t)$$

Taking the difference of these two quantities we obtain:

$$P^{\ell}_{m,n} - \tilde{P}^{\ell}_{m,n} = Z^{\ell}_{m,n} \qquad (4.32)$$

Now for stability to exist, $Z^{\ell}_{m,n}$ must remain bounded as ℓ increases, while Δt remains fixed for all m and n.

The Von Neumann method of analysis claims that a harmonic decomposition can be made of the error Z at discrete grid points at a given time level, leading to the error function

$$E(x) = \sum_j A_j e^{i\beta_j x} \qquad (4.32a)$$

where in general the frequency (β_j) and j are arbitrary. For an analysis it is necessary only to consider a single term of Eq. (4.32a), $e^{i\beta_s x}$ where β_s is any real number. To investigate the error propagation as time increases then it is necessary to find a solution of the finite-difference equation which reduces to $e^{i\beta_s x}$ when t = 0. Let this solution be

$$e^{\alpha_s t} e^{i\beta_s x} \qquad (4.33)$$

where $\alpha_s = \alpha_s(\beta_s)$ is, in general, complex. Now the original error component $e^{i\beta_s x}$ will not grow with time provided that:

$$\left| e^{\alpha_s l} \right| \leq 1 \qquad (4.33a)$$

for all α_s. This is Von Neumann's criteria for stability.

When using the Von Neumann method the following points should be remembered (28):

1. The method which is based on the Fourier series applies only if the coefficients of the linear

differential equation are constant. No method has been derived for non-constant coefficients at present. If the difference equation has variable coefficients the method can still be applied locally and it might be expected that a method will be stable if the Von Neumann condition derived as though the coefficients are constant, is satisfied at every point of the field. There is much numerical evidence to support this contention (28).

2. For two-level difference schemes with one dependent variable and any number of independent variables, the Neumann condition is sufficient as well as necessary for stability. Otherwise, the condition is only necessary.

3. Boundary conditions are neglected by the Von Neumann method, which applies strictly only to pure initial value problems with periodic initial data.

Now taking the finite-difference equation as found in Eq. (3.20) we have:

$$\left[1 - \frac{r_{11}}{2B_o} \delta_x (BD_x \delta_x) \right] \left[1 - \frac{r_{22}}{2B_o} \delta_z (BD_z \delta_z) \right]$$

$$\left[1 + \frac{r_1}{2B_o} \delta_x (UB) \right] \left[1 + \frac{r_2}{2B_o} \delta_z (WB) \right] P_{m,n}^{\ell+1} =$$

$$\left[1 + \frac{r_{11}}{2B_o} \delta_x (BD_x \delta_x) \right] \left[1 + \frac{r_{22}}{2B_o} \delta_z (BD_z \delta_z) \right]$$

$$\left[1 - \frac{r_1}{2B_o} \delta_x (UB) \right] \left[1 - \frac{r_2}{2B_o} \delta_z (WB) \right] P_{m,n}^{\ell} \qquad (3.20)$$

To begin the stability analysis it is assumed that at a given instant B_o, W, U, D_x and D_z are locally constant. Therefore, we may group constants, letting

$$a \equiv \frac{r_{11}}{2} \frac{B}{B_o} D_x$$

$$b \equiv \frac{r_{22}}{2} \frac{B}{B_o} D_z$$

$$c \equiv \frac{r_1}{2} \frac{UB}{B_o} \qquad (4.34)$$

$$d \equiv \frac{r_2}{2} \frac{WB}{B_o}$$

Substituting Eq. (4.34) into Eq. (3.20) and using Eq. (4.31) results in:

$$[1 - a\delta_x^2]\ [1-b\delta_z^2]\ [1+c\delta_x]\ [1 + d\delta_z]\ z_{m,n}^{l+1} =$$

$$[1+a\delta_x^2]\ [1+b\delta_z^2]\ [1-c\delta_x]\ [1-d\delta_z]\ z_{m,n}^{l} \qquad (4.35)$$

Now we can assume a solution form for $z_{m,n}^{l}$

$$z_{m,n}^{l} = e^{\alpha_s l \Delta t}\ e^{i\beta_s m \Delta x}\ e^{i\gamma_s n \Delta z} \qquad (4.36)$$

where α_s, β_s, γ_s are arbitrary constants. Remembering that for a stable solution Eq. (4.33) is applicable, we may expand Eq. (4.35). Neglecting higher order terms, and subsequently substituting Eq. (4.36), the result is:

$$\xi_s^{l+1}\, e^{i\beta_s m\Delta x}\, e^{i\gamma_s n\Delta z}\,(1+2a+2b) + \xi_s^{l+1}\, e^{i\beta_s(m+1)\Delta x}\, e^{i\gamma_s n\Delta z}\,(-a+c/2) + \xi_s^{l+1}\, e^{i\beta_s(m-1)\Delta x}\, e^{i\gamma_s n\Delta z}\,(-a-c/2) +$$

$$+ \xi_s^{l+1}\, e^{i\beta_s m\Delta x}\, e^{i\gamma(n+1)\Delta z}\,(-b+d/2) + \xi_s^{l+1}\, e^{i\beta_s m\Delta x}\, e^{i\gamma_s(n-1)\Delta z}\,(-b-d/2) =$$

$$\xi_s^{\ell} e^{i\beta_s m\Delta x} e^{i\gamma_s n\Delta z}(1-2a-2b) + \xi_s^{\ell} e^{i\beta_s(m+1)\Delta x} e^{i\gamma_s n\Delta z}(a-c/2) + \xi_s^{\ell} e^{i\beta_s(m-1)\Delta x} e^{i\gamma_s n\Delta z}(a+c/2) + \xi_s^{\ell} e^{i\beta_s m\Delta x} e^{i\gamma_s(n+1)\Delta z}(b-d/2) + \xi_s^{\ell} e^{i\beta_s m\Delta x} e^{i\gamma_s(n-1)\Delta z}(b+d/2)$$

(4.37)

where

$$e^{\alpha_s \ell \Delta t} = \xi_s^{\ell} \tag{4.38}$$

and now letting

(1 + 2a + 2b)	=	a1
(-a + c/2)	=	a2
(-a - c/2)	=	a3
(-b + d/2)	=	a4
(-b - d/2)	=	a5
(1-2a-2b)	=	a6

(4.39)

Then using the relations in Eq. (4.39) and dividing Eq. (4.37) by $\xi_s^{\ell} e^{i\beta_s m\Delta x} e^{i\gamma_s n\Delta z}$ and rearranging we obtain:

$$\xi_s = \frac{a6 - e^{i\beta_s \Delta x}(a2) - e^{-i\beta_s \Delta x}(a3) - e^{i\gamma_s \Delta z}(a4) - e^{-i\gamma_s \Delta z}(a5)}{a1 + e^{i\beta_s \Delta x}(a2) + e^{-i\beta_s \Delta x}(a3) + e^{i\gamma_s \Delta z}(a4) + e^{-i\gamma_s \Delta z}(a5)}$$

(4.40)

To separate ξ_s into a real and an imaginary portion, the exponential terms are expanded to obtain:

$$\xi_s = \frac{AA - iAB}{BB + iBC} \tag{4.41}$$

where

$$\begin{aligned}
AA &= a6 - a2\cos(\beta_s \Delta x) - a3\cos(\beta_s \Delta x) - a4\cos(\gamma_s \Delta z) \\
&\quad - a5\cos(\gamma_s \Delta z) \\
AB &= a2\sin(\beta_s \Delta x) - a3\sin(\beta_s \Delta x) + a4\sin(\gamma_s \Delta z) - \\
&\quad a5\sin(\gamma_s \Delta z) \\
BB &= a1 + a2\cos(\beta_s \Delta x) + a_3\cos(\beta_s \Delta x) + a4\cos(\gamma_s \Delta z) \\
&\quad + a5\cos(\gamma_s \Delta z) \\
BC &= a2\sin(\beta_s \Delta x) - a3\sin(\beta_s \Delta x) + a4\sin(\gamma_s \Delta z) \\
&\quad - a5\sin(\gamma_s \Delta z)
\end{aligned}$$

(4.42)

or in an alternate form:

$$\xi_s = \frac{(AA)\ (BB) - (AB)\ (BC)}{(BB)^2 + (BC)^2} - i\,\frac{(BB)\ (AB) + (AA)\ (BC)}{(BB)^2 + (BC)^2} \qquad (4.43)$$

From previous results the solution to the finite-difference scheme is stable if $|\xi_s| \leq 1$. Numerical computations of Eq. (4.43) for arbitrary values of β_s and γ_s show that the scheme is unconditionally stable. Results of the computations are shown in Figs. 4-6 and 4-7 and show similar behavior as those outlined in Figs. 4-2 through 4-5.

CONVERGENCE

As was previously mentioned, for a finite-difference approximation to be valid not only has the solution to be stable but it also must be convergent. By convergent we mean that the theoretical solution of the differential and difference equations at a fixed point P (x,z,t), tends to zero uniformly as the net or grid size is refined in such a way that $\Delta x,\ \Delta z,\ \Delta t \longrightarrow 0$ and $m,n,\ell \longrightarrow \infty$

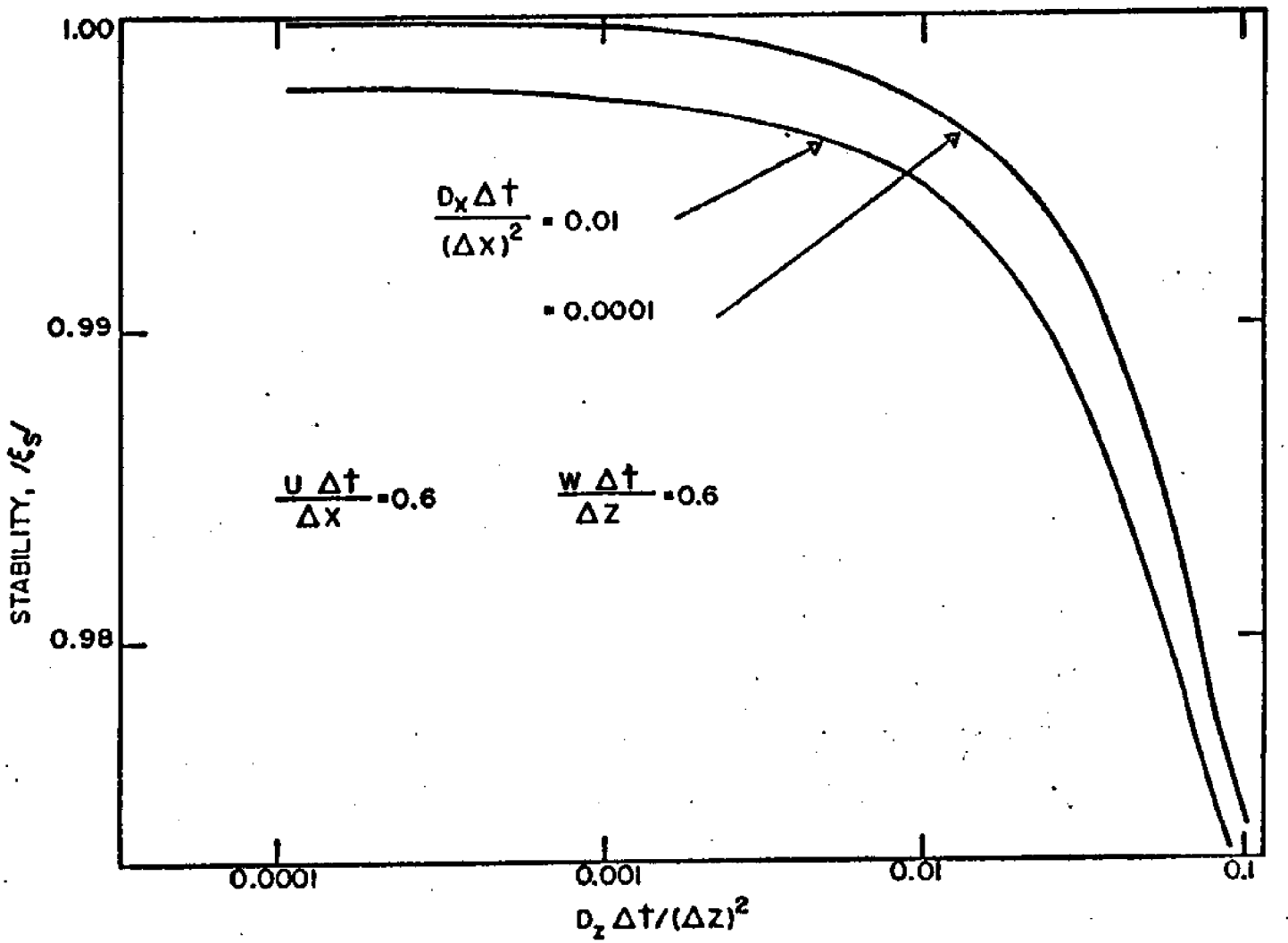

FIG. 4-6 STABILITY CHANGES CAUSED BY VARIATIONS IN $D_x \Delta t/(\Delta x)^2$

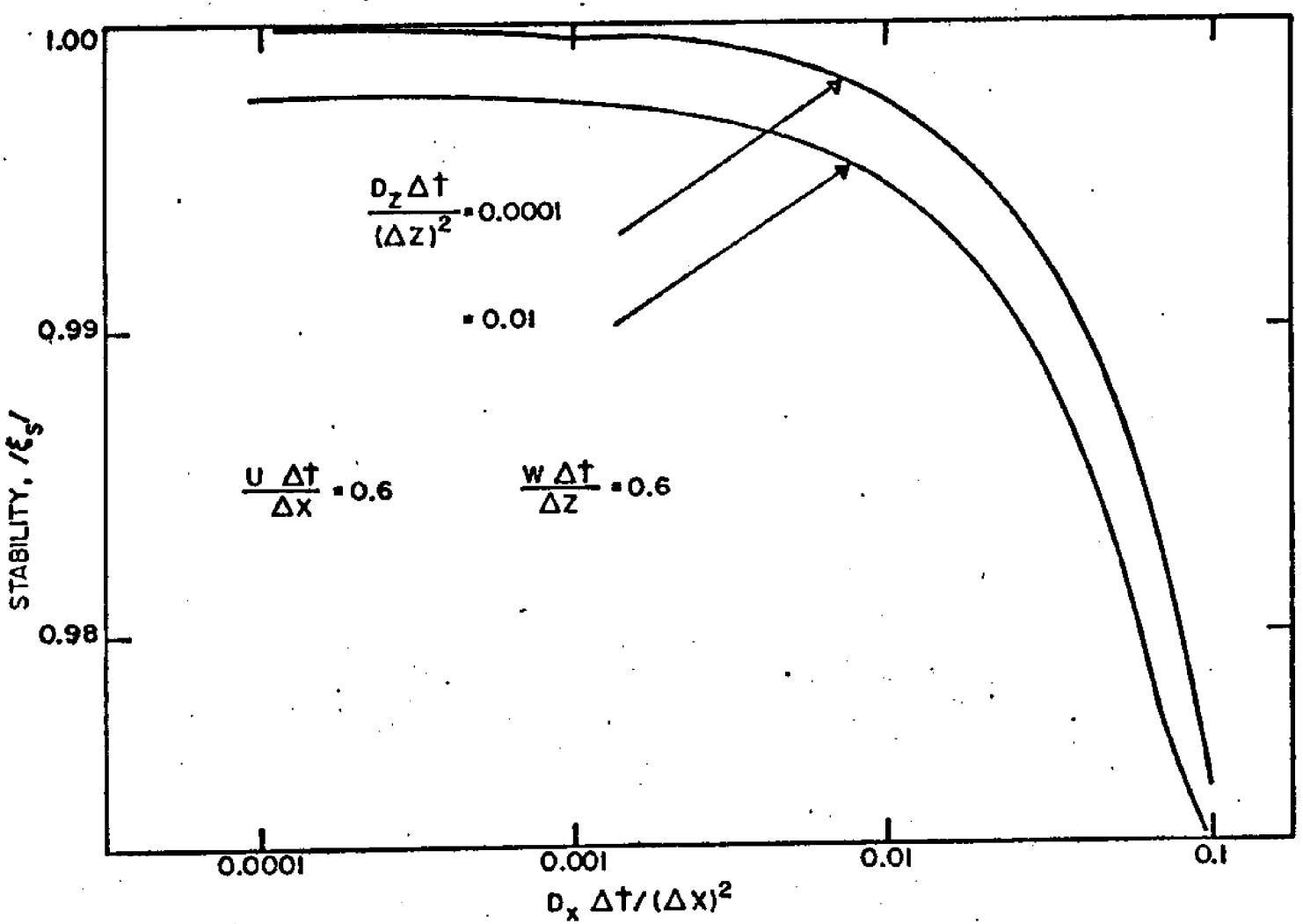

FIG. 4-7 STABILITY CHANGES CAUSED BY VARIATIONS IN $D_z \Delta t/(\Delta z)^2$

with $m\Delta x$, $n\Delta z$, and $\ell\Delta t$ remaining fixed. The fixed point $P(x,z,t)$ is anywhere within the solution region.

From the analysis carried out in the section on dispersive and dissipative aspects it can be seen that the solution of the difference equations converges to the theoretical solution of the differential equation. Further evidence that convergence is obtained is provided by the modeling efforts of Leenderste(6).

NUMERICAL DAMPING

The dispersion term in the parabolic equation for mass transport acts as a numerical damping term, since it helps to eliminate oscillations of a finite-difference solution about the true convergent solution. Such oscillations are frequently found in computational schemes (23). Perkins (30) has also shown similar results for attaining of both a stable and convergent solution. Figure 4-3 clearly displays this effect for the computational scheme which is being developed.

DISCONTINUITES

As has been mentioned previously finite-difference methods of the type developed in approximating the mass transport equation are well suited to slowly changing variables. In most estuarine problems, however, the sources of pollutant enter the model at discrete points. This is unfortunate from a computational view point since a finite-difference equation assumes immediate and complete mixing of the pollutant in a particular grid and thus a local disturbance is generated in the solution.

Just upstream of the discharge, a discontinuity in mass density exists. The computational scheme is unable to represent this discontinuity adequately since the Fourier series decomposition of this jump leads to many very short waves which cannot be resolved into the grid network and become aggregated into waves with a few parts per wavelength. These waves, because of dispersive effects, underestimate the influence of dispersion and lead to incorrect representations of the solution in the surrounding areas.

To overcome this problem artifical dispersion at the

location of discontinuities is often used (23), thus locally smoothing the solution. A convenient and expedient manner to accomplish this is by upstream flux differencing, which usually increases dispersion just enough to counter the generation of a spatial disturbance.

For example, if a source is located at the point m,n and the velocity U ((m + $\frac{1}{2}$)Δx, n Δz, ℓΔt) 0, then at the location (m + $\frac{1}{2}$)Δx, n Δ z,ℓΔt the mass flux flowing toward the point of discharge is computed to be UP where P is taken "upstream" at the location (m+1)Δx, n Δz,ℓΔt rather than being an averaged value, $\bar{P}^{x}$. This technique is more graphically presented in Table 4-1. Using this mass flux in the advective transport m Δx, n Δ z, (ℓ + $\frac{1}{2}$)Δt according to Leenderste(6) achieves conservation of mass of the substance and eliminates the problem. Numerical experiments with the two models confirm this mass conservation. With this approach the influence of the source at location m,n is not felt upstream other than through the contribution of the dispersion term. If, however, the normal finite-difference

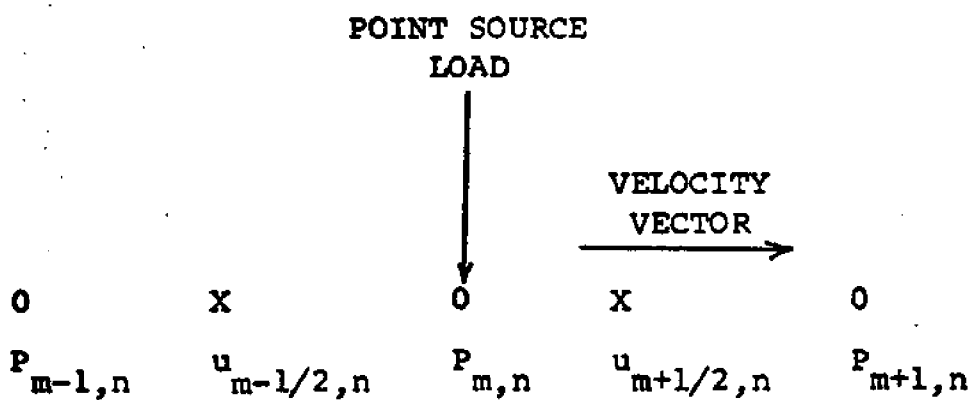

CONDITION: $u_{m+1/2} > 0$, SOURCE LOCATED AT POINT M, GOING FROM TIME LEVEL $\ell + \frac{1}{2}$ to $\ell + 1$.

OPERATION: AT POINT M

TERM	$P_{m-1,n}u_{m-\frac{1}{2},n}$	$P_{m,n}u_{m-\frac{1}{2},n}$	$P_{m,n}u_{m+\frac{1}{2}}$	$P_{m+1,n}u_{m+\frac{1}{2},n}$
	WEIGHTING FACTORS			
UPSTREAM FLUX DIFFERENCING	2	0	1	1
NORMAL TECHNIQUE	1	1	1	1

OPERATION: AT POINT M-1

TERM	$P_{m-2,n}u_{m-\frac{3}{2},n}$	$P_{m-1,n}u_{m-\frac{3}{2},n}$	$P_{m-1,n}u_{m-\frac{1}{2},n}$	$P_{m,n}u_{m-\frac{1}{2},n}$
	WEIGHTING FACTORS			
UPSTREAM FLUX DIFFERENCING	1	1	0	2
NORMAL TECHNIQUE	1	1	1	1

OPERATION: AT POINT M+1, NORMAL TECHNIQUE

TABLE 4-1 VARIATION IN COMPUTATIONAL SCHEME FOR POINT LOADING

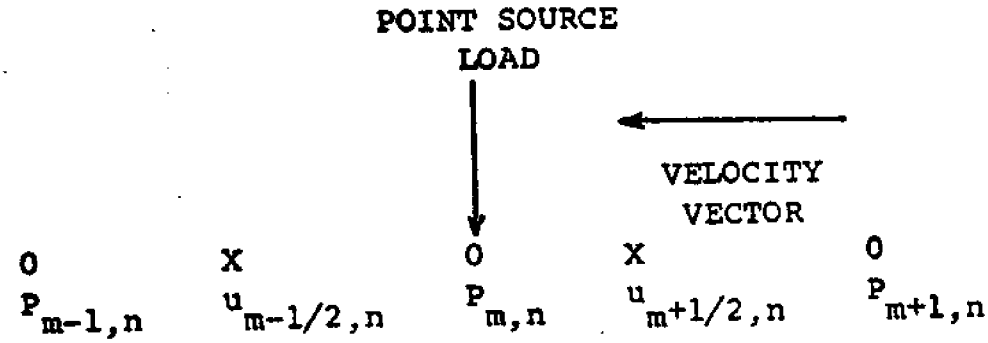

CONDITION: $u_{m+1/2}$ 0, SOURCE LOCATED AT POINT M GOING FROM TIME LEVEL $\ell + 1/2$ to $\ell + 1$

OPERATION: AT POINT M

WEIGHTING FACTORS

TERM	$P_{m-1,n}u_{m-\frac{1}{2},n}$	$P_{m,n}u_{m-\frac{1}{2},n}$	$P_{m,n}u_{m+\frac{1}{2},n}$	$P_{m+1,n}u_{m+\frac{1}{2},n}$
UPSTREAM FLUX DIFFERENCING	1	1	0	2
NORMAL TECHNIQUE	1	1	1	1

OPERATION: AT POINT M + 1

WEIGHTING FACTORS

TERM	$P_{m,n}u_{m+\frac{1}{2},n}$	$P_{m+1,n}u_{m+\frac{1}{2},n}$	$P_{m+1,n}u_{m+\frac{3}{2},n}$	$P_{m+2,n}u_{m+}$
UPSTREAM FLUX DIFFERENCING	2	0	1	1
NORMAL TECHNIQUE	1	1	1	1

OPERATION: AT POINT M-1, NORMAL TECHNIQUE

TABLE 4-1 (CONT'D) VARIATION IN COMPUTATIONAL SCHEME FOR POINT LOADING

equation is employed at the local discontinuity, the upstream mass density generally becomes severly suppressed and subsequentially leads to a dampened spatial oscillation.

In two-dimensional flows, the exact location of the discharge is not always known, and a highly complicated line of discontinuities can appear in the spatial field. Different approaches can be tried to remedy this effect. First we can neglect the effect altogether and interpret the computational model results accordingly, or secondly try to adjust the dispersion values, as considered previously. To accomplish this second method, results of numerical work on shock wave analysis by Lax and Wendroff as presented by Ritchmyer and Morton (23) are employed.

An added artifical dispersion, in this method, is employed whenever the mass density values are significantly different from surrounding values and no artifical dispersion is used if the mass density values are approximately equal to near-field values. For example, the dispersion terms take the form

$$D_{m+\frac{1}{2},n} = D_{m+\frac{1}{2},n}\left\{1 + \left[\frac{(P_{m+1,n} - P_{m,n})}{(P_{m+1,n} + P_{m,n})}\right]^2 e_D\right\}$$

$$D_{m,n+\frac{1}{2}} = D_{m,n+\frac{1}{2}}\left\{1 + \left[\frac{(P_{m,n+1} - P_{m,n})}{(P_{m,n+1} + P_{m,n})}\right]^2 e_D\right\} \qquad (4.44)$$

where e_D = constant

and similarly for $D_{m-1/2,n}$ and $D_{m,n-1/2}$

The addition of Eq. (4.44) to the computational scheme adds considerably to the computational time and the method of ignoring the complicated line discontinuity is usually chosen.

INTERMEDIATE BOUNDARY APPROXIMATIONS

The intermediate value $P^{\ell+\frac{1}{2}}$ introduced into the finite difference computational scheme outlined is not necessarily an approximation to the solution at any value of the time, despite the fact that we have referred to is as "the first-half of the time step" and in similar terms.

As a result, the boundary values at the intermediate level must be obtained, if possible, in terms of the boundary values at $t = \ell \Delta t$ and $t = (\ell + 1) \Delta t$. Mitchell (28) however states that as long as the boundary conditions do not display rapid changes with time and a lower accuracy method is used, that a simple averaging of the boundary conditions at the two time levels should be adequate. For the case of water quality parameters these assumptions are usually justified and the above intermediate boundary approximations are used.

COMMENTS ON HIGHER ORDER SCHEMES

In mathematical modeling, the spatial representation or discreteness is often a limiting factor, since large arrays must be kept in active computer memory. The representation of hydrographic data and the finite-difference approximations which are used give a rough approximation. Consequently higher order approximations in the spatial dimensions seldom provide a noticeable increase in accuracy. A better approach is to refine the size of the spatial grid spacing.

CHAPTER 5

COMPUTER MODELING VERIFICATION AND APPLICATION

CHOICE OF MODEL

It has been indicated that both a dimensional and a non-dimensional z-axis model have been developed for the laterally-averaged, mass-transport equation. An obvious question that arises is which model to use. To determine the appropriate choice one must first realize the constraints on each model. The dimensional z-axis model has a fixed surface - there can be no variation of the surface with time, as is found in all tidal situations - while the non-dimensional z-axis model can account for tidal height variations. Therefore, in general, when significant tidal height variations are encountered the non-dimensional z-axis model should be employed while for negligible tidal height variation the dimensional z-axis model may be employed. Another factor to consider is the vertical representation of the estuary. The non-dimensional model can easily handle a wide range in depths

whereas the dimensional model is fixed by a given grid size. Since the nondimensional model is the more widely applicable it is the one which has been used for the majority of the modeling verification effort. The dimensional model however has been verified to conserve mass and can therefore be employed as an engineering tool even though it has not been used extensively in this work.

APPLICABILITY OF THE PROPOSED MODEL

The two-dimensional, laterally-integrated, mass-transport model is valid only when the assumption of small lateral variations in mass density across any section in the estuary is true. For Narragansett Bay this assumption is a good approximation in the upper half of the Bay where water quality parameters or more correctly D.O. and B.O.D., display their largest variations.

Other assumptions made are that the dispersion coefficients can be adequately represented by empirical re-

lations. For this water quality model a modified Elder's approximation for longitudinal dispersion and Pritchard's model for vertical dispersion have been used. Of these two assumptions regarding the dispersive transport the second, Pritchard's , poses the most severe assumption since the whole vertical structure is determined by this formulation because the vertical velocities have been assumed to be negligible.

GRID SELECTION FOR NARRAGANSETT BAY

The selection of the grid size and the dimensions of the subsequent computational arrays are governed by several parameters. These variables include accuracy of solution desired, available computer storage space, program turn-around-time, and expense of computer time. For example, if a large grid size is chosen, computer time and storage is minimized, however the loss in accuracy of representation of the actual estuary may cause the results to be numerically correct for the equations but fruitless

in determining any of the significant variations in water quality parameters in the area. On the other hand if the grid size is decreased, computations must be made on more points which increase the computational effort by a factor inversely proportional to the square of the grid size (25). In addition, the time step size has to be decreased, since the dispersive properties of the computational method are related to the ratio of the time step to the spatial grid size and thus the computational effort becomes inversely proportional to the third power of the grid size. Now a better representation of the geographical area is obtained but the limits of computer storage are soon reached. No mention has been made of the expense and turn-around-time of computer operations but these also become important due to the size of computer storage involved. At best, the problem of determining the grid size is complicated and should be weighted very carefully in determining the modeling effort to be expanded.

To verify the mass-transport model, Narragansett Bay as shown in Fig. 5-1 was chosen. The area of interest included a region from Rhode Island Sound to the lower reaches

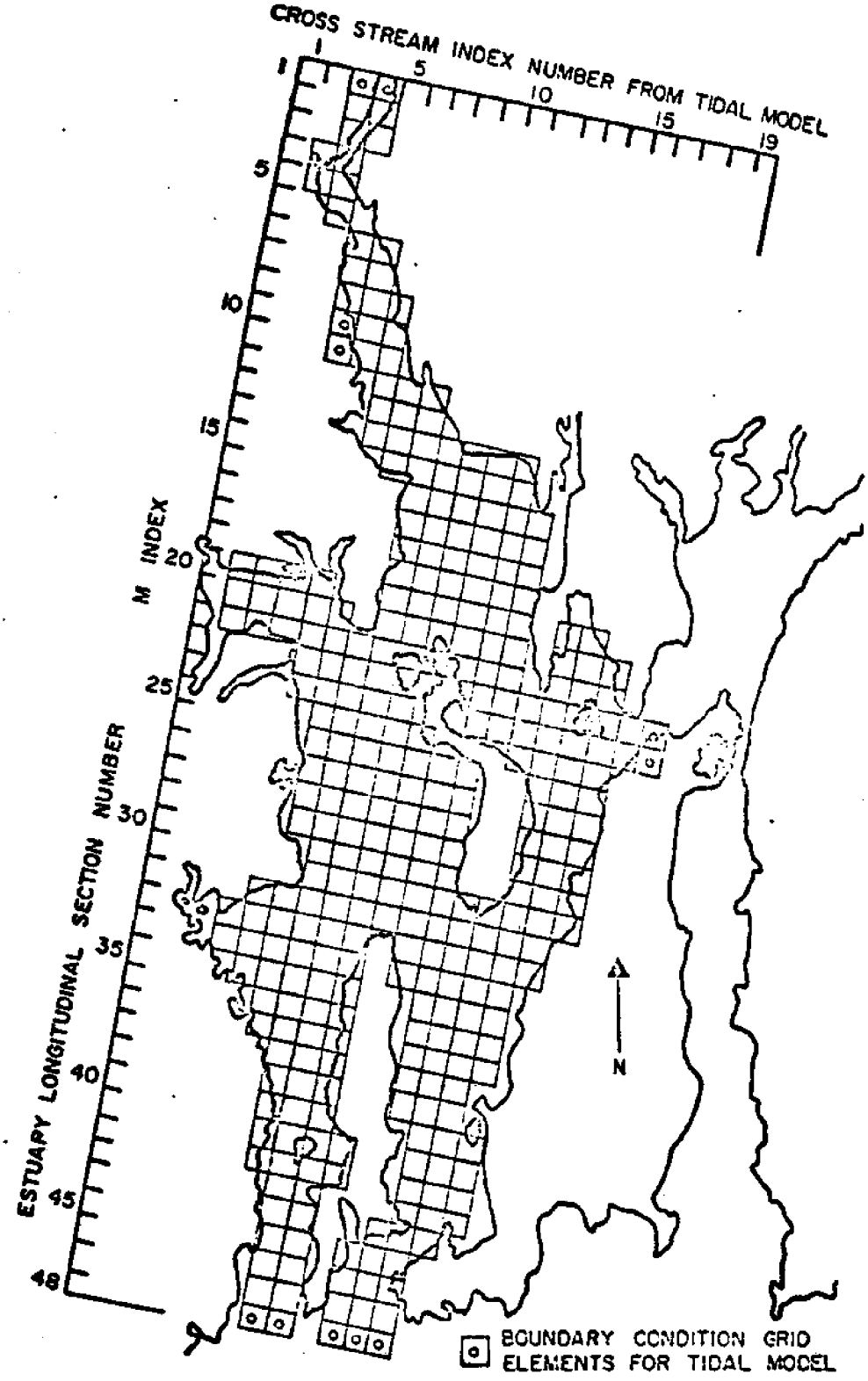

FIG. 5-1 LONGITUDINAL ESTUARY SECTION NUMBER LOCATIONS FOR NARRAGANSETT BAY

of the Seekonk River in Providence. Neither the Sakonnet River nor Mt. Hope Bay was included in this initial modeling program.

In order to achieve good spatial definition, 14 vertical grids for the non-dimensional z-axis model were chosen with 46 longitudinal grids of 3038 ft or 1/2 nautical mile (nm) along the estuary x-axis. With this combination the storage arrays for various water quality parameters were 16 X 50 leading to a total computer storage requirement of approximately 256 K bytes for the entire mass transport program.

GEOGRAPHICAL INPUT DATA

A good representation of the area under study from a geographical or bathymetric viewpoint is the first important step in any modeling effort. To obtain information on the average section depths and widths for Narragansett Bay Chart # 353 of the Coast and Geodetic Survey was employed, Fig. 5-2. In gathering this data however, the basic

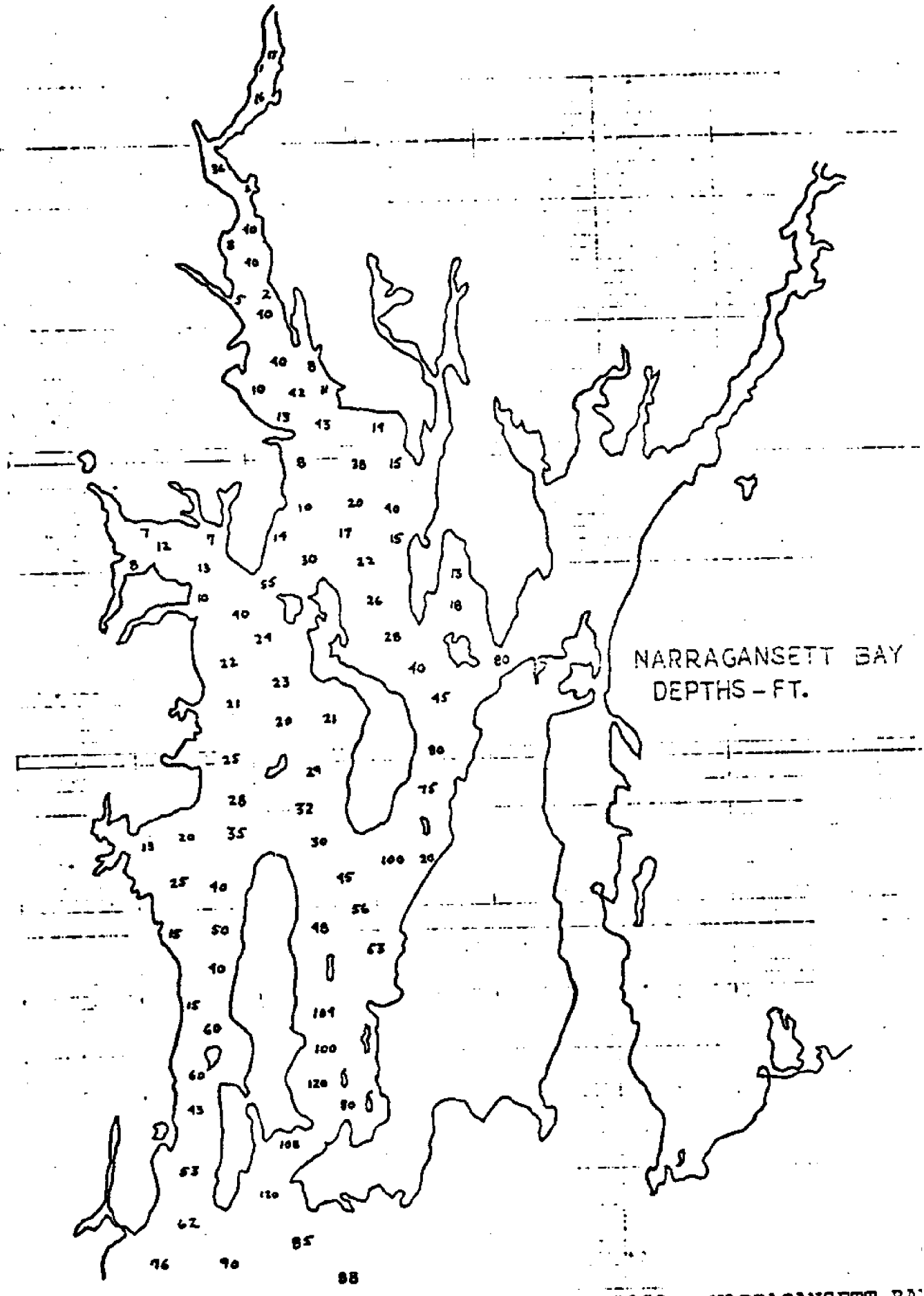

FIG. 5-2 COAST AND GEODETIC SURVEY MAP #353 - NARRAGANSETT BA

assumption of the model must be remembered - laterally integrated. This assumption can also involve averages over depths as well as cross sections. A typical example of this situation is observed at sections across the lower bay over the East and West Passages. Bathymetric data show large differences in the average depths of the two passages. To model the entire cross section then an average depth of the two passages is chosen and a new bottom profile developed. This approximation is used since dispersive relations for the model are directly related to the section depths, and since no cross sectional variations in depths occur in the model, the best estimate of the depth of that cross section for purposes of calculating a reasonable dispersive transport coefficient should be used. Fortunately, in Narragansett Bay, where this averaging process must be extensively employed, at the lower bay region, is the area in which water quality parameter variations are particularly small. However, for other estuaries this may not occur and the results of the model must be interpreted accordingly.

WATER QUALITY INPUT DATA AND BOUNDARY CONDITIONS

Good initial value arrays of the water quality variables help significantly reduce the computational time required to achieve a pseudo steady-state approximation to the water quality variables under investigation. To achieve this goal, data from the actual estuary can be used as initial conditions for the water quality model. In this light, all available D.O. and B.O.D. for Narragansett Bay were collected. laterally-averaged for each section and used as input conditions for the initial model run (8, 31, 32, 33).

For subsequent runs the output of the water quality model included a set of punched cards of the final field concentration which then could be employed as inputs for the next program simulation run.

The data for open boundary conditions for D.O. and B.O.D. were obtained from existing field data (8,31,32,33) and were held constant over the entire program running time. Indications have been made as to how values of mass densities can be extrapolated from within the field but were not used in the model since the simulation effort has initially been on long term variations due to a lack of

good accurate short term data. By long term it is meant that data over a particular season is being used.

HYDRODYNAMICS OF BAY

Since the mass-transport model as developed has no provisions for computing its own velocity fields these data, as a function of time, had to be found from another model or experimental data.

Based on the original tidal model, developed by Leenderste (9) a Narragansett Bay circulation and tidal hydraulics model was completed and verified (34). A grid size of 1/2 nm squares was chosen as shown in Fig. 5-1 for this effort. However, the assumptions of this model were that the momentum and continuity equations are vertically integrated and therefore the tidal velocities represent vertical averages over each section. By simply averaging the u velocities (x direction) across each section using a flow rate and dividing it by the cross sectional area, one obtains a pseudo, one-dimensional velocity field in the

x-direction. One can now assume that this is the driving force for the two-dimensional, vertically-structured water quality model being developed if the cross sectional flows or lateral flows are small and that the vertical velocities are negligible. For Narragansett Bay in the regions of greatest interest for water quality parameters, the upper Bay, both these assumptions are essentially true. The implications of this approximation for the velocity field are that the longitudinal advection and dispersion and the vertical dispersion are the primary mechanisms for constituent transport. The area in which these approximations are worst - in the lower bay - is where the water quality parameters show the least variation.

Therefore to drive the non-dimensional z-axis water quality model, cross-sectional averaged tidal height and tidal velocity, u , for each longitudinal section of the Bay were generated by the tidal hydraulics model and stored in computer memory. These data were taken by the above water quality model, forced to satisfy continuity of water over each grid in the field and then used as the velocity data for the model.

Numerical results show that this procedure leads to a fairly accurate representation of the velocity field, even considering that it has been forced to conform to a new grid system. A better approximation of course could be obtained by completely developing the corresponding non-dimensional z axis hydrodynamic model for the area.

The biggest drawback in employing this type of hydraulics model is its poor representation of the Providence River area. Since the hydrodynamics model attempts to match such a large area with as few grids as possible it was inevitable that areas with relatively small cross sections as the Providence River would be poorly modeled. An idea of the amount of this deviation from actual estuary geometry can be obtained by comparing the area modeled by the hydraulics model with the actual estuary cross-sectional area. Performing this operation shows that in the Providence River this ratio has values as large as 4.5 while in the remainder of the estuary the ratio falls between .85 and 1.2. Also, when the velocity field is forced to obey a continuity equation, before being used in the mass-transport equation, the small but yet all important net outward trans-

port due to river inputs and land runoff is lost. To counter this loss a source of inflow term was added to the continuity equation.

A comparison of all velocity profiles determined from the hydraulics model, forced to obey a continuity equation with and without corrections for river inputs can be seen in Fig. 5-3. It is noted that the agreement between the continuity equation forced velocity profile and that supplied by simply obtaining the average u velocity field for each section is remarkably good. The places of significant deviation occur, as can be noted from Fig. 5-1, when the actual estuary area being modeled displays significant cross stream velocities. Observation of the addition of the river inflows shown only slight variation from the forced continuity equation results and only in the Providence River area are the values noticeable where the cross sectional areas are particularly small in comparison to tidal model areas. Several runs were made which tried to correct the river inflows by using the tidal model cross sectional area, actual estuary cross sectional area ratio in

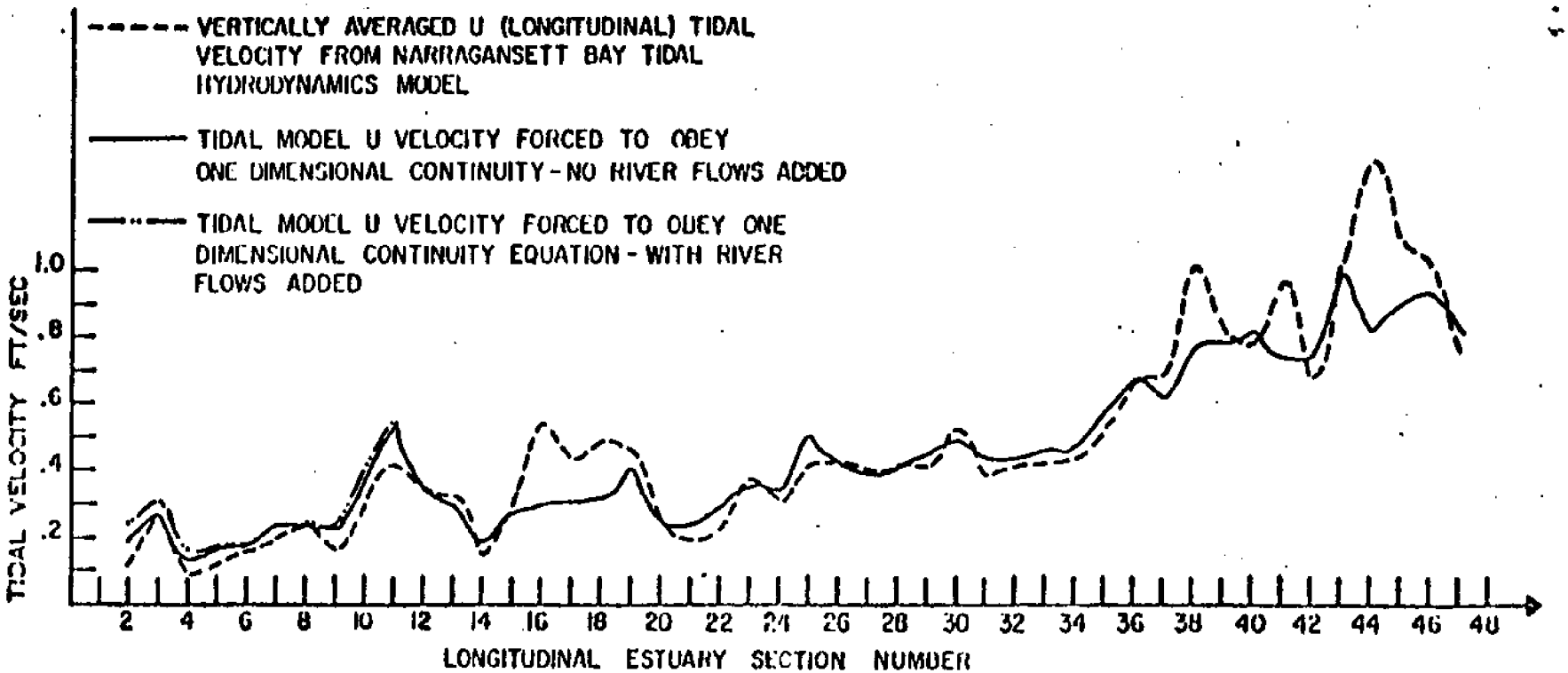

FIG. 5-3 COMPARISON OF LONGITUDINAL TIDAL VELOCITY FROM VERTICALLY AVERAGED TIDAL HYDRAULICS MODEL TO ONE DIMENSIONAL FORCED CONTINUITY EQUATION WITH AND WITHOUT RIVER INFLOWS FOR A GIVEN TIME

an attempt to make the model more representative of actual conditions. This approach however proved fruitless since the magnitude and variability of these correction factors caused the solution to oscillate considerably. Therefore the uncorrected river input continuity equation is used as the tidal velocity input and the results interpreted accordingly.

MODEL VERIFICATION OF DISSOLVED OXYGEN-BIOCHEMICAL OXYGEN DEMAND SYSTEM

In order to verify the reaction scheme for the D.O.-B.O.D. system the model with geometry for Narragansett Bay was run under a zero B.O.D. loading condition. It is important to realize that this exercise does not imply any final results of estuary cleanup time but merely demonstrates the response of the model and the subsequent changes in D.O.and B.O.D. concentrations.

Using initial profiles of D.O. and B.O.D. obtained from existing data for the Bay (8,31,32,33) the model was run for a period of about 24 days. All boundary conditions were linearly extrapolated to their cleanup values over a 2 day period (i.e. B.O.D. concentration to 0.0 and D.O. concentration to saturation value) and remained constant at that level throughout the following days. Since the reareation process is particularly slow for large deep bodies of water a value of thirty times the Dobbins-O'Connor (35) reareation coefficient was chosen to accelerate the surface reoxygenation phenomena. The decay coefficient was also chosen with similar reasoning in regards to the decay of

B.O.D. with a value of .25 day $^{-1}$.

Figures 5-4 and 5-5 display the vertically-averaged profiles of D.O. and B.O.D. respectively, in four day intervals beginning with the initial conditions, where the longitudinal estuary section numbers are equivalent to the M values shown in Fig. 5-1. The decrease of B.O.D. due to flushing and natural decay processes is readily demonstrated in Fig. 5-4. It is also to be noted that the decay model for B.O.D. is a first order process which is clearly demonstrated by the decreasing difference between the B.O.D. profiles as time progresses. Simultaneous with the decrease of these B.O.D. concentrations, the D.O. (Fig. 5-5) exhibits the expected increase due to dispersion and reareation. In the early stages, between the initial profile and the levels at 12 days, however the vertically-averaged D.O. concentration display levels below the initial. This phenomena can be attributed to the large loadings of B.O.D. during the first few days, again due to the first order decay process. Another point of interest is the peak which occurs in the neighborhood of estuary longitudinal section numbers 11, 12, 13 . Careful observation of the grid sectioning in Fig. 5 - 1

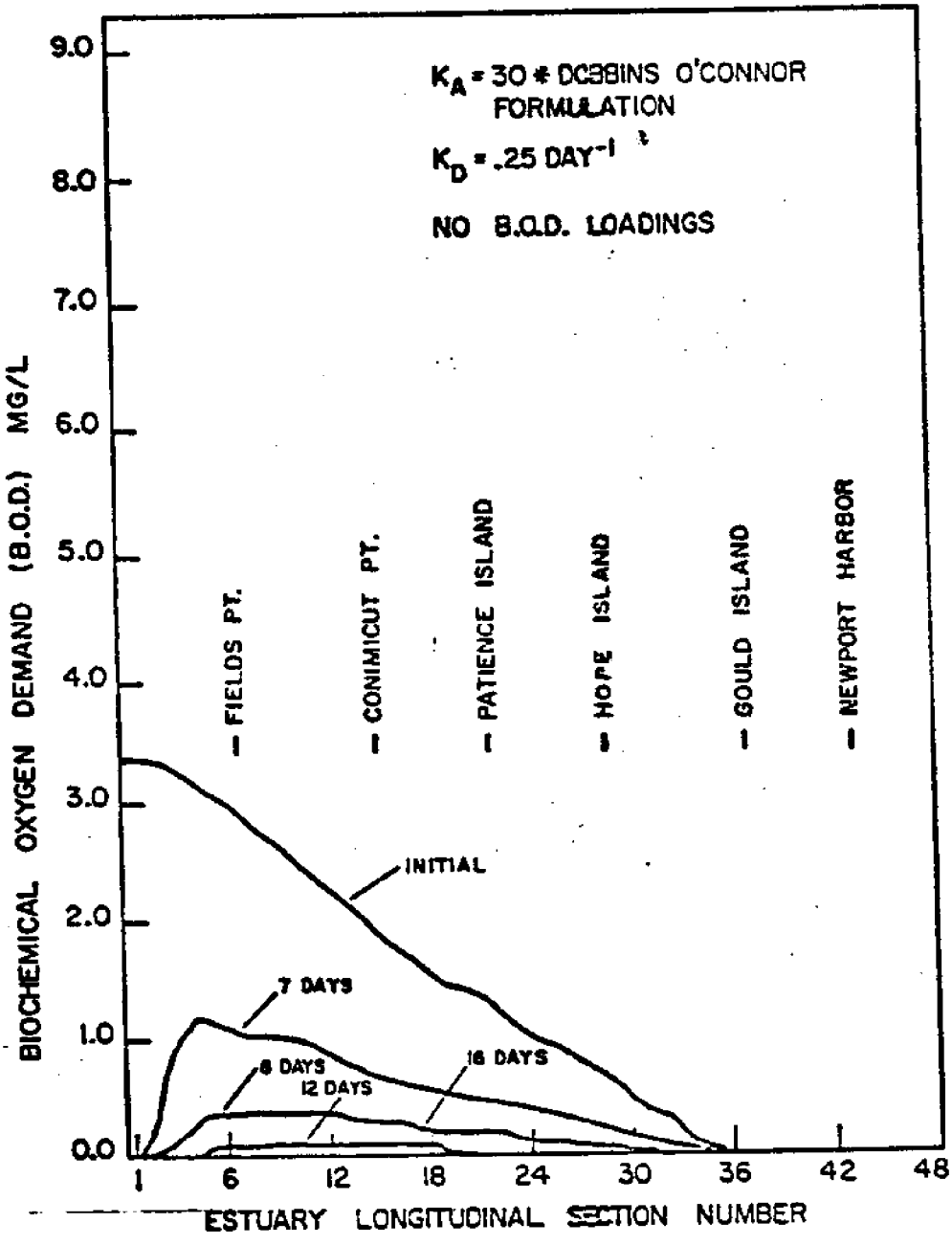

FIG. 5-4 VARIATIONS IN DEPTH AVERAGED BIOCHEMICAL OXYGEN DEMAND FOR ESTUARY CLEANUP CASE (NO. B.O.D. LOADINGS)

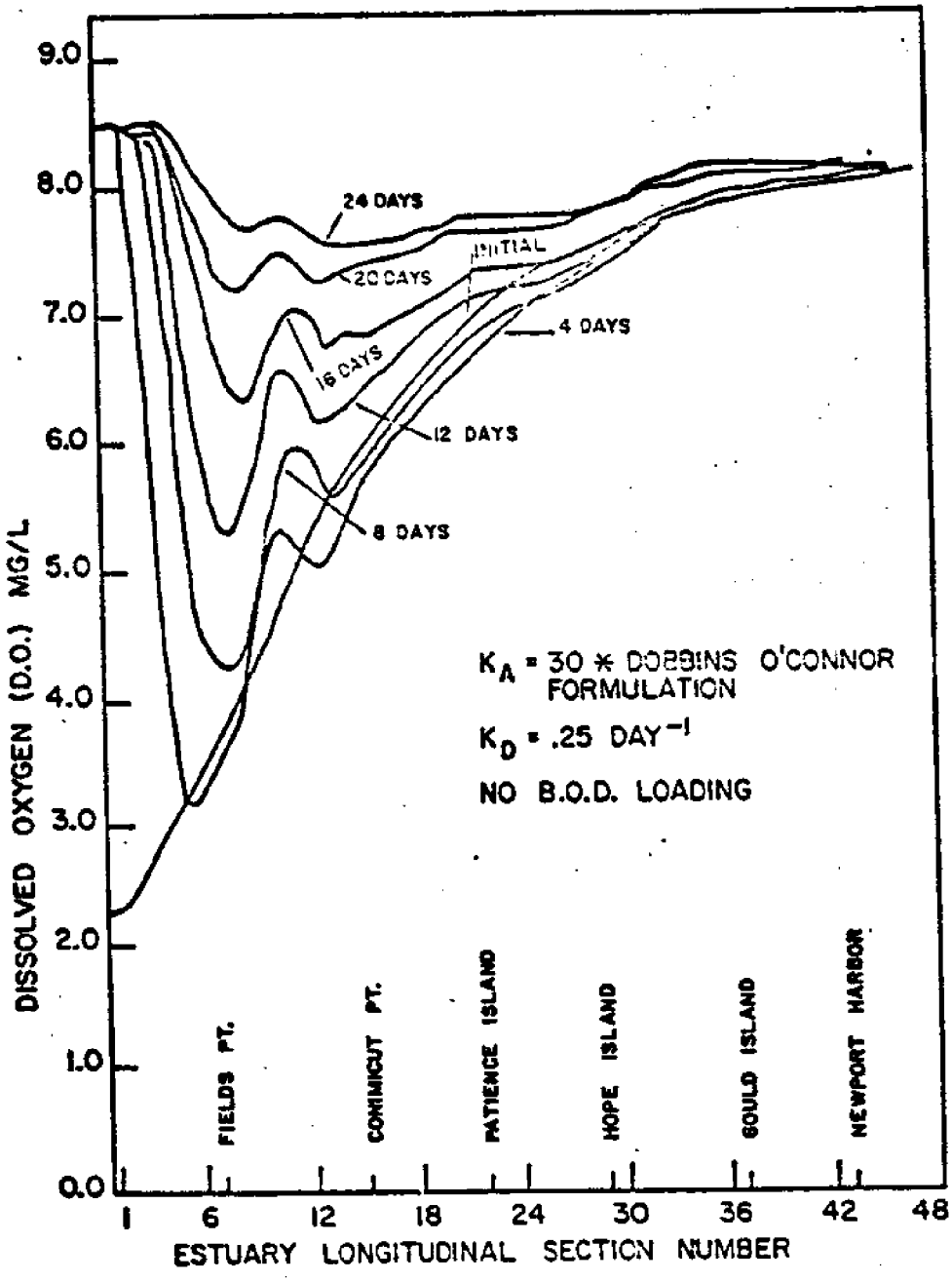

FIG. 5-5 VARIATIONS IN DEPTH AVERAGED DISSOLVED OXYGEN FOR ESTUARY CLEANUP CASE (NO. B.O.D. LOADINGS)

shows that there is a factor of about 2 change in the cross sectional area which leads to large velocity changes and subsequent increases in the reareation coefficient.

MODEL EXPERIMENTS WITH THE D.O. - B.O.D. SYSTEM

In order to further verify that the coupled D.O. - B.O.D. system has been correctly modeled and in addition obtain information on how changes in the basic coefficients of reareation and B.O.D. decay affect overall profiles, several computer runs were executed varying these parameters. Figures 5-6 and 5-7 show the D.O. and B.O.D. profiles, respectively, plotted against the estuary longitudinal section numbers, as defined in Fig. 5-1 for a constant reareation coefficient and variable B.O.D. decay constants.

The reareation coefficient chosen was that developed by O'Connor and Dobbins (35) and adjusted by a factor of 3 to obtain a fairly good approximation to general estuarine reareation processes for the area. The decay coefficients for B.O.D. were then chosen to represent both the

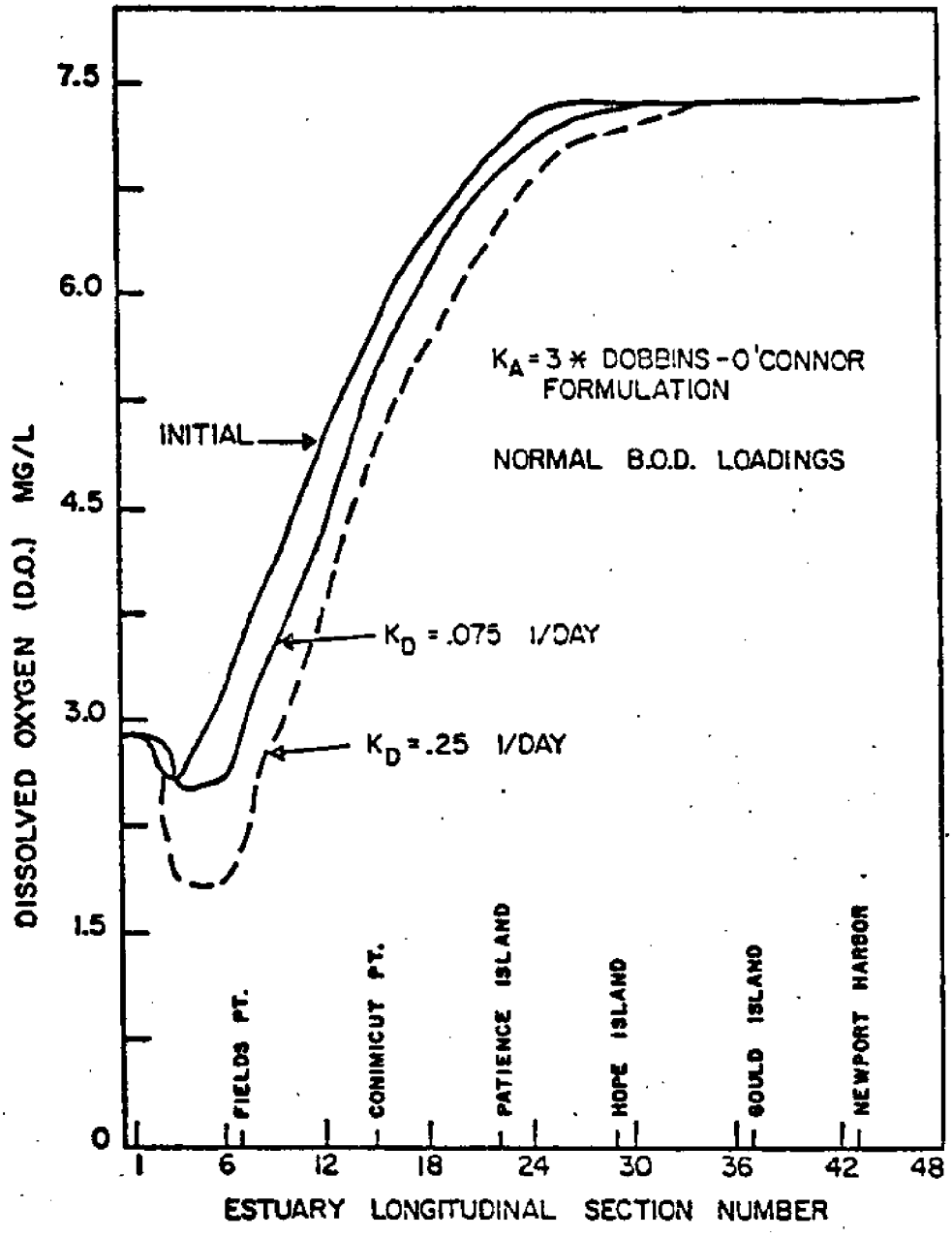

FIG. 5-6 INFLUENCE OF K_D ON DEPTH AVERAGED D.O. PROFILE FOR CONSTANT K_A AFTER 2 DAY SIMULATION TIME

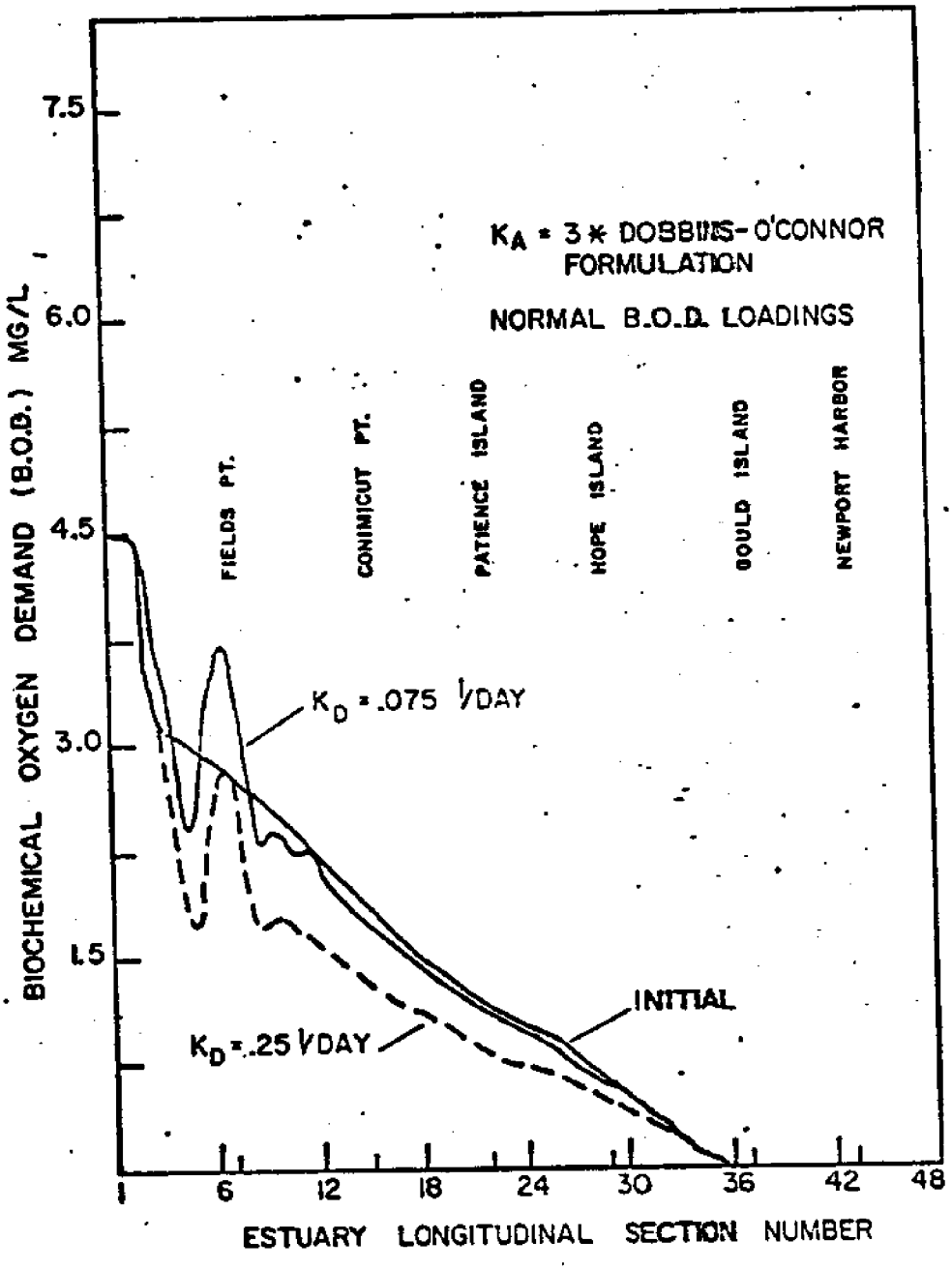

FIG. 5-7 INFLUENCE OF K_D ON DEPTH AVERAGED D.O. PROFILE FOR CONSTANT K_A AFTER 2 DAY SIMULATION TIME

high and low values for a typical estuary system. In obtaining Figure 5-6 and 5-7 initial estimates of D.O. and B.O.D. profiles were selected and the computer model of the oxygen system was begun with a typical sewage loading distribution as shown in Table 5-1, and geometry for Narragansett Bay. These initial estimates do not represent steady state values but are taken from a summation of the available data. The largest load of pollutants can readily be seen occuring at estuary longitudinal section number 7. The depression on either side of this large load, as noted in Fig. 5-7, can be attributed to a lack of adequate dispersion where concentration gradients become increasingly large. In such circumstances in a natural environment the dispersion coefficient is locally increased to smooth out the discontinuity of concentration. If left to continue on its present path for a period longer than the two day simulation run shown, the concentration on either side of the grid which is heavily loaded will become negative - an unrealistic situation for an actual estuary. However, of particular interest here is that as the B.O.D. coefficient is raised from .075 day^{-1} to .25 day^{-1} there appears a significant decrease in the amount

of B.O.D. present. This phenomena can be attributed to the normal first-order decay process of B.O.D. Subsequently, the D.O. profile shows a considerable decrease with increase in B.O.D. decay coefficient which again may be attributed to the first-order decay process drawing on the available oxygen in the surrounding water column.

Using similar starting conditions as have been previously noted - the D.O. - B.O.D. system model was again run for Narragansett Bay with constant B.O.D. decay coefficient of .1 day^{-1} but variable reareation coefficient, 3. and 30. times the O'Connor-Dobbins (35) formulation. Figures 5-8 and 5-9 present the results of these runs. It can be seen from Fig. 5-8 that as the reareation coefficient is increased more oxygen is forced into the water mass. A peculiarity shown by Fig. 5-8 is the large amount of oxygen added around estuary longitudinal grid section number 3-4, this can be attributed to a change in depth of the water column at that point of a factor of 3. Now since the Dobbins-O'Connor reareation formulation is proportional to $H^{-3/2}$ the reason for this large input is explained. In addition Fig. 5-9 shows that variations of reareation coefficient have essentially no effect on the

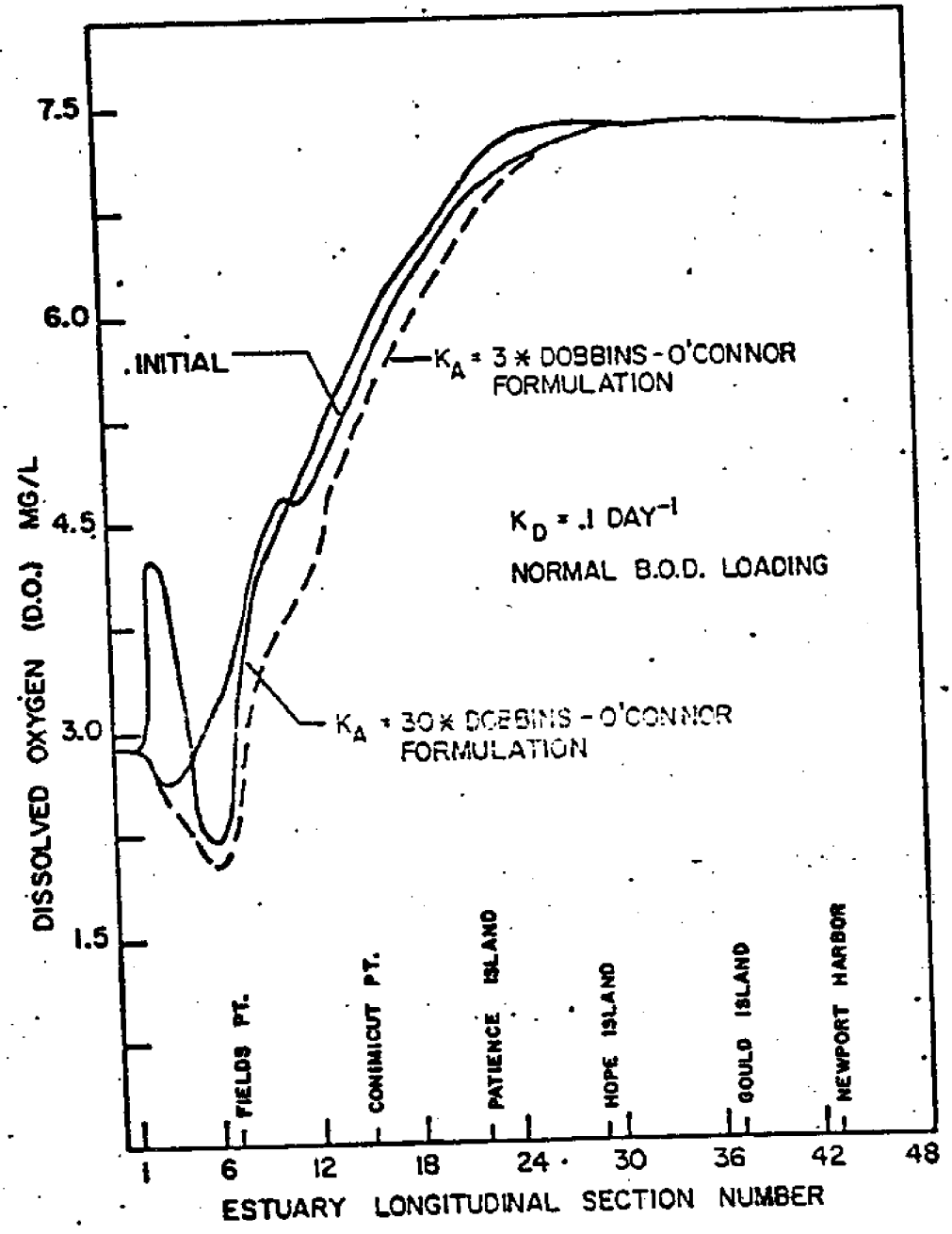

FIG. 5-8 INFLUENCE OF K_A ON DEPTH AVERAGED D.O. PROFILE FOR CONSTANT K_D AFTER 2 DAY SIMULATION TIME

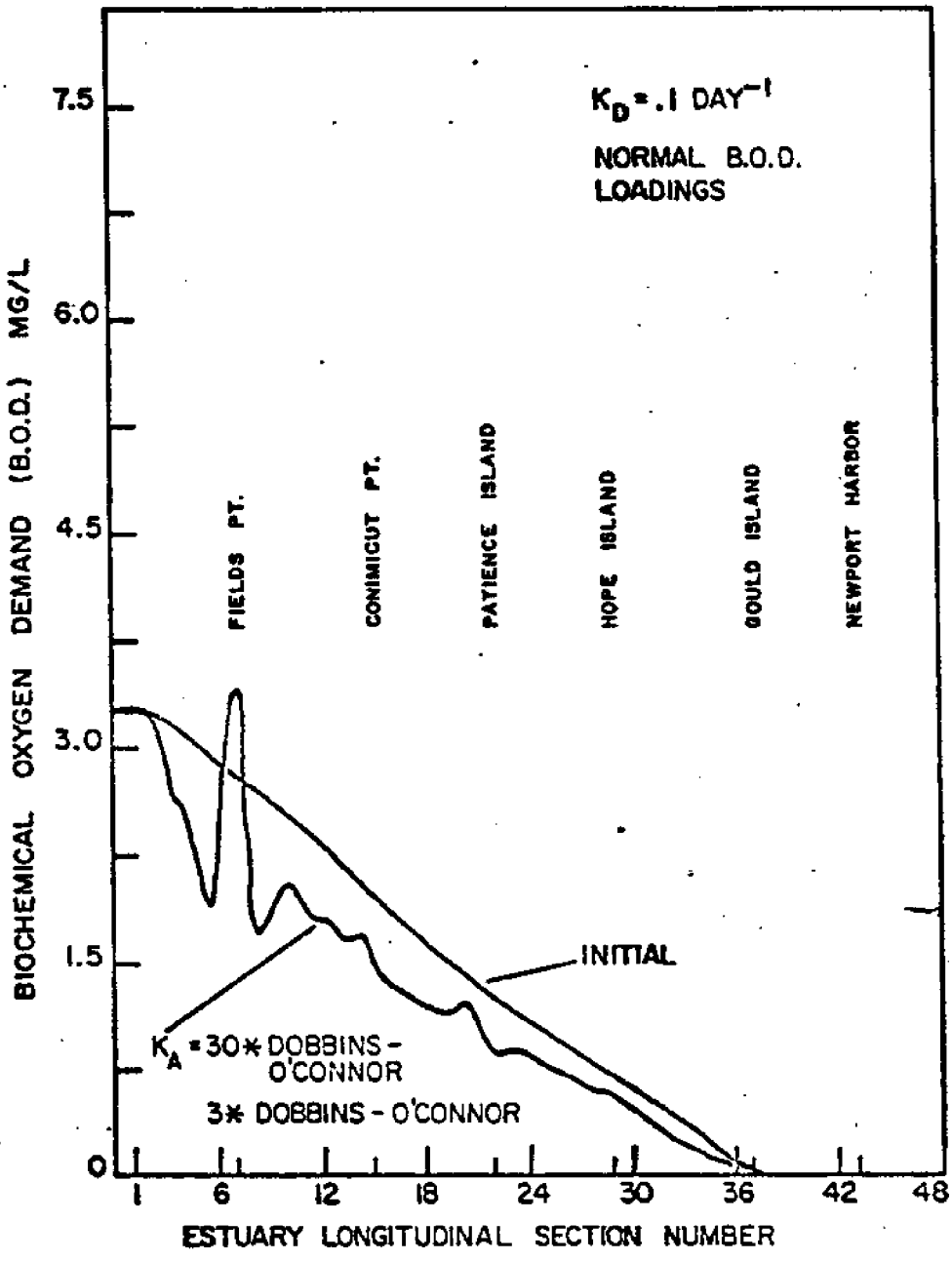

FIG. 5-9 INFLUENCE OF K_A ON DEPTH AVERAGED D.O. PROFILE FOR CONSTANT K_D AFTER 2 DAY SIMULATION TIME

B.O.D. profile. This can be easily understood since the D.O. - B.O.D. equation coupling occurs only through a B.O.D. decay term or, in other words, the D.O. has no direct effect on the B.O.D. profile.

TEMPERATURE EFFECTS ON THE D.O. - B.O.D. PROFILES

To simulate the effect of variation in water temperature on the D.O. - B.O.D. profiles the non-dimensional vertical axis computer model was run for two different water surface temperature levels of 65 and 55° F which were kept constant over the entire Bay until a quasi steady-state was achieved. Figure 5-10 presents the comparison of the D.O. and B.O.D. profiles for each case. Since the effect of temperature is included only in the saturation and reareation values of D.O. at the estuary surface one would expect changes only to occur in the level of D.O. in the water column. This indeed is the case as shown in the figure for these vertically-averaged profiles.

Vertical profiles of D.O. show that the increase in

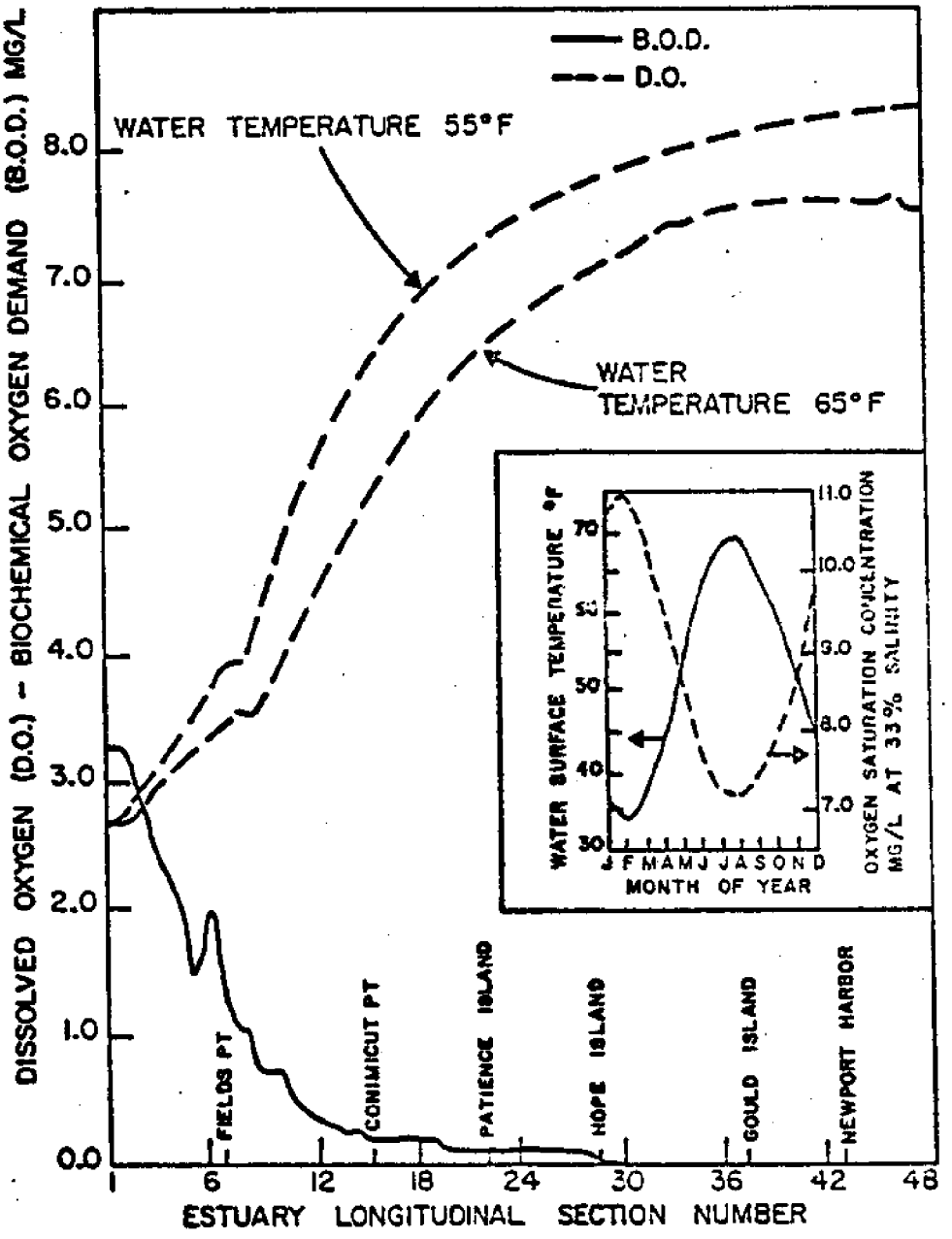

FIG. 5-10 COMPARISON OF DEPTH AVERAGED D.O. - B.O.D. PROFILES FOR VARIATION IN SURFACE WATER TEMPERATURE

oxygen saturation levels increases the D.O. levels at all depths with little change in the overall vertical structure. It is evident from viewing this simple comparison that slight changes in water temperature have drastic effects on the oxygen saturation and reareation processes.

VERIFICATION OF NARRAGANSETT BAY D.O. - B.O.D. PROFILE

In order to verify the nondimensional z axis computer modeled D.O. - B.O.D. reaction scheme and both the processes of reareation and B.O.D. decay, as well as pollutant point loading, the model was used to compute the D.O. - B.O.D. values for Narragansett Bay under typical summer time conditions. Using data published by the Providence Journal Bulletin Company (36) which was compiled from the Northeastern area Environmental Protection Agency and the Rhode Island Department of Public Health, a current list of pollution sources for the Bay was obtained. A summary of the sewage loads that are deposited directly into the estuary is presented in Table 5-1 and the locations

DIRECT POLLUTION SOURCES FOR NARRAGANSETT BAY (36)
AS OF OCTOBER 1971

STATION NO.	POLLUTERS NAME	LOCATION	RAW	TO WATER	ESTUARY LONGITU SECTION NUMBER (FIG.5-
1	PROVIDENCE SEWAGE TREATMENT PLANT	PROVIDENCE	54000	14000	7
2	NARRAGANSETT VILLAGE	WARWICK	80	15	11
3	EAST GREENWICH SEWAGE TREATMENT PLANT	E.GREENWICH	420	40	22
4	QUONSET-DAVISVILLE NAVAL BASE	N.KINGSTON	2700	1100	31
5	NAVY HOUSING DEV-ELOPMENT	WICKFORD	280	30	34
6	UNIVERSITY OF RHODE ISLAND	NARRAGANSETT	40	2	44
7	BLACKSTONE VALLEY SEWER DISTRICT COMMISSION	E.PROVIDENCE	52200	42300	-
8	EAST PROVIDENCE SEWAGE TREATMENT PLANT	E.PROVIDENCE	5000	1000	8
9	RHODE ISLAND LARE WORKS INC.	BARRINGTON	2160	2160	12
10	WARREN SEWAGE TREATMENT PLANT	WARREN	1900	1300	15
11	BRISTOL SEWAGE TREATMENT PLANT	BRISTOL	3900	2000	21
12	PEARSON YACHT DIV-ISION GRUMMAN ALLIED INDUSTRIES INC.	PORTSMOUTH	40	4	25
13	MELVILLE NAVAL FUEL DEPOT	PORTSMOUTH	181	161	29
14	RAYTHEON CO.	PORTSMOUTH	164	15	29
15	NEWPORT SEWAGE TREATMENT PLANT	NEWPORT	6700	6200	39
16	JAMESTOWN SEWER	JAMESTOWN	260	260	42
17	JAMESTOWN SEWER	JAMESTOWN	30	30	42
18	FORT ADAMS NAVY HOUSING COMPLEX	NEWPORT	170	130	43

TABLE 5-1 SOURCES OF SEWAGE POLLUTION FOR NARRAGANSETT BAY OCT. 1971

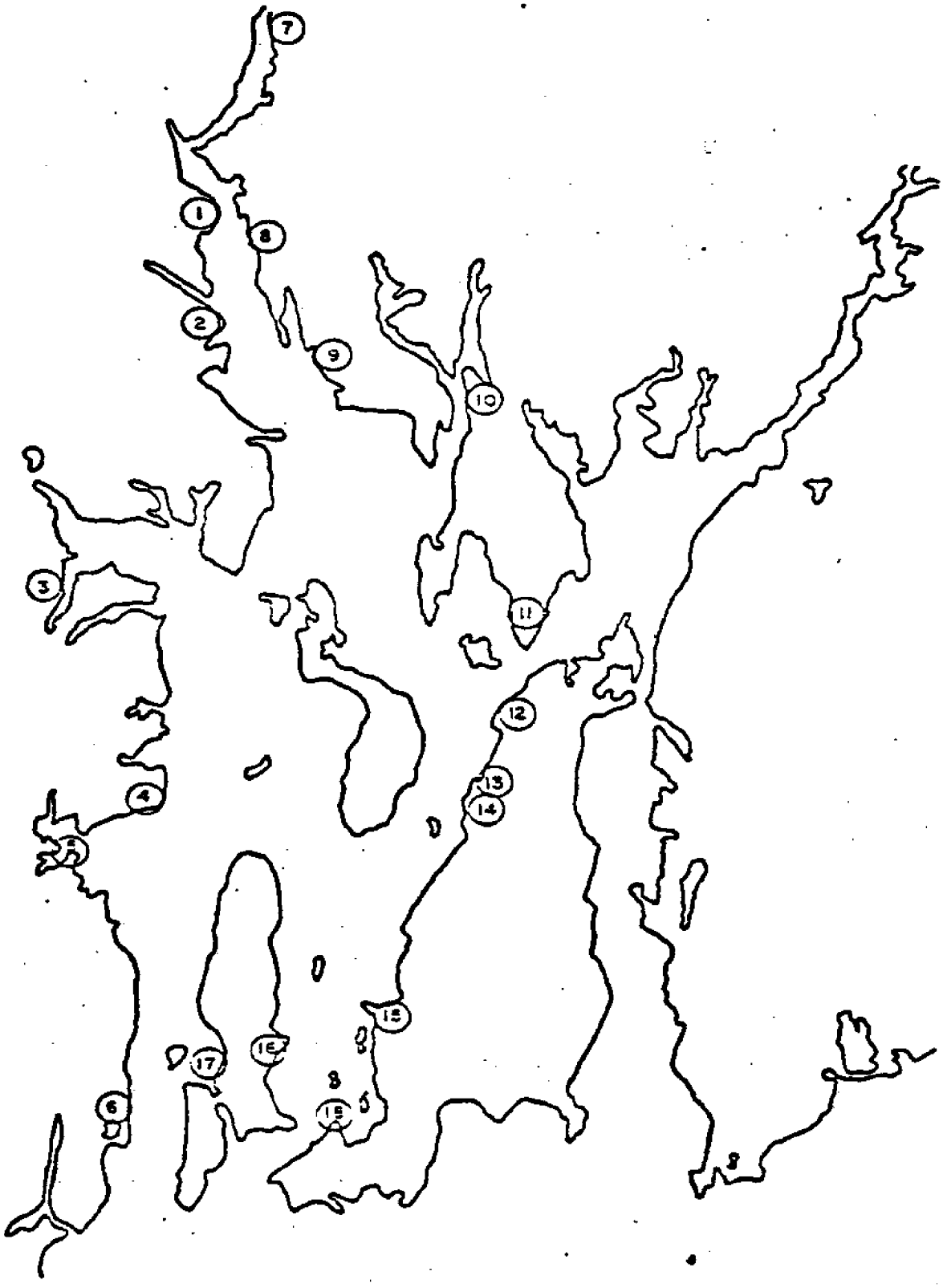

FIG. 5-11 LOCATION OF SEWAGE POLLUTION SOURCES AS LISTED IN TABLE 5-1

are suitably noted in Fig. 5-11. The table lists both normal (to river) and overflow (raw) loading conditions characteristic of dry and rainy weather conditions respectively. These pollutant load levels were then taken to represent the simple carbonaceous loads and were multiplied by the ratio of the model estuary cross-sectional area to the actual estuary cross-sectional area in an attempt to correct loadings to fit the tidal model geometry. The reasons for these corrections in geometry has been previously discussed in the section of this chapter concerning the estuarine hydrodynamics.

The simulation of the tidal movements has been previously outlined, in which a net outward flow has been added to the laterally averaged longitudinal velocity components from the two-dimensional vertically-averaged tidal hydraulics model. The results of this procedure seem adequate to complete the modeling effort at present.

Determination of a preliminary characteristic value for the B.O.D. decay coefficient was performed by the author using samples acquired from the Providence River. Employing a log daily difference approach with the 1,3,5 and 7 day B.O.D. values the decay coefficient was found to be in the

range between .065 day^{-1} and .25 day^{-1}. Therefore, as a preliminary estimate the B.O.D. decay coefficient was approximated as .08 day^{-1} over the entire Bay area. Further work will undoubtedly be necessary to determine more accurate values for this coefficient.

The reareation coefficient formulation for the model use was taken from the work of Krenkel and Thackston (37) and modified to obtain an average value of about .25 day^{-1}. Considerable difficulty was encountered in application of this classical reareation formulation, since like all other presently available empirical formulation techniques of reareation it incorporates both the actual molecular surface transport of oxygen as well as a dispersion coefficient for the entire water column which characterizes the movement of oxygen to the lower depths. However, to overcome this problem, instead of using the difference between the surface saturation value of D.O. and the value in the grid at the surface as the driving potential for reareation, the difference between the saturation level and the average value of D.O. for the whole column of water was employed. This technique appears to have substantially solved the problem and provided reasonable

reareation rates for the Bay.

The dispersion coefficients chosen for the study were a modified version of Elder's formulation with values of approximately 45 ft^2/ sec for longitudinal dispersion and Pritchard's density-corrected vertical dispersion coefficient with values ranging between .0001 ft^2/sec. and .02 ft^2/sec. depending on the gradients in the salinity field, which was employed to define the density structure of the Bay.

To help summarize the input for the D.O. - B.O.D. simulation of Narragansett Bay Table 5-2 presents the values employed in the computer modeling effort. Indications have also been made in this table as to the location of the data or formulation scheme.

To compare the results of the computer model to actual Bay conditions data for both B.O.D. and D.O. were collected from the Rhode Island Department of Public Health (31), the Army Corps. of Engineers Hurricane Barrier Study (8), and the University of Rhode Island's Bay Watch water sampling program (32). The values were then averaged over the summer season for each sampling program and station and then averaged again across each longitudinal

MODEL DATA INPUT	RANGE OR VALUE	COMMENTS
TIDAL VELOCITIES AND HEIGHTS	-	DETERMINED BY FORCING ONE DIMENSIONAL CONTINUITY ON TIDAL MODEL (34) OUTPUT WITH NET OUTWARD FLOW.
LONGITUDINAL DISPERSION COEFFICIENT	45 ft^2/sec	MODIFIED ELDER FORMULATION (p.321) WITH 25 ft^2/sec. ADDED FOR WIND EFFECT
VERTICAL DISPERSION COEFFICIENT	.0001-.01ft^2/sec.	PRITCHARD FORMULATION (p.321) WITH VERTICAL STRUCTURE DETERMINED BY SALINITY PROFILES AND WIND EFFECT INCLUDED WITH WH = 3.ft; WT = 6 sec. WL = 200 ft.
TEMPERATURE	65^oF	APPROXIMATE SUMMER AVERAGE VALUE
B.O.D. DECAY K_D	.08 day^{-1}	EXPERIMENTALLY DETERMINED
REAREATION K_A	.25 day^{-1}	MODIFIED THACKSTON-KRENKEL FORMULATION (p.319 TO OBTAIN .25 day^{-1}.

TABLE 5-2 SUMMARY OF INPUT CONDITIONS FOR COMPUTER MODELING OF D.O. - B.O.D. PROFILE FOR NARRAGANSETT BAY

MODEL DATA INPUT	RANGE OR VALUE	COMMENTS
WATER QUALITY BOUNDARY CONDITIONS FOR D.O. AND B.O.D.	SEEKONK RIVER BOUNDARY B.O.D. = .2077 (VSN) + 1.485 D.O. = .1538 (VSN) + 1.392 OCEAN BOUNDARY B.O.D. = 0.0 D.O. = SATURATION VALUE (p.318)	DETERMINED FROM EXISTING DATA (8,31,32,33) WHERE VSN - VERTICAL SECTION NUMBER 2 → 15, BOTTOM TO TOP, RESPECTIVELY
B.O.D. LOADING FROM POINT SOURCES	-	GIVEN IN TABLE 5-1 WITH DISTRIBUTION OVER VERTICAL AS NOTED ON PAGE 467.
SALINITY	27.2-34.%	DETERMINED FROM EXISTING DATA (8,32). SEE PAGE 470.

TABLE 5-2 (Cont'd) SUMMARY OF INPUT CONDITIONS FOR COMPUTER MODELING OF D.O. - B.O.D. PROFILES FOR NARRAGANSETT BAY

estuary section as defined in Fig. 5-1. The sampling results for D.O. and B.O.D. for both top (5 ft. below water surface) and bottom (5 ft. above estuary bottom) samples were then plotted against the longitudinal estuary section number. Starting with a set of initial conditions for both D.O. and B.O.D. taken from these data the computer model was run with the conditions as presented in Table 5-2. The model runs were continued until a quasi-steady condition was reached as determined by no significant changes in the depth-averaged D.O. and B.O.D. profiles. This process required approximately 30 days simulation time. Figures 5-12 and 5-13 show a comparison of the computed profiles for both depth-averaged and top and bottom stations compared to actual data for the D.O. and B.O.D. values, respectively. Error bars used on both figures show maximum levels found in the computer model results, or minimums.

Figure 5-12 shows that both for the depth-averaged and top sampling stations the comparison between estuary D.O. data and modeled results is good to excellent while the bottom sampling station results agreement to model results

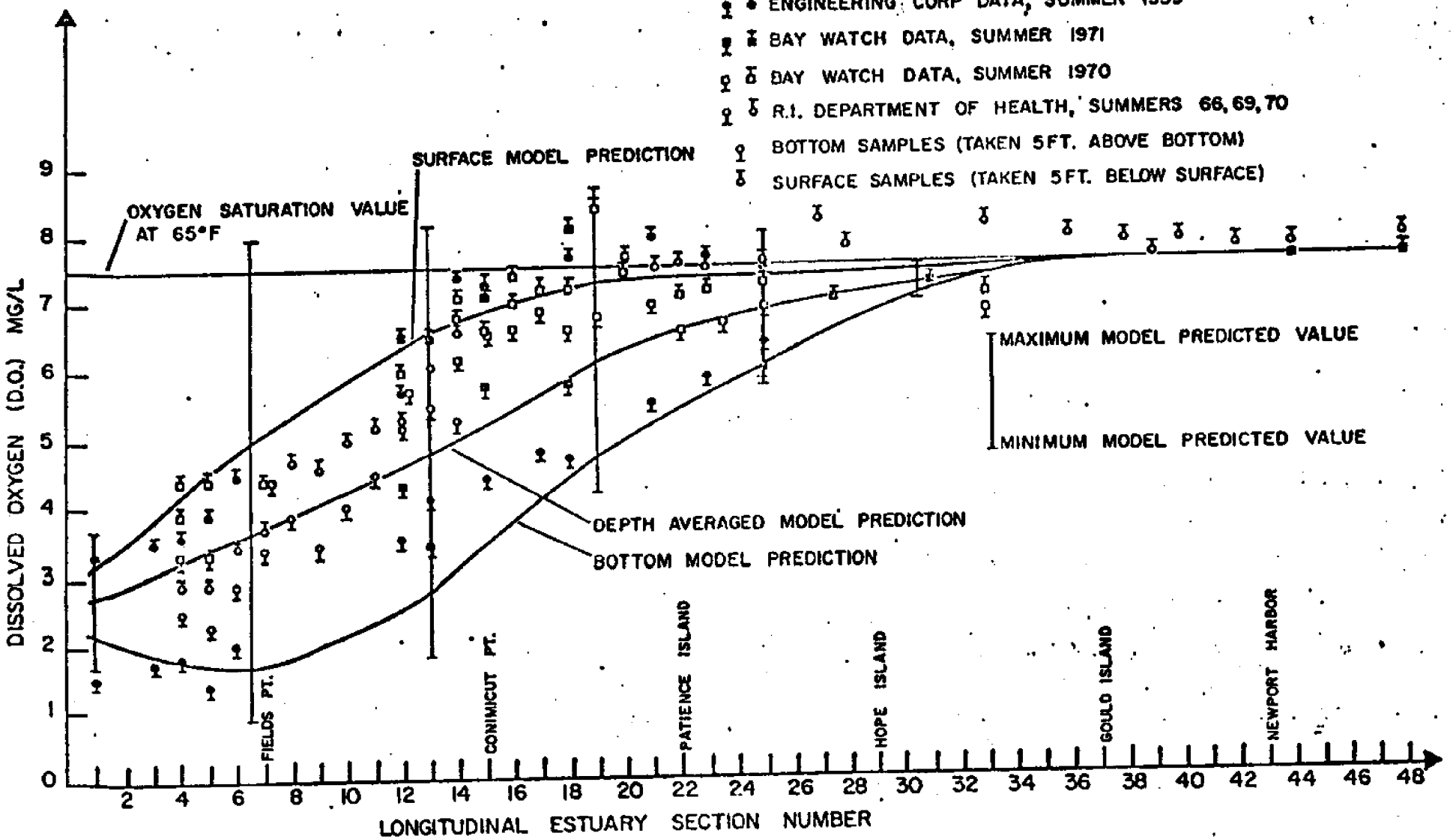

FIG. 5-12 COMPARISON OF MODEL PREDICTED D.O. PROFILES TO DATA FOR NARRAGANSETT BAY

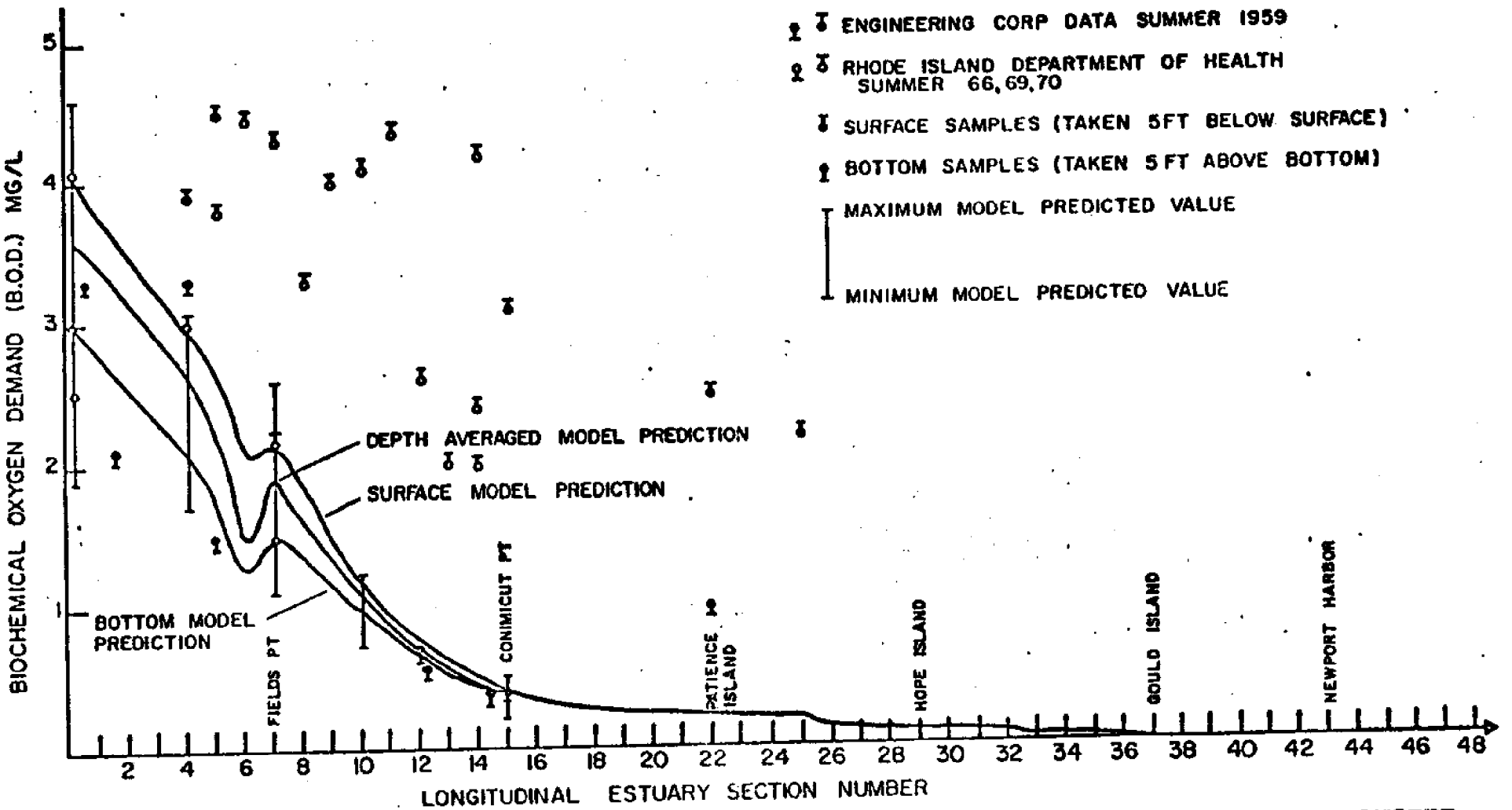

FIG. 5-13 COMPARISON OF MODEL PREDICTED B.O.D. PROFILES TO DATA FOR NARRAGANSETT BAY

is only fair to good. B.O.D. profiles, as shown in Fig. 5-13 appear to be in good agreement in the upper estuary but display considerable variation between model results and actual data in the lower portions of Narragansett Bay.

The major contributors to the poor representation between model and data are chiefly caused by the following factors - lack of inclusion of any B.O.D. loading due to the nitrogenous or benthic demands, less than adequate representation of the actual structure for the vertical dispersion coefficient, need for a biological model to predict sources of D.O. or B.O.D. caused by interaction between phytoplankton and zooplankton populations, lack of knowledge as to loading distribution over the vertical sections and only fair estimates of the coefficients for both reareation and B.O.D. decay. In light of all these difficulties however, the computer model results appear to be in good agreement with the Narragansett Bay data.

Another important model output is a time varying plot of the D.O., B.O.D. and tidal height for any particular location in the estuary. Typical outputs from the model appear similar to the graph in Fig. 5-14. Of particular

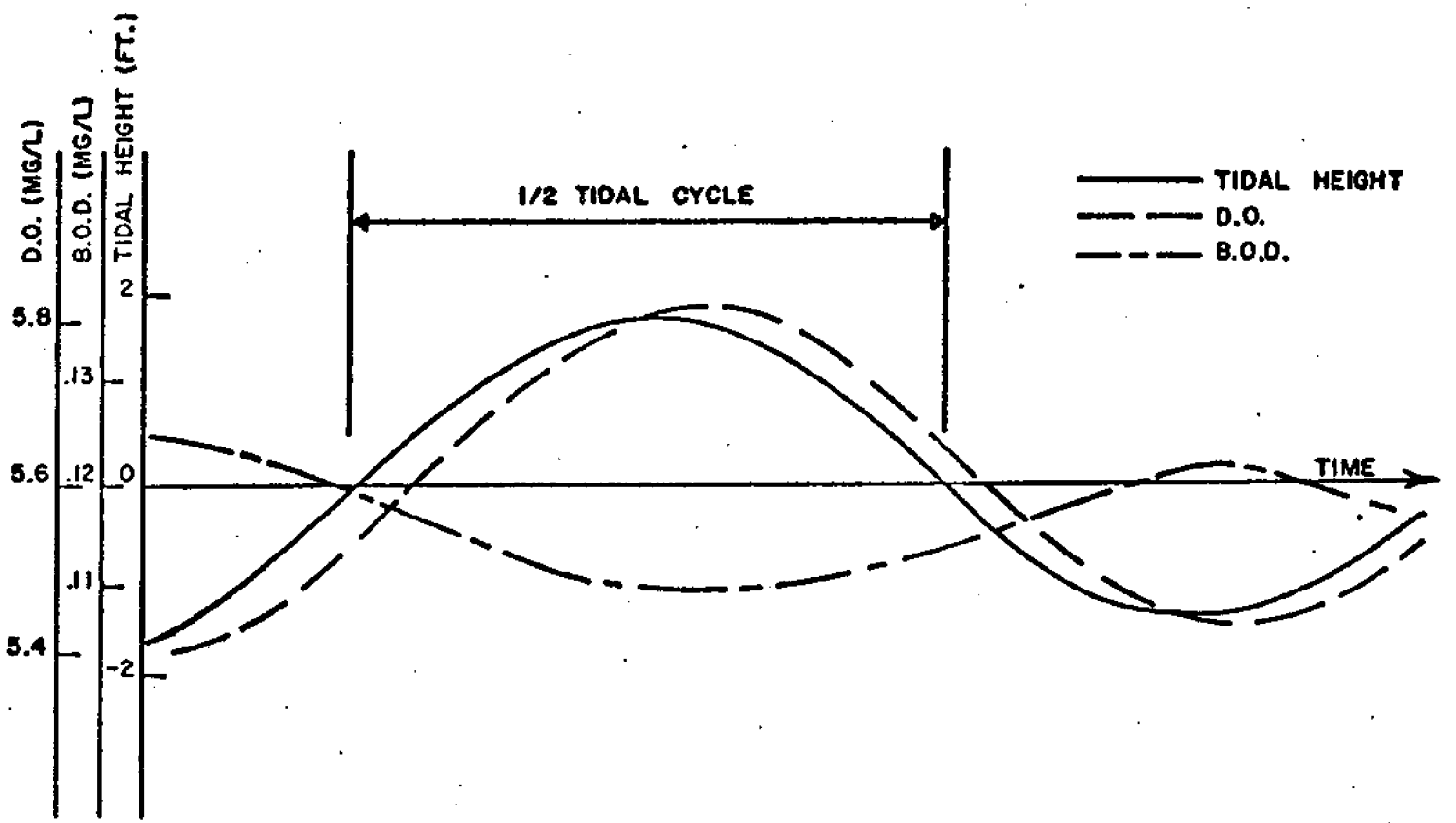

FIG. 5-14 TYPICAL VARIATIONS OF D.O. B.O.D. AND TIDAL HEIGHT FOR A GIVEN LOCATION IN NARRAGANSETT BAY

significance is that the variation of D.O. and tidal height are approximately in phase while the B.O.D. profile is consistently out of phase. Physically this effect can be quite simply explained. As water progresses up the Bay (flood, tidal level on the rise) cleaner water (higher D.O. levels) characteristic of each higher longitudinal section number of the Bay is carried up toward Providence, while the opposite process occurs during ebb tidal flow. Thus we can see why the D.O. and tidal height are in phase. Using a similar argument about the B.O.D. levels becoming higher as one proceeds from the Bay mouth to Providence, the B.O.D. levels should increase as the tidal flow ebbs. There are however, cases where both the D.O. and B.O.D. are in phase but 180^{o} out of phase with the tidal height. This situation can occur when there is a dip in the D.O. profile such as seen in Fig. 5-12 in the bottom values predicted by the model. Also of concern is the variation in D.O. and B.O.D. levels over a tidal cycle. Typical changes between mean low water and mean high water and over all depths range between 10% and 20% of the mean tidal cycle averaged value. These variations appear to be

considerably smaller than variations noted during the Engineering Corp Survey (8) of 1959, but the differences are more than likely attributable to inadequacies in incorporating short term and transit phenomena in the present model development.

Probably the single most important feature of the model is it ability to predict vertical structure for both D.O. and B.O.D. The variations over depth in each of these cases are determined by loading distributions for B.O.D. and D.O. sources as well as the vertical dispersive structure. The variations caused by vertical velocity components has been considered small and thus they have been neglected in the present modeling effort. To determine the loading distribution for sources of B.O.D. it was assumed that sewage discharge was buoyant when entering the estuaries environment therefore the loading for all cases was evenly distributed over the top five non-dimensional grids except when the loading in shallow water areas was large ($>$10,000 lbs. B.O.D./ day). In these cases the load was evenly distributed over the entire water column. In regards to reareation, it was assumed that oxygen was to enter only

at the estuarine surface. Defining accurate values for the vertical dispersion formulation variable coefficients was impossible due to lack of any data of this kind for Narragansett Bay. Hence, the standard Pritchard constants were used and the results viewed accordingly.

A partial view of the vertical structure has already been noted in Fig. 5-12 and 5-13 which show that the trends of higher B.O.D.'s and D.O.'s that occur near the surface have been qualitively predicted by the model. Figures 5-15 through 5-20 show comparisons of actual D.O. field data plotted against depth for several sections of the Bay. The figure order shows a logical progression from upper to lower Bay vertical D.O. structure. The depths listed on the figures often do not correspond to actual estuar depths at those stations, but are actually cross-sectional averages and should be interpreted in that manner. Careful observation of Fig. 5-16 through 5-20 shows a progressive case of increased vertical mixing as one proceeds from the Providence Hurricane Barrier to Beavertail at the mouth of Narragansett Bay. This fact has been well confirmed by observation of salinity profiles in the area over many years.

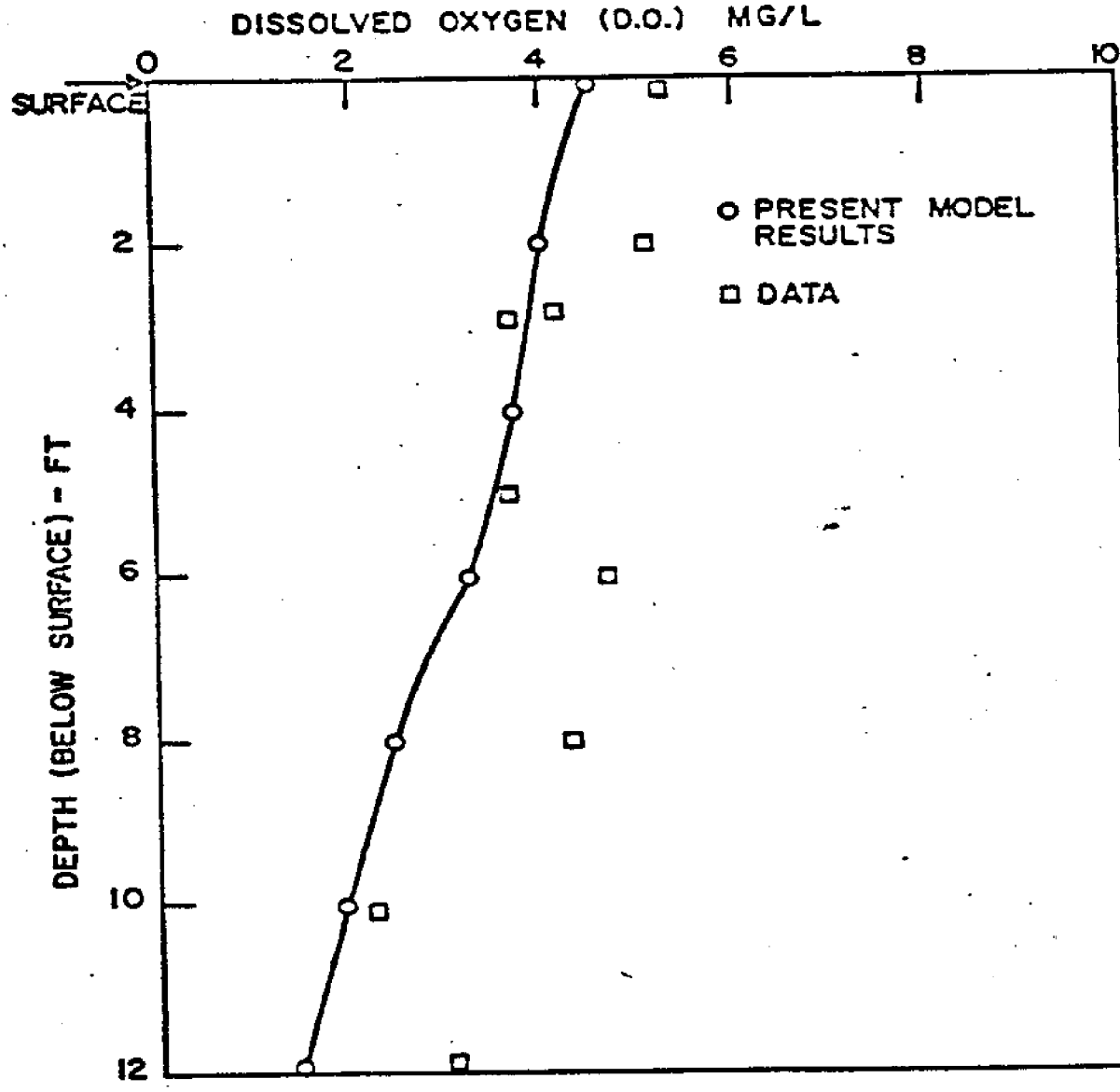

FIG. 5-15 COMPARISON OF D.O. VS. DEPTH FOR DATA AND MODEL RESULTS AT RED BRIDGE AREA, EAST PROVIDENCE

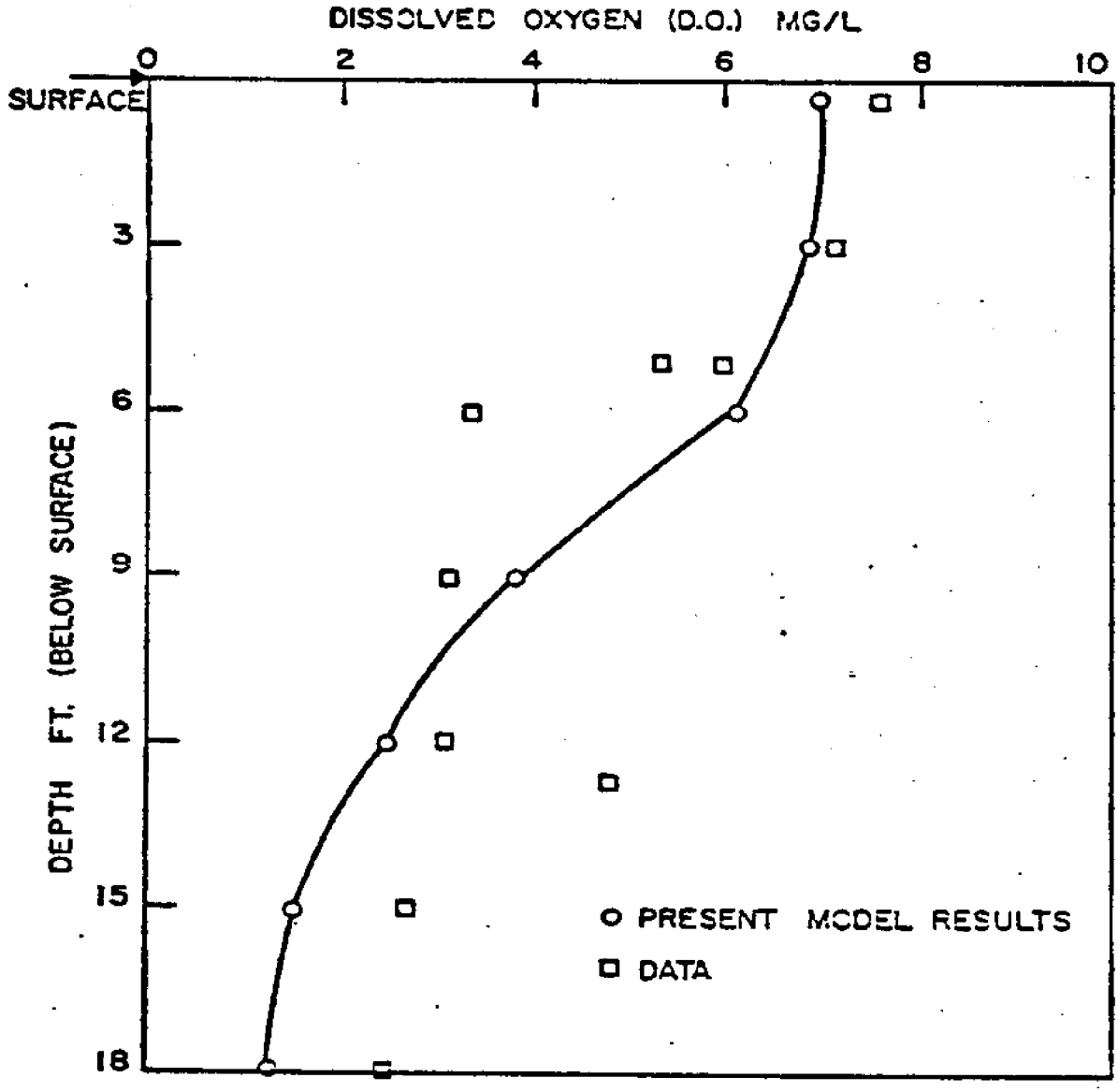

FIG. 5-16 COMPARISON OF D.O. VS. DEPTH FOR DATA AND MODEL RESULTS AT HEAD OF SABIN PT. REACH, PROVIDENCE

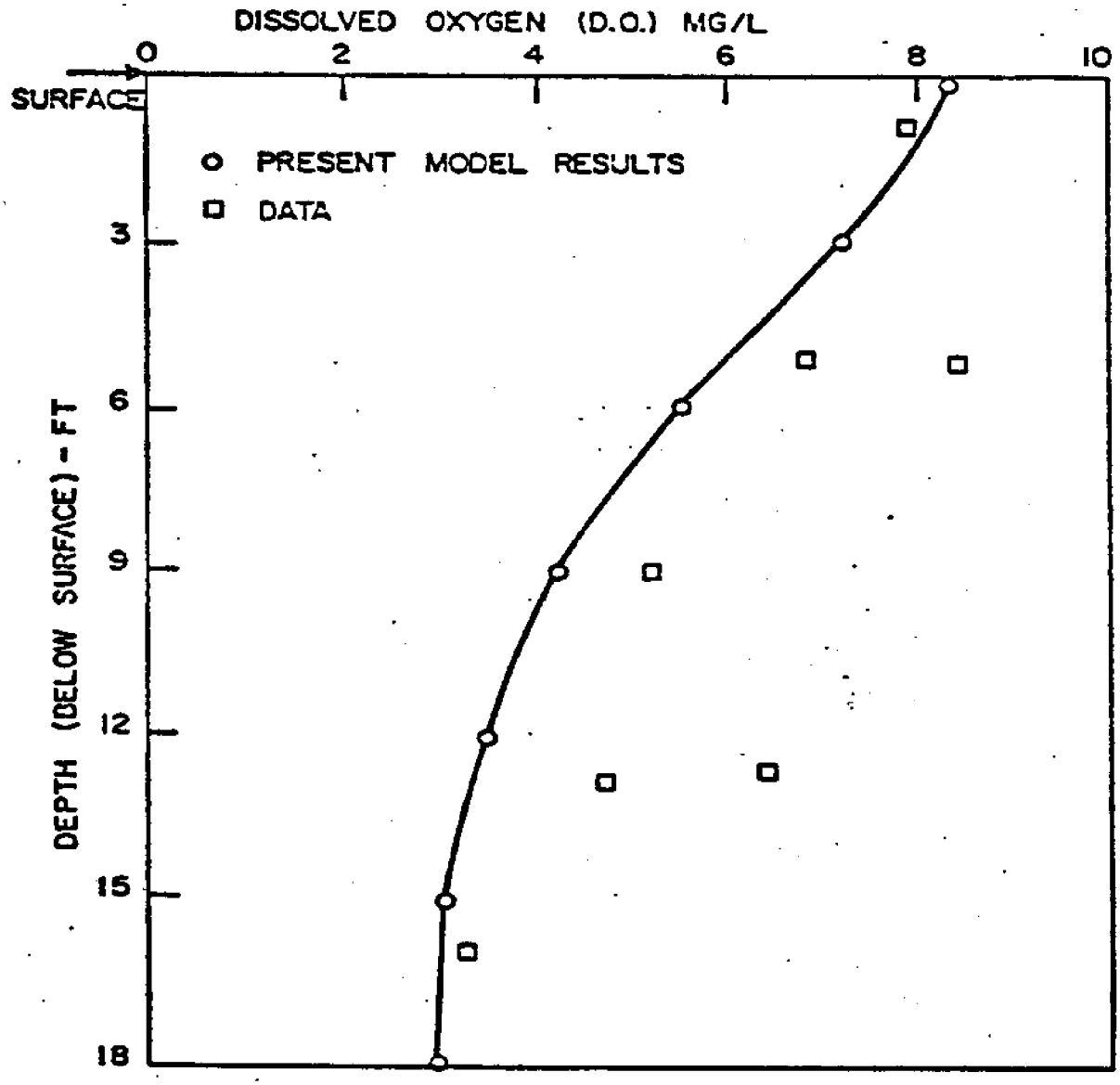

FIG. 5-17 COMPARISON OF DO VS. DEPTH FOR DATA AND MODEL RESULTS AT RUMSTICK REACH - ROCKY PT. AREA

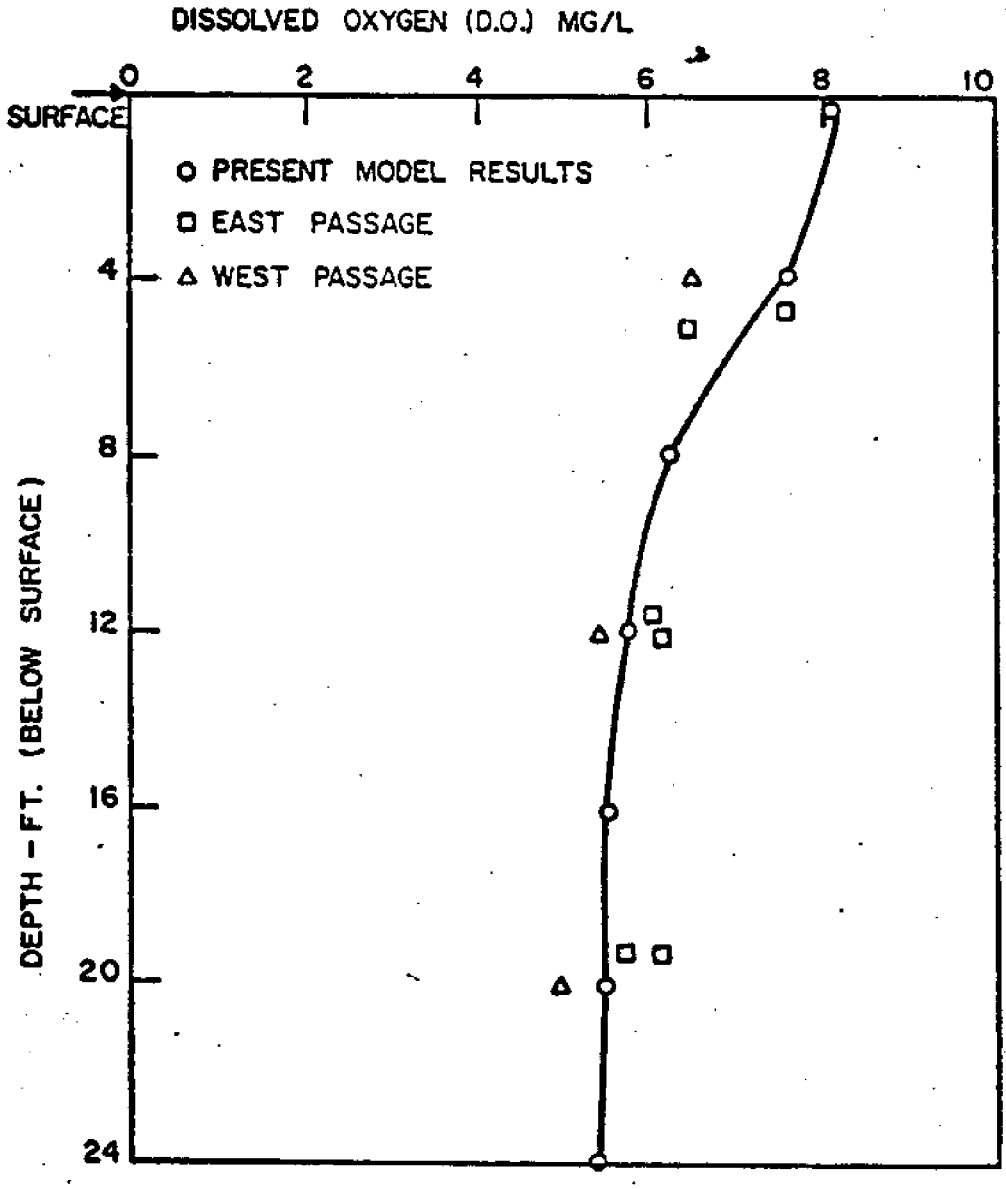

Fig. 5-18 COMPARISON OF D.O. VS. DEPTH FOR DATA AND MODEL RESULTS AT THE HOG ISLAND - PATIENCE ISLAND AREA

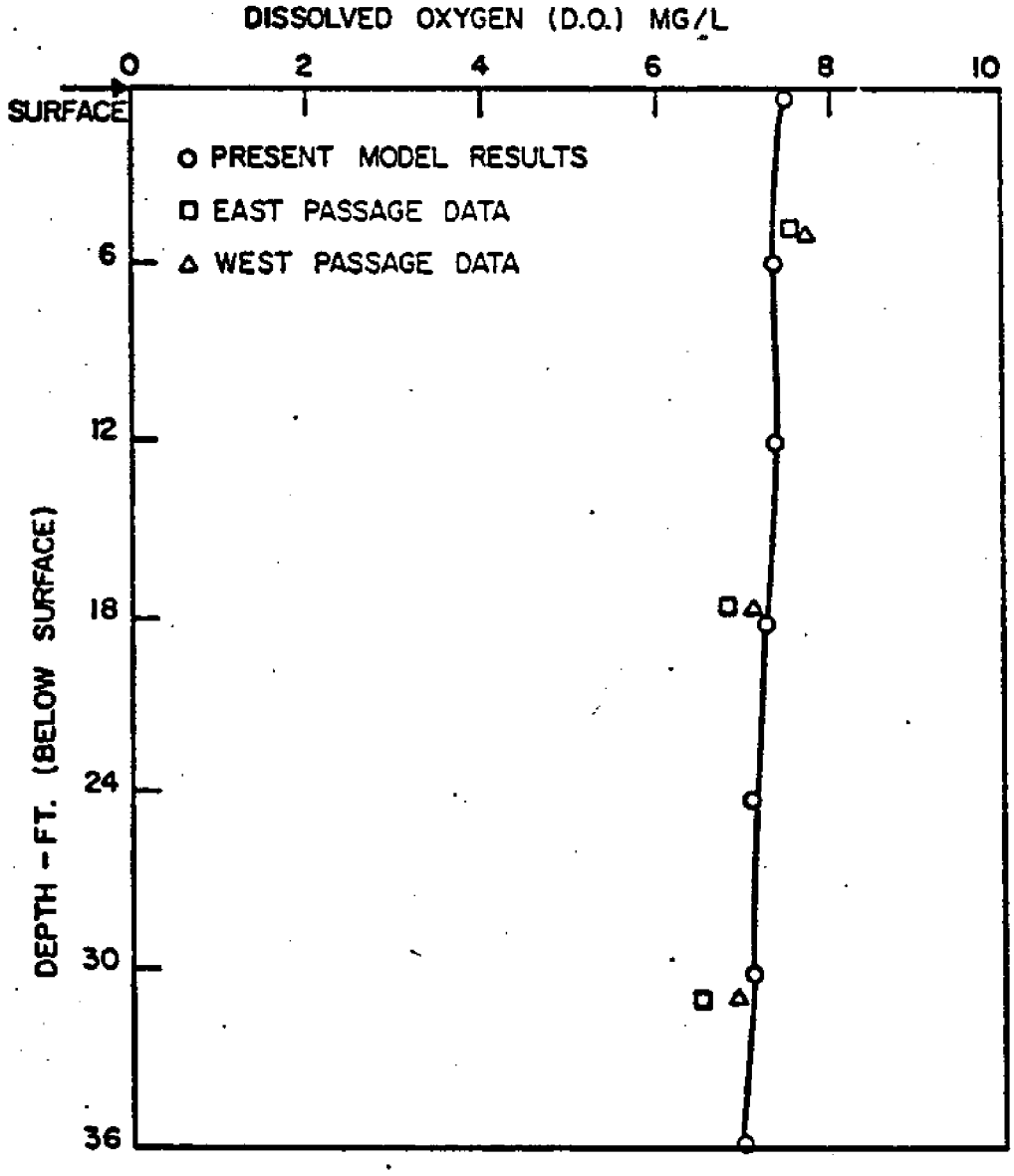

FIG. 5-19 COMPARISON OF D.O. VS. DEPTH FOR DATA AND MODEL RESULTS AT CONANICUT PT. AREA, JAMESTOWN

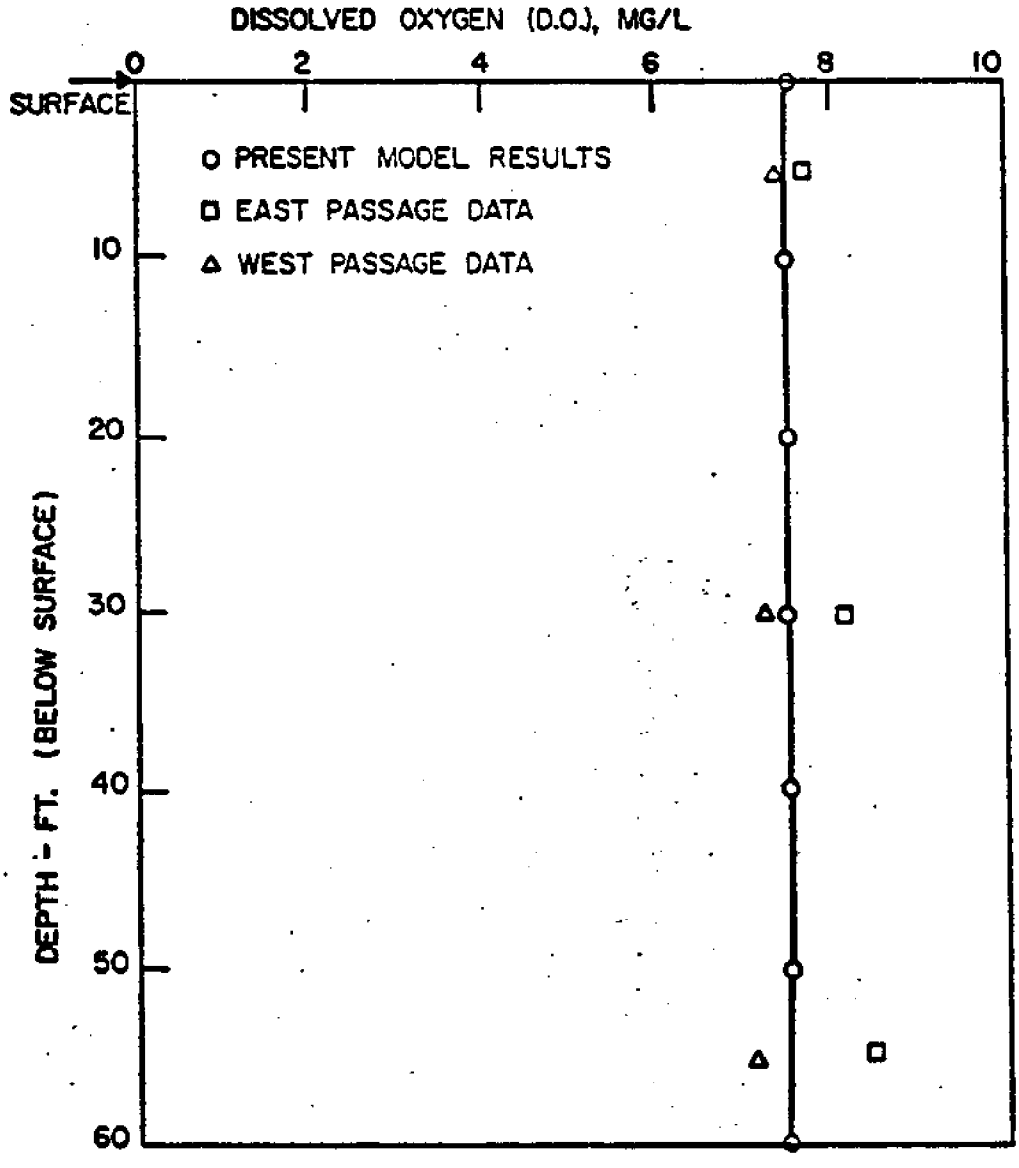

FIG. 5-20 COMPARISON OF D.O. VS. DEPTH FOR DATA AND MODEL RESULTS AT BEAVERTAIL, JAMESTOWN

The upper boundary condition (Seekonk River - Red Bridge) area (Fig. 5-15) does not display the severly inhibited vertical mixing structure due to the upper boundary condition approximations and large land and river inflows in the area. Comparison of the data which have been obtained from references (8,31,32,33) and a current U.R.I. Bay Watch sampling program show that the model results are remarkably good when considering the vertical structure of the dispersion coefficient has been taken from a standard Pritchard formulation and B.O.D. - D.O. loading distributions have been rather crudely approximated. The model results as shown in the figures represent approximate mean tidal averages and therefore are subject to a 10-20% deviation in either direction due to the influence of a tidal cyclic variation.

Profiles of the vertical structure of B.O.D. have not been presented since all data sets available have taken only top and bottom samples of B.O.D. and these results have already been adequately presented in Fig. 5-13. They however, would more than likely display a somewhat similar vertical structure, varying only where large B.O.D. loadings were made in a given section.

APPLICATION TO STORM-SEWAGE OVERFLOW

Once a model has been developed and verified to predict actual estuary D.O. and B.O.D. levels with a reasonable accuracy, the next step is to apply that model to some specific application. To that end the steady state model for Narragansett Bay was subjected to typical sewerage overflow characteristics for a one day period and then allowed to reach its quasi steady-state value once again. The level of these overflows was taken as the raw loadings as given in Table 5-1, while normal loads correspond to river values.

Figures 5-21 and 5-22 display the values of the D.O. and B.O.D. depth-averaged profiles, respectively. From the insert graph we can determine the approximate time of overflow conditions and the subsequent return to normal loading situations. As expected, the levels of D.O. drop due to the excess loads while the B.O.D. values rise rather substantially especially in high load areas, and both appear to reach their maximum or minimum levels respectively at the end of 40 hrs. This trend is to be expected

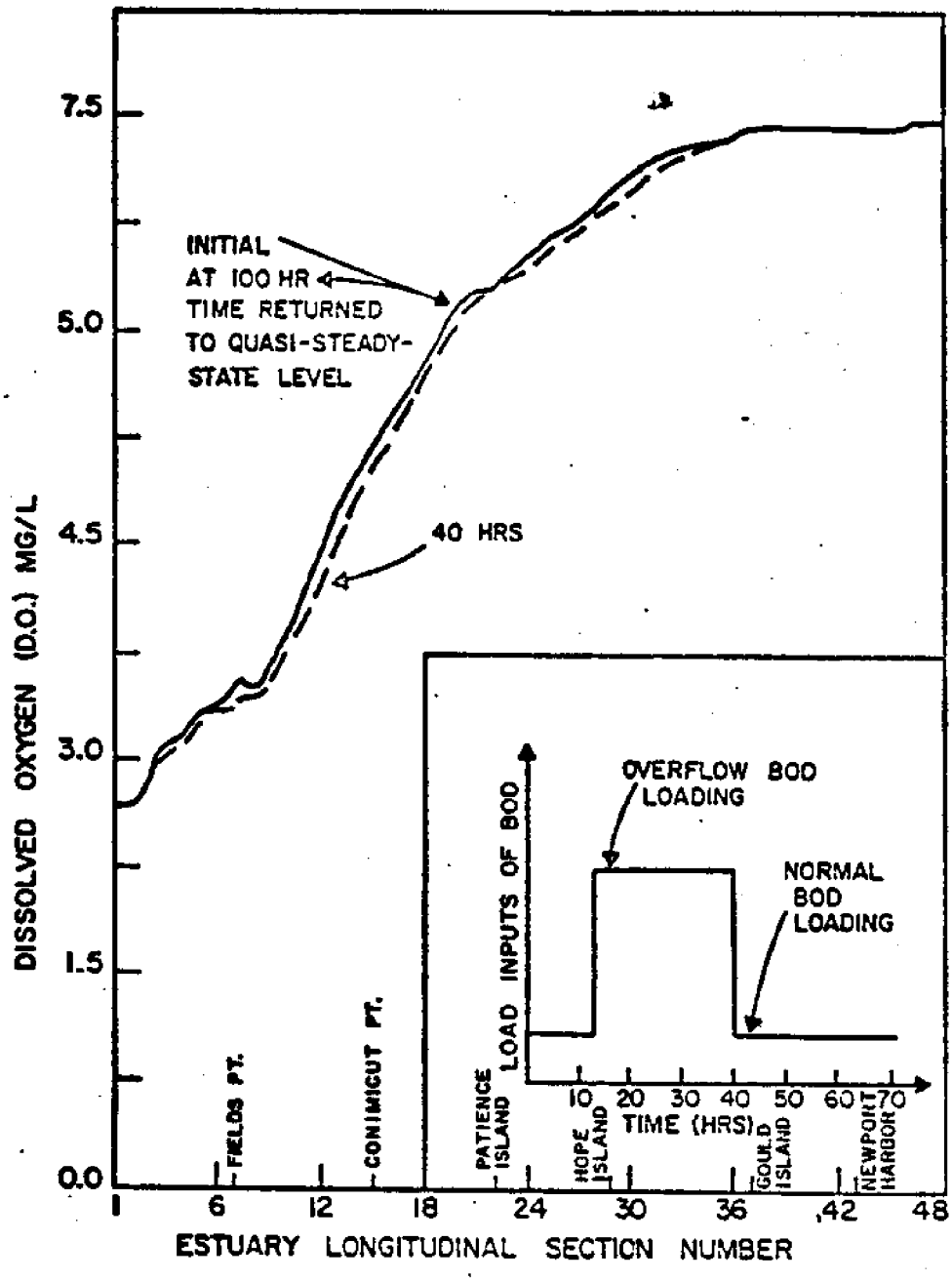

FIG. 5-21 DEPTH AVERAGED D.O. VALUE VARIATION CAUSED BY OVERFLOW B.O.D. LOADING

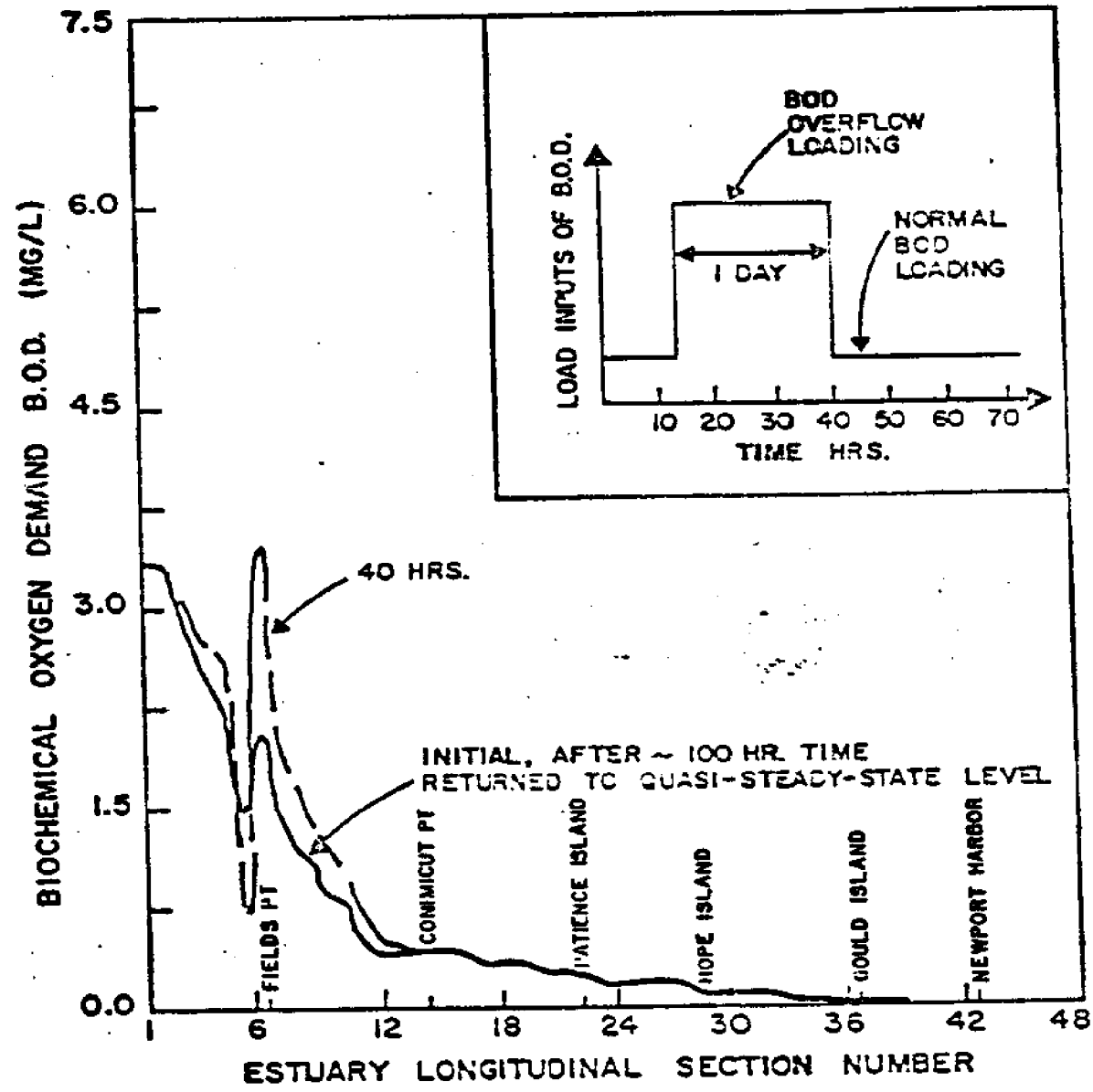

FIG. 5-22 DEPTH AVERAGED B.O.D. VALUE VARIATION CAUSED BY OVERFLOW B.O.D. LOADING

since when the excess loading ceases the process of B.O.D. decay continues in its customary concentration dependent manner to decay B.O.D. levels. Variations in D.O. between initial levels and minimum value show values of approximately 2% - 5% decrease of the initial, while B.O.D. levels display deviations as large as 175% from the initial value.

It is also noted that in the area of longitudinal estuary section number 6 and 7 there appear large differences in the B.O.D. levels. This effect for section number 7 can be explained by an excessively large load in that grid while the relatively low value in grid 6 is attributable to a depression of that value caused by the finite-difference approximation adjustment for the large point loading in 7 and insufficient local dispersion.

The next major point of interest is to determine the approximate period of time required for the estuary to recover from this excess load and return to its normal quasi-steady values for both D.O. and B.O.D. With this goal then the section-depth averaged profiles for D.O. and B.O.D. were compared to the initial values until agreement

between the two was achieved - both at the same-depth averaged value for a given longitudinal section. Preliminary results show that the time from which the excess load was stopped to approximate steady state levels occurred in about 2 1/2 days. This number appears reasonable when compared to the 5-7 day estimate used by the R.I. Department of Public Health to determine closing times for the shell fish areas in the upper Bay after periods of significant rainfall.

Plots of the vertical structure for the Bay were not performed since they show similar trends as in the normal sewage loading verification run. Variations of D.O. and B.O.D. levels show the expected increases in B.O.D. and decrease in D.O. where loading is high and vice versa.

The results of this application run with the computer model are surprisingly good in giving an order of magnitude estimate of the "excessive load cleanup time", considering the numerous gross approximations made in setting up the model parameters. Further work in this area however, is undoubtedly needed to provide more accurate predictions.

CHAPTER VI

SUMMATION

CONCLUSIONS

The development of the laterally-averaged mass-transfer equation and its subsequent finite-difference approximation have been shown to be valuable in providing a vertical water quality structure for a given estuary or estuary river system within a reasonable computational framework regarding both computer storage and run time. Verification of mass conservation and D.O. - B.O.D. reaction scheme have in addition indicated that the present model development has significant potential for estuarine water quality prediction.

Simulation runs of the finite-difference computer model involving the reaction scheme for the B.O.D. - D.O. system have displayed the models ability to predict rather excellent vertical structure definition for D.O. and reasonable values for B.O.D., in addition to which variations over a tidal cycle show expected phase relationships between

D.O. and B.O.D. Applications of the model to storm-sewerage overflow situations has also shown an order of magnitude estimate comparison with the scanty data available for "excessive load cleanup times". Hence, in conclusion, even considering the gross variations between estuary geometry and actual conditions with subsequent changes in tidal flow, crude approximations to the vertical dispersion coefficient, lack of accounting for all B.O.D. and D.O. sources and sinks caused by B.O.D. nitrification and estuarine biology and gross approximations as to the coefficients of B.O.D. decay and reaeration, the model predictions are surprisingly good.

RECOMMENDATIONS

Although the model results show good agreement to the data during quasi steady state conditions there are considerable problems yet to be tackled which would even make transit phenomena predictions a possibility. In the following list, recommendations of a specific nature for

the present Narragansett Bay model will be presented.

(1). A new more realistic tidal hydraulics model needs to be developed for the area of study including more accurate representation of actual estuarine geometry in the upper portion of the Bay. Possible development of a two dimensional laterally integrated tidal model and good one dimensional model is indicated here.

(2). An experimental program should be performed to determine the vertical dispersion coefficient structure for short term time varying cases for the Bay. These results can be compared with Pritchard's work to determine possible correlation between that formulation and actual data.

(3). The distribution of point loadings of B.O.D. should be further studied to determine a more reasonable approximation.

(4). The present model should be extended to include not only carbonaceous B.O.D. loads but also nitrogenous B.O.D. loading.

(5). The B.O.D. decay coefficients, both carbonaceous and nitrogenous, and the reareation coefficient should be determined from experimental data and compared with existing formulations.

(6). Modeling efforts should continue in the area of the estuarine biological sources and sinks of dissolved oxygen. Both distribution and times of these loadings are of particular importance.

(7). Present model work has been terminated at a simple D.O. - B.O.D. reaction scheme. Obvious generalizations to other water quality parameters, conservative substances and temperature distributions are indicated.

(8). Simulation runs of the conservative mode model should be performed to determine limits on the dispersion coefficients to achieve a solution which adequately conserves mass for each different estuarine geometry employed.

(9). Boundary condition approximation should be corrected to include transit effects due to tidal motion, wind, and land runoff.

(10). Applications of the present model to storm sewage overflow problems should be continued with a more realistic estimate of the loading levels as a function of time after a rainfall and inclusion of direct land runoff loadings into the Bay.

(11). In a more general view the present model has shown the surface process of reareation to be rather inadequately defined as regards to the vertical structure modeling. Also extension

of the present model to handle three dimensional time varying water quality predictions driven by a two dimensional vertically averaged tidal hydraulics model appears to be within reach by using some of the larger existing computer facilities available.

EXTENSION TO ESTUARINE WATER POLLUTION MANAGEMENT

The present model development has proven, through verification on Narragansett Bay D.O. - B.O.D. reaction scheme, to be of significant use in predicting the vertical structure of these water quality parameters. It therefore can be expected that with even better input data for the system constants that the model will provide a reliable predictive tool to note changes in estuary conditions under different loadings of pollution. It has already been shown in the application to storm sewage overflow conditions that the results appear to be qualitatively and quantitatively

reasonable.

The extension of this work from a simple verification process to an actual predictive model marks the true value of any water quality model. Once this transition is achieved we then have a model that can aid in the management of our coastal areas by allowing us to quantitatively predict the change in water quality caused by changes in sewage loading, channel dredging, barrier construction, and methods of sewage treatment.

BIBLIOGRAPHY

1. Lee, C.H., "One Dimensional, Real Time Model for Esturaine Water Quality Prediction", Ph.D. Thesis, M.I.T., September, 1970.

2. Hess, K.W., "Pollution in Narragansett Bay", Department of Ocean Engineering, Sea Grant Publication, Memorandum Number 5M, University of Rhode Island, 1970.

3. DiLuzio, F.C., "The Role of the Federal Government in Estuarine Pollution Abatement", National Symposium on Estuarine Pollution, Stanford University, August, 1967.

4. Thomann. R.V. "Mathematical Model for Dissolved Oxygen", Journal of Sanitary Engineering Division, ASCE, 89, October, 1963.

5. Jeglic, J.M., "DECS III, Digital Computer Program for Simulation of the Delaware Estuary's Behavior", General Electric Company Document, DCT & P, Memo No. 1027, August, 1965.

6. Leenderste, J.J., "A Water Quality Simulation Model for Well Mixed Estuaries and Coastal Seas: Vol. I, Principles of Computation", The Rand Corporation, RM-6230-RC, February, 1970.

7. TRACOR, "Estuarine Water Quality Modeling. An Assessment of Pollution Control Capabilities", Three Volumes. Work performed under contract 14-12-551, for the Federal Water Quality Administration, U.S. Department of the Interior, 1970.

8. U.S. Army Engineers District, New England Division, Corps of Engineers, "Effects of Proposed Hurricane Barriers on Water Quality of Narragansett Bay," 1959.

9. Leenderste, J.J., "Aspects of a Computational Model for Long Period Water Wave Propagation", The Rand Corporation, RM-5294-PR, May, 1967.

10. Bird, R.B., W.E. Stewart, and E.N. Lightfort, Transport Phenomena, John Wiley & Sons, Inc., New York, 1960.

11. Ippen, Arthur T., Estuary and Coastline Hydrodynamics, McGraw Hill, New York, 1966.

12. Fisher, H.B., "Methods for Predicting Dispersion Coefficients in Natural Streams, with Applications to Lower Reaches of the Green and Dawamesk River," Department of the Interior, Washington Geological Survey Professional Paper 582-4, U.S. Government Printing Office, Washington, D.C., 1958.

13. Taylor, G.I. "The Dispersion of Matter in a Turbulent Flow Through a Pipe", Proc. Roval Society of London 223, 1958.

14. Thomas, E.I., "Dispersion in Open Channel Flow", Ph.D. Thesis, Northwestern University, August, 1958.

15. Elder, J.W., "The Dispersion of Marked Fluid in Turbulent Shear Flow", Journal of Fluid Mechanics 5, (1959).

16. Fischer, H.B., "Longitudinal Dispersion in Laboratory and Natural Streams", Ph.D. Thesis, California Institute of Technology, 1966.

17. Wilson, J.R., and F.D. Masch, "Field Investigation of Mixing and Dispersion in a Deep Reservoir," The University of Texas, Hydraulic Engineering Laboratory Report 10-6701, June, 1967.

18. Pritchard, D.W., "A Study of the Salt Balance in a Coastal Plain Estuary", Journal Mar. Res., Vol. 13., No. 1, 1964.

19. Pritchard, D.W., "The Movement and Mixing of Contaminants in Tidal Estuaries", 1960. Proceedings 1st International Conference on Water Disposal in the Marine Environment, E.A. Pearson, Ed.

20. Montgomery, R.B., "Generalization for Cylinders of Prandtl's Linear Assumption for Mixing Length": Am. New York Acad. Sci. XLIV, Art. 1, 1943.

21. Kent, R.E., and D.W. Pritchard, "A Test of Mixing Length Theories in a Coastal Plain Estuary", Journal of Mar. Res., Vol. 18, No. 1.

22. Holley, E.R., "Unified View of Diffusion and Dispersion", Proc. ASCE, Vol. 45, HY2, 1969.

23. Richtmeyer, R.D., and E.W. Morton, Difference Methods for Initial Value Problems. 2nd ed., Interscience Publishers, New York, 1967.

24. Leenderste, J.J., and E.C. Gritton, "A Water Quality Simulation Model for Well Mixed Estuaries and Coastal Seas: Vol. II Computational Procedures", The Rand Corporation, July, 1971.

25. Leenderste, J.J., and E.C. Gritton, "A Water Quality Simulation Model for Well Mixed Estuaries and Coastal Seas: Vol. III, Jamacia Bay Simulation" The New York City Rand Corporation, R-709-NYC, July, 1971.

26. Peaceman, D.W., and H.H. Rachford, "The Numerical Solution of Parabolic and Elliptic Differential Equations", Journal Soc. Industrial Appl. Math. Vol. 3,No. 1, March, 1955.

27. Douglas, J. and J. Gunn, "A General Formulation of Alternating Direction Methods", Numerical Mathematics, Vol. 6, 1964.

28. Mitchell, A.R., Computational Methods in Partial Differential Equations, J. Wiley & Sons, New York, New York, 1969.

29. Hildebrand, F.B., Introduction to Numerical Analysis, McGraw Hill, New York, 1956.

30. Perkins, F.E., "The Role of Damping in Numerical Stability", A.S.C.E. National Meeting on Environmental Engineering, Chattanoga, Tennessee.

31. Rhode Island Department of Public Health, unpublished reports on Narragansett Bay Water Quality Sampling program.

32. University of Rhode Island, Bay Watch Project, unpublished data, 1970, 1971, 1972.

33. Oviatt, C., Graduate School of Oceanography, University of Rhode Island, unpublished data, 1971.

34. Hess, K.W. and F.M. White, "Hydrodynamics Model of Narragansett Bay", to be published as U.R.I. Marine Technical Report, 1972.

35. O'Connor, D.J. and W.E. Dobbins, "Mechanism of Reareation in Natural Streams", Trans. ASCE, Vol. 123, 1958.

36. The Providence Sunday Journal, The Providence Journal and Evening Bulletin, "Our Dirty Water", October, 1971.

37. Thackston, E.L. and P.A. Krenkel, "Reareation Prediction in Natural Streams", ASCE, Sanitary Engineering Division Journal, February, 1969.

NOMENCLATURE

A	Estuary cross sectional area
B	Estuary width
c	Dissolved oxygen (D.O.) concentration
C_o	Coliform bacteria concentration
Co_s	Source or sink coliform bacteria
c_{SAT}	Saturation value of dissolved oxygen
C_z	Chezy coefficient
D_1	Partial Differential operator $\partial/\partial x$
D_2	Partial Differential operator $\partial/\partial z$
D_x	Laterally averaged longitudinal (x) dispersion coefficient
D_z	Laterally averaged vertical (z) dispersion coefficient
E	Finite difference recursion value
e_D	Dispersion coefficient modification constant
e_x	x-directed diffusion coefficient
e_y	y-directed diffusion coefficient
e_z	z-directed diffusion coefficient
F	Generalized finite difference function
F_p	Position function

f_g	Generalized function operator
g	Gravitational acceleration
g_a	Amplification matrix
H	Mean sea level (MSL) depth of the estuary
H_T	Total estuary depth
J	Biochemical oxygen demand (B.O.D.) point loads
K_A	Reareation coefficient
K_D	B.O.D. decay coefficient
K_{cd}	Coliform decay coefficient
$[K]$	Reaction matrix
L	Biochemical oxygen demand (B.O.D.) concentration
L_o	Linear operator
L_w	Wavelength of mass concentration wave
ℓ	Integer index number for temporal spacing
l_c	Characteristic length of channel
m	Integer index number for longitudinal spacing
n	Integer index number for vertical spacing
P	Laterally integrated value of mass concentration ρ_A
$\vec{P}$	Laterally averaged mass concentration vector
P^*	Complex mass concentration amplitude
$\tilde{P}^{\ell}_{m,n}$	Numerical solution of finite difference equation for mass concentration P
$P^{\ell}_{m,n}$	Finite difference recursion value

Q	Finite Difference recursion value
R	Ratio of computed to physical mass concentration wave speeds
R_i	Richardson number
r	Hydraulic radius
S	Laterally integrated value of a source or sink S_A
$\vec{S}$	Source or sink vector
S_a	Conservative constituent
S_{DO}	Source or sink of D.O.
T	Propagation factor
T_t	Lagarangian time scale
t	Time
U	Laterally integrated longitudinal velocity (u)
u	x or longitudinal velocity component
$\bar{u}$	Uniform flow velocity in the x direction
u'	Perturbation of u velocity component
u''	Local depth averaged velocity distribution
u^*	Friction or shear stress velocity
u^{**}	rms turbulent velocuty fluctuations
v	y or lateral velocity component
W	Laterally integrated vertical velocity w

WH	Wave height of water wave
WT	Wave period of water wave
WL	Wavelength of water wave
w	z or vertical velocity component
w'	Pertubation of w velocity component
x	Longitudinal direction in orthogonal coordinate system
y	Lateral direction in orthogonal coordinate system
$z^{\ell}_{m,n}$	Error between numerical and theoretical solutions of the finite difference equation
z	Vertical direction in orthogonal coordinate system
α	Finite difference weighting factor
α_i	Reaction matrix weighting factor
α_p	Wind induced vertical dispersion emoirical constant
α_s	Stability constant for temporal term
β_i	Reaction matrix weighting factor
β_p	Density structure vertical dispersion empirical constant
β_s	Stability constant for longitudinal term
γ_s	Stability constant for vertical term
Δt	Temporal grid spacing
Δx	Longitudinal grid spacing

ΔZ	Vertical grid spacing
ϵ_y	Lateral dispersion coefficient
η	Nondimensionalized vertical axis (Z/H_T)
η_p	Turbulent flow induced Vertical dispersion empirical constant
λ	Eigenvalue
ζ	Tidal height referenced to mean sea level (MSL)
ζ_s	Stability parameter
ρ	Density
ρ_A	Mass concentration of Substance A
ρ_A'	Perturbation of ρ_A
σ_j	Wave number for constituent j
τ	Half temporal spacing ($\Delta t/2$)
τ_x	Bed shear stress
ϕ	Characteristic dispersive mixing length
χ	,4
ω_j	Wave number of constituent j

APPENDIX A

TWO - DIMENSIONAL
LATERALLY - INTEGRATED ESTUARINE
NUMERICAL WATER QUALITY MODEL

VOLUME II - USER'S MANUAL

MALCOLM L. SPAULDING

FRANK M. WHITE

DEPARTMENT OF MECHANICAL ENGINEERING AND APPLIED MECHANICS

UNIVERSITY OF RHODE ISLAND

KINGSTON, RHODE ISLAND

1974

THIS WORK WAS SUPPORTED BY THE UNIVERSITY OF RHODE ISLAND SEA GRANT PROGRAM. ADDITIONAL COPIES OF MARINE TECHNICAL REPORT XX ARE AVAILABLE FROM THE URI MARINE ADVISORY SERVICE, NARRAGANSETT BAY CAMPUS, NARRAGANSETT, RHODE ISLAND 02882. COST PER COPY IS $X.00.